AWARD NUMBER: W81XWH-15-1-0192

TITLE: Msi2 Regulates the Aggressiveness of Non-Small Cell Lung Cancer (NSCLC)

PRINCIPAL INVESTIGATOR: Yanis Boumber, MD, PhD

CONTRACTING ORGANIZATION: University of New Mexico
Albuquerque, NM 87131

REPORT DATE: October 2016

TYPE OF REPORT: Annual

PREPARED FOR: U.S. Army Medical Research and Materiel Command
Fort Detrick, Maryland 21702-5012

REPORT DOCUMENTATION PAGE

Form Approved
OMB No. 0704-0188

1. REPORT DATE *(DD-MM-YYYY)*	2. REPORT TYPE	3. DATES COVERED *(From - To)*
October 2016	Annual	15 Sep 2015 - 14 Sep 2016

4. TITLE AND SUBTITLE

Msi2 Regulates the Aggressiveness of Non-Small Cell Lung Cancer (NSCLC)

5a. CONTRACT NUMBER

5b. GRANT NUMBER
W81XWH-15-1-0192

5c. PROGRAM ELEMENT NUMBER

6. AUTHOR(S)
Yanis Boumber, MD, PhD

5d. PROJECT NUMBER

5e. TASK NUMBER

5f. WORK UNIT NUMBER

7. PERFORMING ORGANIZATION NAME(S) AND ADDRESS(ES)

University of New Mexico Health
Sciences Center
MSC09 5220
1 University of New Mexico
Albuquerque, NM 87131-0001

8. PERFORMING ORGANIZATION REPORT NUMBER

9. SPONSORING / MONITORING AGENCY NAME(S) AND ADDRESS(ES)
U.S. Army Medical Research
Fort Detrick, Maryland
21702-5012

10. SPONSOR/MONITOR'S ACRONYM(S)

11. SPONSOR/MONITOR'S REPORT NUMBER(S)

12. DISTRIBUTION / AVAILABILITY STATEMENT
Approved for public release; distribution unlimited

13. SUPPLEMENTARY NOTES

14. ABSTRACT `200 words-fit in the box`

Purpose, scope: The objective of this project is to expand our mechanistic data to characterize the functional roles of MSI2 in human NSCLC cells and test whether MSI2-overexpressing cells are more sensitive to γ-secretase and TGF-β receptor Type I kinase (TGF-βRI) inhibitors (Aim 1). I also aim to investigate if MSI2 expression is clinically predictive in tumor specimens from lung cancer patients (Aim 2). **Major findings and progress:** Depletion of MSI2 in multiple independent metastatic murine and human NSCLC cell lines reduced invasion and metastatic potential, independent proliferation effects. MSI2 depletion significantly induced expression of proteins associated with epithelial identity, including tight junction claudin proteins and down-regulated direct translational targets associated with EMT, and unexpectedly upregulated NOTCH pathways. Depletion of TGFβRI or SMAD3 resulted in reduced invasion, while overexpression of TGFβRI reversed the loss of invasion associated with MSI2 depletion. Interestingly, MSI2 depletion reduced E-cadherin expression, while increasing fibronectin (FN1), reflecting a mixed epithelial–mesenchymal phenotype. MSI2 provides essential support for TGFβR1/SMAD3 signaling, contributes to NSCLC progression and may be a predictive biomarker of NSCLC aggressiveness. TGF-βRI and γ-secretase drug studies in vitro and in vivo are ongoing, while immunohistochemistry studies are starting Fall 2016.

15. SUBJECT TERMS
Non-small cell lung cancer, invasion, metastasis, pro-invasive signaling, RNA binding proteins, Musashi, TGF-beta, epithelial mesenchymal transition (EMT), Notch, gamma-secretase, tissue microarrays (TMA).

16. SECURITY CLASSIFICATION OF:			17. LIMITATION OF ABSTRACT	18. NUMBER OF PAGES	19a. NAME OF RESPONSIBLE PERSON
U					USAMRMC
a. REPORT	b. ABSTRACT	c. THIS PAGE	UU	77	19b. TELEPHONE NUMBER *(include area code)*
U	U	U			

Standard Form 298 (Rev. 8-98)
Prescribed by ANSI Std. Z39.18

Table of Contents

Page

1. INTRODUCTION

Analyzing tumors from a mouse model of NSCLC, we identified upregulation of Msi2 as a previously unrecognized marker of invasion and metastasis in NSCLC. Msi2 knockdown in metastatic murine NSCLC cell lines decreased invasion and metastasis. Candidate pathway analysis and reverse-phase protein array screening identified EMT-associated proteins including the TGF-β receptor Type I (TGF-βRI), the Notch inhibitor Numb, and fibronectin, as strongly regulated by Msi2. An initial probe of 123 primary human NSCLC specimens, we have found that Msi2 is significantly elevated in tumors versus normal lung epithelium, suggesting relevance to physiological NSCLC in patients. The objective of this project is to expand our mechanistic data to characterize the functional roles of MSI2 in human NSCLC cells.

2. KEYWORDS

Non-small cell lung cancer, invasion, metastasis, pro-invasive signaling, RNA binding proteins, Musashi, TGF-beta, epithelial mesenchymal transition (EMT), Notch, gamma-secretase, tissue microarrays (TMA).

3. ACCOMPLISHMENTS

What were the major goals and objectives of the project?
Our preliminary data suggest the hypothesis that Msi2 is a master switch for invasion and metastasis that provides essential support for TGF-β and Notch-dependent oncogenic in a subset of metastatic NSCLC. The objective of this proposal is to expand our mechanistic data to characterize the functional roles of Musashi proteins in human NSCLC cells and to test whether Msi2 overexpressing cells are more sensitive to γ-secretase and TGF-β receptor Type I kinase (TGF-βRI) inhibitors (Aim 1): as a developing physician-scientist, my bigger goal would then be to develop a Phase I/II trial focused on evaluation of these inhibitors using Msi2 as a biomarker for response. I also aim to investigate if the expression of Msi2 is clinically predictive in tumor specimens from lung cancer patients (Aim 2). A functional role for Msi proteins has never been identified or studied in NSCLC; of the two Msi proteins, has almost all work has focused on Msi1. I hope these studies of Msi2 will improve understanding of what drives NSCLC, and suggest improved treatment strategies.

Aim 1: Evaluate the functional role of Msi2 in human lung cancer cell lines. Human and murine cell lines with depleted or overexpressed Msi2 will be used for functional assays in vitro and orthotopic xenograft studies in mice. The functional role of Msi2 in regulating Numb/Notch, TGF-β and markers of epithelial-mesenchymal transition (EMT) in NSCLC pathogenesis will be characterized. Msi2 manipulated lung cancer cells will be treated with γ-secretase and TGF-β receptor Type I kinase (TGF-βRI) inhibitors, to determine if those are differentially sensitive to these drugs, and that treatment with these agents will reduce tumor invasion and metastasis.
Overall, 65% completed.

Subtask 1: Confirmation of Msi2 function in human NSCLC models. Cell lines: H358, A549; H441, H322, 293T (MD Anderson / ATCC). *SA1:* Cell proliferation assays: second method of measuring proliferation, performing automated counting DAPI-stained nuclei using high throughput equipment in the institutional translational science facility. 1-6 months. 100% completed.
Subtask 2: Validation of functional significance of Msi2-dependent signaling effectors. Cell lines used: 344SQ, A549, H358, H441, H322, 293T (MD Anderson / ATCC). 1-18 months. 100% completed.
Subtask 3: Determination of the role of Msi2 in NSCLC response to Notch and TGF-β targeting drugs (in SCID mice). Cell lines used: H358, A549 (MD Anderson / ATCC). 12-24 months. 40% completed.

Aim 2: Establish how Msi2 expression predicts tumor phenotypes, patient outcomes, and invasion-related signaling in primary human NSCLC tumors. We will analyze lung cancer tissue microarrays for Msi2 expression

relative to normal lung tissues, and Msi2 correlation with stage, grade, and survival in lung cancer patients. We will determine whether Msi2 expression correlates with expression of Numb, Notch pathway activity, TGF-β R1 and SMAD3 expression, and therapeutic response.
Overall, 5% completed.
Subtask 1: Obtain UNM SRC and FCCC Committee Approvals for the construction and use of TMAs. 1-3 months. 100% completed.
Subtask 2: Analyze expression of Numb, activated Notch, and HES1, TGF-βRI, phosphorylated SMAD3 and correlate it with Msi2 expression and patient and tumor data in lung cancer tissue microarrays (UNMHSC), using Aperio Scan Scope CS. 12-22 months. 0% completed.
SA1: Msi2 Specificity control experiments on the TMAs using MSI2-knockdown vs control cell lines that will be paraffin embedded and stained in parallel manner to TMA. In addition, we will use 2d alternative Msi2 antibody to validate our data if needed (Abcam #ab50829, or ab156770).12-22 months. 0% completed.

Generally, the goals will not change from one reporting period to the next and are unlikely to change during the final reporting period. However, if the awarding agency approved changes to the goals during the reporting period, list the revised goals and objectives. Also explain any significant changes in approach or methods from the agency approved application or plan.

What was accomplished under these goals?
Major activities for this project as per major goals outlined above included an extensive series of experiments as outlined in (3) below and required applications of various molecular, cancer biology and cell biology experimental procedures, and included primarily in vitro and cell culture approaches, with currently ongoing animal experiments which have not yet resulted, being performed in mice.

Specific objectives, once again, included expanding our mechanistic data to characterize the functional roles of Musashi proteins in human NSCLC cells and to test whether Msi2 overexpressing cells are more sensitive to γ-secretase and TGF-β receptor Type I kinase (TGF-βRI) inhibitors (Aim 1): as a developing physician-scientist, my bigger goal would then be to develop a Phase I/II trial focused on evaluation of these inhibitors using Msi2 as a biomarker for response. I also aim to investigate if the expression of Msi2 is clinically predictive in tumor specimens from lung cancer patients (Aim 2). A functional role for Msi proteins has never been identified or studied in NSCLC; of the two Msi proteins, has almost all work has focused on Msi1.

Significant results and major findings. The narrative and 8 corresponding figures below generally match Aim 1 of the grant, which has been 65% completed. Sub-Aim 3 experiments (“mouse trials”) are nearly half done, and

remaining experiments are currently ongoing.***MSI2 depletion in metastatic NSCLC cells inhibits invasion in vitro and has minimal effect on proliferation in NSCLC.*** Based on expression profiles of NSCLC cell lines available through the Cancer Cell Line Encyclopedia[1], we identified the human NSCLC cell lines A549 ($KRAS^{mut}$) and H358 ($KRAS^{mut}$;$TP53^{-/-}$) as metastasis-competent adenocarcinoma cell lines with high expression of MSI2. We previously used shRNA depletion of these and two metastatic murine NSCLC cell lines (344SQ and 531LN2) to further study the role of MSI2 in metastasis. Similar results were obtained using transient siRNA transfections to deplete MSI2 as well, which we recently published (Kudinov et al[2]). To complement these studies, we now generated two additional MSI2-depleted and control human cell lines, A549 and H358 (Figure 1A). MSI2 depletion consistently and significantly reduced invasion through Matrigel for all lines, including A549 and H358 cell line models (Figure 1 B, C). As indicated in the CDA, we also analyzed cell proliferation upon MSI2 depletion. For three of the four cell lines (344SQ, A549, and H358), depletion of MSI2 had no effect on cell proliferation in vitro (Fig 1 L, M), using both CellTiterBlue (CBT) and complementary DAPI cell counting as was requested by the DOD CDA grant reviewers per SA1 goals.

In a reciprocal approach, as outlined in Aim1 of the proposal, we recently overexpressed MSI2 in cell lines with low MSI2 levels. We initially planned to overexpress MSI2 in H441 and H322 cell lines. However, we were unable to reliably overexpress MSI2 in H441 cell line, and therefore we used an alternative approach by overexpressing MSI2 in 393P murine cell line. Later, we were able to successfully overexpress MSI2 in H322 cell line as well. In view of these slight, likely technical, changes, we first generated functional data for the 393P cells, and we have recently generated the H322 cell lines, control and MSI2-overexpressing lines (Fig. 5 H; functional

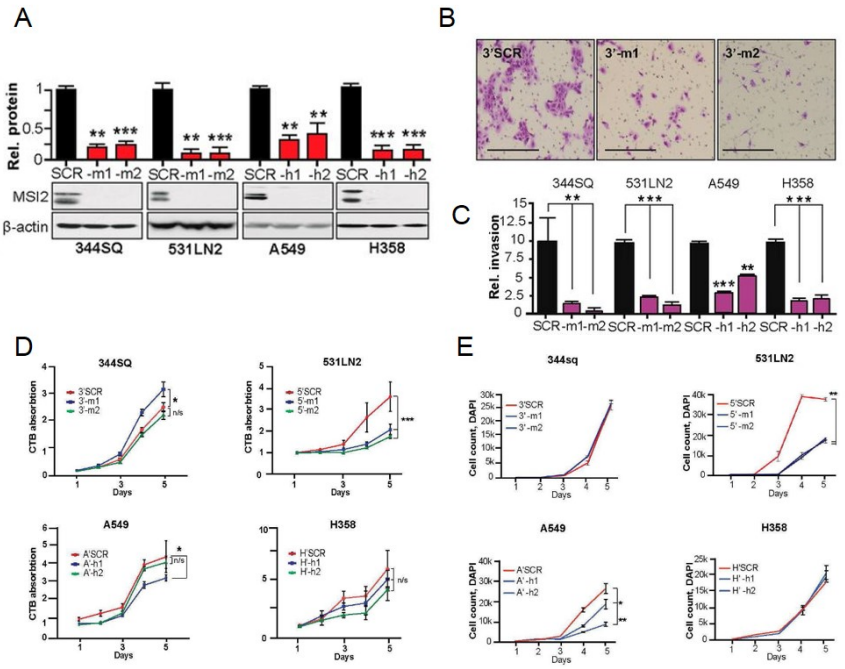

Fig. 1. Elevated MSI2 expression supports NSCLC invasion with minimal effects on proliferation. (A) Western validation of MSI2 depletion with two independent shRNAs (–m1, –m2, –h1, and –h2) in indicated cell lines, relative to control shRNA (SCR)-depleted cells. (B, C) Quantified (H) and representative (I; for 344SQ cells) data for invasion for models shown (D, E) proliferation results for indicated cell lines using CBT (D) and DAPI (E).

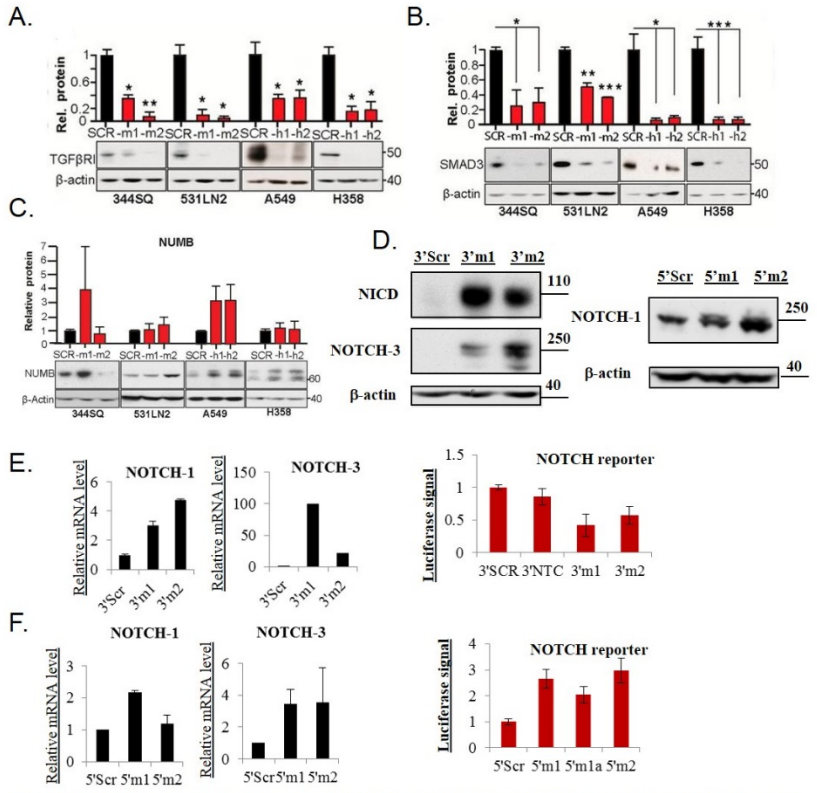

Fig. 2. MSI2 depletion controls the expression of TGFbR1, SMAD3 and NOTCH pathway proteins. (A, B and C) Western analysis of expression of TGFβR1 (A) and SMAD3 (B) and NUMB (C) in murine and human NSCLC cell lines with stably depleted MSI2. Graphs represent data from 3 independent runs. For all graphs,*P < 0.05, **P < 0.01, and ***P < 0.001 relative to SCR (scrambled shRNA) controls. (D) Western analysis of expression of Notch pathway –related proteins in 344SQ and A549 MSI2-expressing (3'SCR, 5'SCR) and MSI2-depleted (3' and 5' m1, m2) cells (E, F) RT-PCR expression of NOTCH pathway related genes in 344SQ (E) and A549 (F) MSI2-expressing (3'SCR, 5'SCR) and MSI2-depleted (3' and 5' m1, m2) cells.

proliferation and invasion data for H322 cell line are currently pending/ ongoing). In 393P non-metastatic cells, which have low endogenous levels of Msi2. MSI2 overexpression did not affect 393P proliferation (Fig 4A), but greatly increased invasion through Matrigel (Fig 4B, C). Finally, analysis of migration independent of invasion (Kudinov et al[2]) showed limited effects of MSI2 depletion. We therefore focused subsequent analysis on mechanistic analysis of invasion-related signaling.

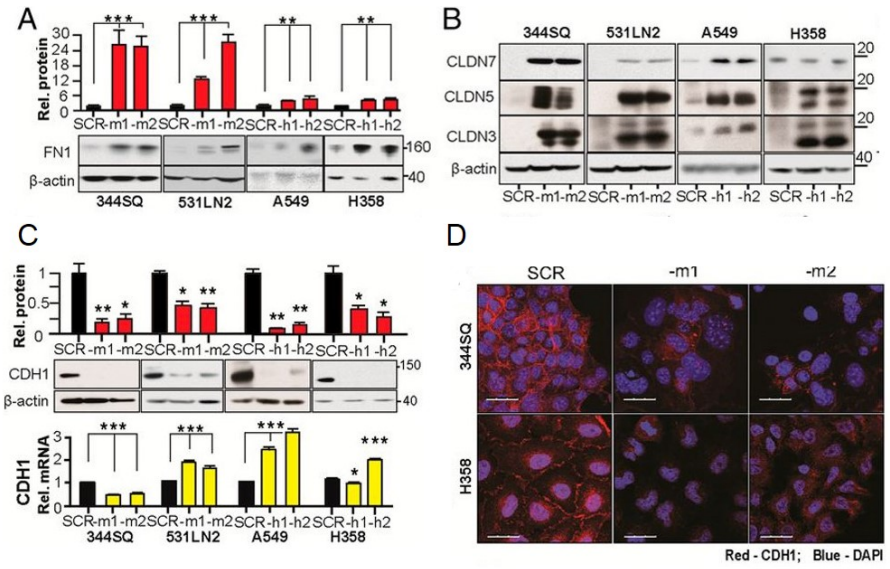

Fig. 3. MSI2 depletion controls the expression of indirect and direct targets relevant to invasion and EMT. (A and B) Western analysis of FN1 (A) and CLDN7, CLDN5, and CLDN3. (B) In murine and human NSCLC cell lines in the context of MSI2 depletion with independent targeting shRNAs (–m1/–m2, –h1/–h2). SCR, control scrambled shRNA. Graphs represent data from four independent runs .) (C) Western (Top) and qRT-PCR (Bottom) analysis of E-Cadherin expression in 4 NSCLC cell line models with / without depleted MSI2. Graphs represent data from 3 independent runs. For all graphs, *P < 0.05, **P < 0.01, and ***P < 0.001 relative to SCR (scrambled shRNA) controls. (D) Immunofluorescence analysis of E-Cadherin staining in 344SQ murine (Top) and H358 human (Bottom) NSCLC cell lines, with or without depleted MSI2. Blue, DAPI; red, E-Cadherin. (Scale bars, 30 μm).

Candidate-based and unbiased investigation of MSI2-regulated signaling.

Direct MSI2 translational targets defined in other cell types that might be relevant to the invasiveness of NSCLC cells and tumors include the TGF-β receptor (TGFβR1) and its effector SMAD3[3], which promote epithelial-mesenchymal transition (EMT) by downregulating E-cadherin (CDH1) and inducing other transcriptional changes[4]. We found that stable or transient MSI2 knockdown caused strong downregulation of TGFβR1 and SMAD3, predominantly at the protein level, in all 4 models (Fig 2A, B). Reciprocally, exogenous overexpression of MSI2 induced TGFβR1 and SMAD3 expression in 393P, H322 cells and caused loss of CLDN3, CLDN5 and CLDN7 expression in the 393P cell line (Fig 5 D, E, H).

While some studies suggested expression of the NOTCH regulator NUMB, is influenced by MSI1/2[5], we found no consistent and significant differences in NUMB in MSI2-depleted cells (Fig S6D), supporting the idea that regulation of NUMB by MSI1/2 may depend on cellular context[3, 6]. To investigate NOTCH pathways signaling in more depth, we tested for NOTCH-3 / NOTCH-1 RNA and protein expression in 344SQ and 531LN2 cells (NICD protein level was tested in 344SQ cells as well), Fig. 2 D-F. Surprisingly, this data demonstrated an upregulation of NOTCH pathway upon MSI2 depletion. Luciferase reporter data using RBP-Jk reporter (Qiagen) in 344SQ and 531LN2 cells has shown

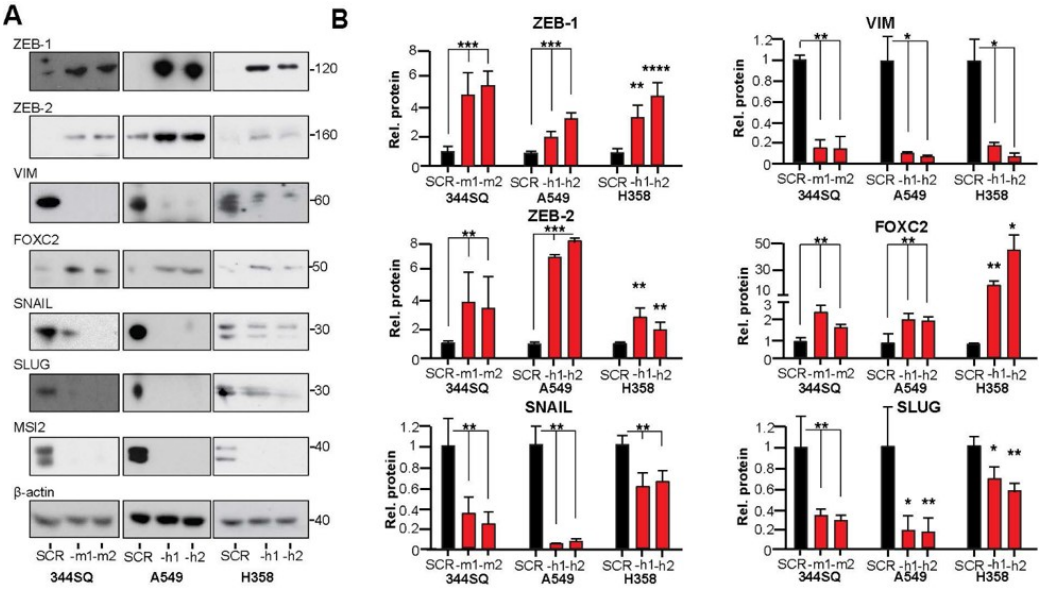

Fig. 4. MSI2 depletion: discovery of additional relevant MSI2-regulated EMT proteins. Western blot analysis (**A**) and quantification (**B**) of MSI2, ZEB-1, ZEB-2, FOXC2, SNAIL, SLUG, VMN (vimentin) versus beta-actin loading control in 344SQ, A549 and H358 cell lines expressing MSI2 (SCR) or depleted of MSI2 (-m1, -m2, -h1, -h2).

inconsistent results which varied depending on cell line (Fig. 2 E-F).

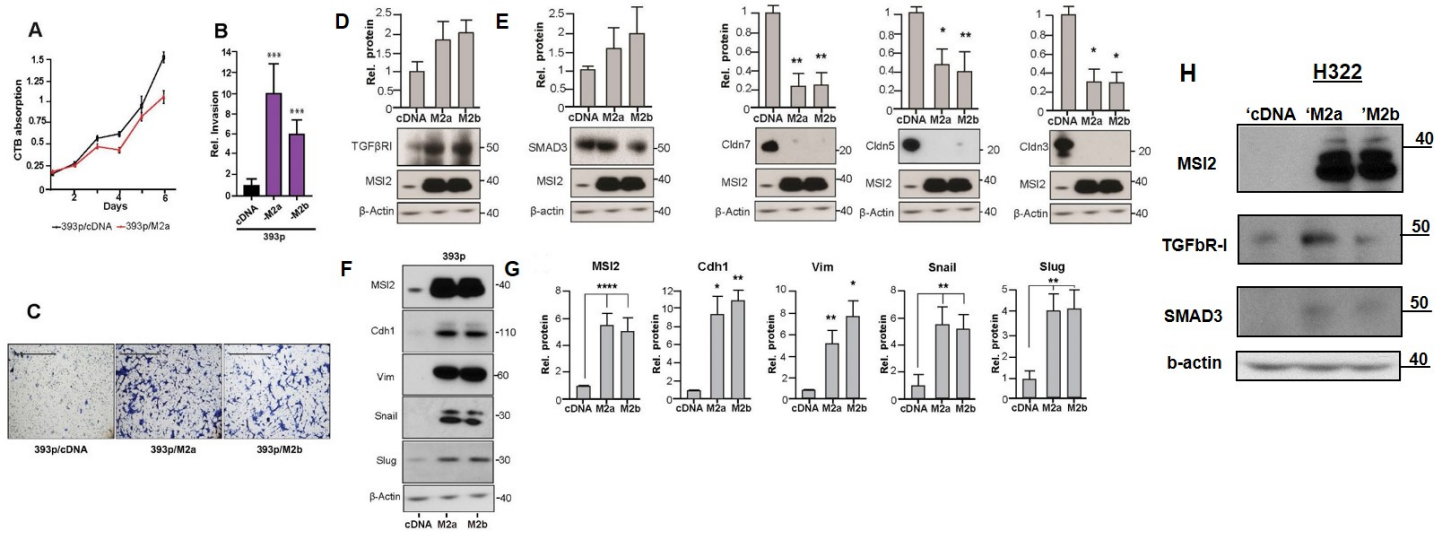

Fig. 5. MSI2 overexpression: functional and signaling effects validation of MSI2 effects in 393P cell line. A. Quantification of CellTiterBlue (CTB) proliferation assays of 393p/M2a and 393p/M2b MSI2-overexpressing clones vs 393p/cDNA control cell lines. **B.**, **C**. Quantification (**B**) and representative image (**C**) of Matrigel invasion analysis of 393p/cDNA control and 393p/M2a and 393p/M2b MSI2 overexpressing cell lines. **D, E.** Western blot analysis of indicated proteins in the 393P cell line, overexpressing MSI2 (393p/M2a and 393p/M2b versus the 393p/cDNA control cell line). All graphs: *, p≤0.05; *, p≤0.01; ***, p≤0.001 relative to controls. **F., G.** Western blot analysis (C) and quantification (D) of MSI2, E- Cadherin, vimentin, SLUG and SNAIL protein expression 393p/cDNA control and 393p/M2a and 393p/M2b MSI2 overexpressing cell lines. All graphs: *, p≤0.05; *, p≤0.01; ***, p≤0.001 relative to controls. **H.** Western blot analysis of indicated proteins in the H322 cell line, overexpressing MSI2 (H322/M2a and H322/M2b versus the H322/cDNA control cell line).

We previously used Reverse Protein Phase Array (RPPA) to query 171 total and phospho-proteins for expression changes associated with Msi2 knockdown using control shRNA and Msi2-targeted shRNA derivatives of 344SQ cells[2]. This work suggested a number of novel candidates associated with Msi2 expression and relevant to control of EMT and invasion. Proteins with the greatest magnitude of response to Msi2 depletion that were subsequently validated by low throughput Western analysis included the tight junction (TJ)-associated protein claudin 7 (CLDN7)[7-9], elevated 19.4-fold, and the ECM protein fibronectin (FN1)[10-13], elevated 2.5-fold[2]. Subsequent independent evaluation confirmed these RPPA results, as MSI2 depletion significantly elevated FN1 mRNA (4.0-9.4-fold) and protein (2.4-23 fold) in all 4 cell lines. While initially not planned, we expanded investigations of the EMT-related claudin proteins, and we indeed found elevated CLDN7 protein (2.5-28 -fold) in 3 of the 4 cell lines (Fig 3B). Results were independently confirmed using transient siRNAs to deplete MSI2 (Kudinov et al[2]). NSCLC cells have been shown to express multiple claudins with partially redundant function[14], most not represented in the RPPA panel. In direct testing, we found MSI2 depletion also induced CLDN3 and CLDN5 in all 4 cell lines at the protein level (3.8-22 fold for CLDN3 and 3.4-41 fold for CLDN5) (Fig 3B), making restraint of claudin expression a consistent feature of MSI2 function. Studies of the MSI proteins (predominantly focused on MSI1) have defined these proteins as RNA-binding proteins that regulate mRNA translation[3, 15, 16]. The induction of claudins may reflect a combination of transcriptional and post-transcriptional consequences of MSI2 depletion, as the mRNA level shows induction less marked than at the protein level (Kudinov et al[2]). However, the claudin mRNAs lack [(G/A)U(n)AGU (n = 1–3)] consensus motifs for MSI2 binding described in Wang et al[17], suggesting direct regulation of translation is not involved.

Depletion of MSI2 affects the composition of cell-cell junctions and causes partial EMT. Based on the action of MSI2 in supporting the expression of TGFβR1 and SMAD3, while repressing CLDN3, CLDN5, CLDN7, and FN1, we hypothesized that the reduced invasiveness of MSI2-depleted cells might reflect changes involving TJs and reduced EMT, associated with elevated E-cadherin (CDH1). Unexpectedly, total epithelial protein E-cadherin protein expression was decreased by MSI2 depletion, while mRNA levels were not consistently affected (Fig. 3C); immunofluorescence analysis confirmed that expression of E-cadherin at cell-cell junctions was much reduced by MSI2 depletion (Fig 3D). In contrast, there was a significant increase in CLDN3 and

CLDN7 staining at cell-cell contact points, while TJP1 (ZO-1), which localizes to the cytoplasmic surface of TJs, was unaffected (Kudinov et al[2]).

Based on the effects of MSI2 in regulating EMT-related signaling, we examined expression of additional proteins associated with mesenchymal identity (Fig 4A, 4B). MSI2 depletion upregulated the pro-EMT factors ZEB1, ZEB2 and FOXC2 but downregulated VIM (vimentin), SLUG and SNAIL. Conversely, MSI2 overexpression in 393P cells induced CDH1, VIM, SNAIL and SLUG (Fig 5F, G). Collectively, these data indicated a mixed effect of MSI2 depletion on EMT.

MSI2 regulation of invasion via TGFβR1, SMAD3 and CLDN7. To assess the functional interaction between MSI2, its direct targets TGFβR1 and SMAD3, and claudins, we depleted SMAD3 or TGFβR1 in MSI2-depleted versus control cell lines. SMAD3 knockdown reduced CDH1 expression levels in both parental and MSI2-depleted lines (Fig 6A, B). By contrast, the relationship between TGFβR1 and CDH1 expression was modulated by MSI2 status, with the TGFβR1 knockdown elevating CDH1 expression in the parental cell lines, but reducing it in MSI2-depleted cell lines (Fig 6A, B). Importantly, depletion of TGFβR1 or SMAD3 caused a statistically significant decrease in invasion in SCR-depleted NSCLC cell lines, but not in those with depleted MSI2 (Fig 5C). Conversely, overexpression of TGFβR1 partially but incompletely rescued the decrease in invasion seen in MSI2-depleted cells (Kudinov et al[2]), suggesting other contributing factors.

The profile of mixed pro- and anti-EMT changes, and incomplete rescue by TGFβR1 overexpression, suggested a possible important role for claudin-associated TJs in limiting NSCLC invasion induced by MSI2-dependent TGFβR1/SMAD3 signaling. Exploring the relationship between these proteins, we found that siRNA depletion of TGFβR1 or SMAD3 did not significantly affect the expression of CLDN3, CLDN7, or MSI2. This indicated that MSI2 regulates CLDN3/CLDN7 expression independently of TGFβR1 and SMAD3 (Fig 6A, B). Importantly, depletion of TGFβR1 or SMAD3 caused a statistically significant decrease in invasion in SCR-depleted NSCLC cell lines, but not in those with depleted MSI2 (Fig 6 C).

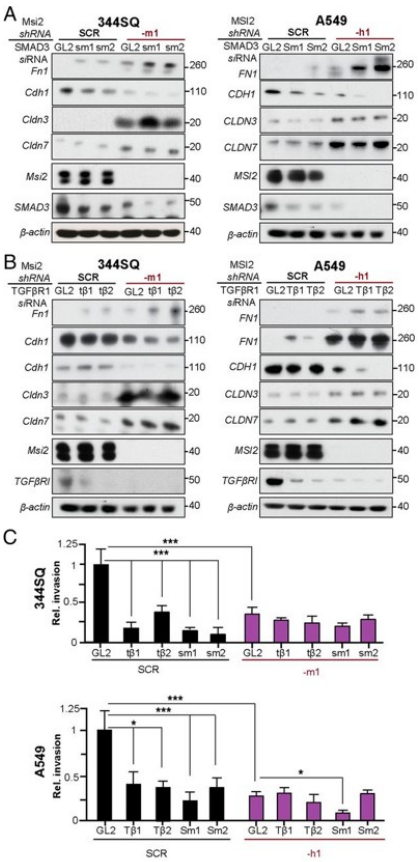

Fig. 6. Functional interaction of MSI2 with TGFβR1, SMAD3, FN1, E-Cadherin, and CLDN3 and CLDN7. (A) Western for expression of indicated proteins in the 344SQ and A549 cell lines with (–m1 and –h1) or without (SCR) shRNA depletion ofMSI2, and with (–sm1, –sm2, and –Sm1, –Sm2) or without (GL2) siRNA depletion of SMAD3. (B) Western for expression of indicated proteins in the 344SQ, A549 cell lines with (m1 and h1) or without (SCR) shRNA depletion of MSI2, and with TGFβR1 (–tβ1, –tβ2 and –Tβ1, –Tβ2) or without (GL2) siRNA depletion of TGFβR1. (C) Quantification of results from 3 independent Matrigel invasion assays for 344SQ and A549 with (–m1 and –h1) or without (SCR) shRNA depletion of MSI2, in the context of additional siRNA depletion of TGFβR1 (–tβ1, –tβ2 and –Tβ1, –Tβ2) or SMAD3 (–sm1, –sm2 and –Sm1, –Sm2) vs siRNA negative control (GL2). *P < 0.05 and ***P < 0.001 relative to controls.

Determination of the role of Msi2 in NSCLC response to Notch and TGF-β targeting drugs.

We hypothesized that MSI2 expression can affect drug responses.

Here, we also initiated experiments to determine whether Msi2 expression conditions response to γ-secretase and TGF-β receptor Type I kinase (TGF-βRI) inhibitors, as predicted by its regulation of NUMB/Notch and TGFβ/SMAD2/3 pathways. We performed IC50 determinations, as well as invasion assays as described in preliminary data, for drugs used in clinical trials against solid tumors. We will assess RO-4929097, a small molecule γ-secretase inhibitor which blocks Notch signaling[48], and LY2157299[17, 18], a small molecule inhibitor of the TGF-βRI kinase activity, in Msi2-manipulated versus control cells. We used A549 and H358 human NSCLC cell lines with endogenous or transiently / stably depleted Msi2, or overexpressed Msi2. Briefly, these cell lines will be plated in 96 well plates; 24 hours after plating, drugs or vehicle will be added, and 72 hours later, cells will be analyzed by CellTiterBlue for reduction in proliferation. As described in Figure 7 (A, B), preliminary in vitro results in 344SQ and A549 cell lines demonstrated increased sensitivity of MSI2-depleted cells (3'74, 3'75 and A'9, A'11) to RO-4929097 gamma-secretase compound. In contrast, we did

not observed significant difference in IC50 curves between MSI2-expressing or MSI2-depleted 344SQ cells treated with LY2157299 TGFbR1 inhibitor. In vivo mouse experiments are currently pending. LY2157299 mouse trials using A549, H358 MSI2-manipulated cell line xenografts are about 70% completed, while RO-4929097 mouse experiments are planned for the Fall of 2016.

Taken together, we conclude that MSI2 stimulates invasion in lung cancer in part by sustaining TGFβR1 signaling and suppressing the expression of CLDN7 and potentially other claudins. Our study for the first time shows that elevation of MSI2 expression progressing NSCLC supports tumor cell invasion and metastasis by modulating TGFβ- dependent EMT, and repressing claudin expression (Fig. 8).

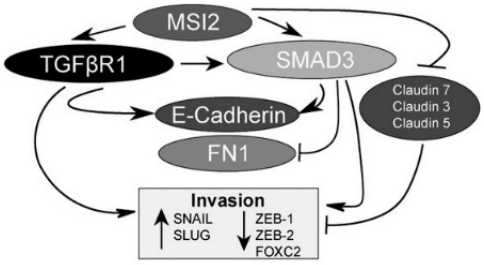

Fig. 8. Model for MSI2 action in coordinating EMT and invasion potential.

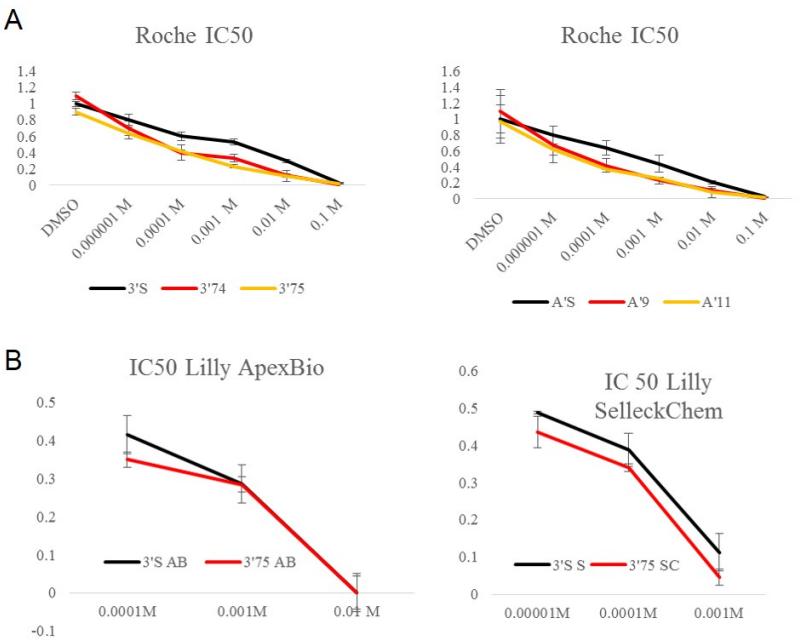

Fig. 7. IC50 curves for gamma-secretase and TGFbR1 inhibitors in NSCLC cell lines. (A) Roche gamma-secretase inhibitor IC50 curve shows increased sensitivity of MSI2-depleted cells to the compound relative to control (3'S) in 344SQ and A' S in A549 (B) Lilly TGFbR1 inhibitor shows similar activity against MSI2-expressing (S) and MSI2-depled (75) cells in 344SQ cell line.

What opportunities for training and professional development has the project provided?

I have attended 2016 AACR where MSI2 data poster was successfully presented. I have interacted with several scientists working on RNA-binding proteins in the USA and Asia.

How were the results disseminated to communities of interest?

Our MSI2 PNAS publication sparked significant interest in scientific community. This was illustrated by a feature report in a weekly publication, June 23, 2016 BioCentury Innovations. BioCentury Inc. was founded in 1992 by David Flores, President and CEO, and Karen Bernstein, Ph.D., Chairman. This is a "first-in-class" biotech-focused business journal that provides independent, authoritative intelligence built on in-depth and accurate reporting. Their mission is to identify and communicate the essential scientific, business, financial and public policy actions required to successfully bring progressive medical solutions to patients. *BioCentury Innovations* (formerly SciBX) specifically identifies commercially promising translational science and assesses the next steps required to develop the technology.

In addition, press release is planned for October 2016 at Fox Chase Cancer Center web-site, to feature MSI2 NSCLC story as one of the innovative scientific breakthroughs at the Center.

What do you plan to do during the next reporting period to accomplish the goals?

We plan to complete the remaining experiments for the Aim 1 (mouse trials using RO-4929097 and LY2157299 compounds, including HE staining of mouse xenograft A549, H358 tumors, and data analysis). We also plan to complete the Aim 2 entirely. Completion of Aim 2 will involve analysis of the human tissue microarrays for signaling proteins supported by MSI2. These specimens will be stained and analyzed for the expression of Ki-67, TGF-βRI, phosphorylated SMAD3 and Numb. Expression of activated, cleaved Notch will also be measured, and

Hes1 expression will be used as an endpoint indicator of Notch pathway activity. TMAs will be analyzed for correlation of Msi2 expression with pathologic stage, lymph node status, presence of metastasis, grade. We will determine whether Msi2 expression correlates with expression of Numb, activated Notch, and HES1, TGF-βRI, phosphorylated SMAD3, as predicted by in vitro studies.

4. IMPACT

What was the impact on the development of the principal discipline(s) of the project?
MSI2 work we published has advanced the field of RNA-binding proteins biology. In particular, it is the first work to describe MSI2 role in driving NSCLC progression. It was also the first report to describe regulation of claudins by MSI2, which may have important implications of understanding how NSCLC develops.

What was the impact on other disciplines?
Our findings may indirectly affect pharmacology and drug development fields. Since NSCLC is being driven by MSI2, our publication may spark an increase interest in developing MSI2 inhibitors for cancer therapy.

What was the impact on technology transfer?
Nothing to report

What was the impact on society beyond science and technology?
I believe that our project that focuses on lung cancer may draw additional interest from general public in understanding and awareness of lung cancer burden and impact on patients around the country.

5. CHANGES/PROBLEMS

Changes in approach and reasons for change
No changes anticipated, nothing to report

Actual or anticipated problems or delays and actions or plans to resolve them
No delays anticipated, nothing to report

Changes that had a significant impact on expenditures
Nothing to report

Significant changes in use or care of human subjects, vertebrate animals, biohazards, and/or select agents
Nothing to report

6. PRODUCTS

Publications, conference papers, and presentations:
Journal publications
Kudinov AE, Deneka A, Nikonova AS, Beck TN, Ahn YH, Liu X, Martinez CF, Schultz FA, Reynolds S, Yang DH, Cai KQ, Yaghmour KM, Baker KA, Egleston BL, Nicolas E, Chikwem A, Andrianov G, Singh S, Borghaei H, Serebriiskii IG, Gibbons DL, Kurie JM, Golemis EA, Boumber Y. Musashi-2 (MSI2) supports TGF-β signaling and inhibits claudins to promote non-small cell lung cancer (NSCLC) metastasis. **Proc Natl Academy Science** U S A. 2016 Jun 6; PubMed PMID: 27274057.
Acknowledgement of federal support (yes)

Alexander Kudinov, Alexander Deneka, Anna Nikonova, Ilya Serebriiskii, Tim N. Beck, Qi Cai, Brian L. Egleston, Emmanuelle Nicolas, Hossein Borghaei, Don Gibbons, Jonathan Kurie, Erica A. Golemis and Yanis

Boumber. "*Musashi-2 (MSI2) drives TGFBR1/SMAD3 dependent partial EMT and supports VEGFR2 expression and metastasis of human and mouse NSCLC cells.*" AACR 2016 abstract # 1584. Proceedings: AACR 105th Annual Meeting; Apr 12-22, 2015; New Orleans, LA. Published.
Acknowledgement of federal support (yes)

Books or other non-periodical, one-time publications
Nothing to report

Other publications, conference papers, and presentations
Alexander Kudinov, Alexander Deneka, Anna Nikonova, Young-Ho Ahn, Xin Liu Liu, Ilya Serebriiskii, Andrey Efimov, Dong-Hua Yang, Mark Andrake, Emmanuelle Nicolas, Brian Egleston, Hossein Borghaei, Don Gibbons, Jonathan Kurie, Erica Golemis and Yanis Boumber. *"Musashi-2 (MSI2) activates TGF-β signaling and inhibits CLDN7 to promote non-small cell lung cancer (NSCLC) metastasis."* Presented at AACR 104th Annual Meeting; Apr 12-22, 2015; Philadelphia, PA.
Acknowledgement of federal support (yes)

Website(s) or other Internet site(s)
Nothing to report

Technologies or techniques
Nothing to report

Inventions, patent applications, and/or licenses
Nothing to report

Other Products
We have generated additional MSI2-depleted (A549, H358) or overexpressing (H322, 393P) cell lines, which are useful research tools to study MSI2. While those are currently only used in our laboratory, we are open to sharing it with scientific community (independent labs or investigators, Addgene, other sources).

7. PARTICIPANTS & OTHER COLLABORATING ORGANIZATIONS

What individuals have worked on the project?
Name: **Alexander Kudinov, MD**
Project Role: Postdoctoral fellow
Researcher Identifier (e.g., ORCID ID): N/A
Nearest calendar month worked: 6
Contribution to Project: Dr. Kudinov performed the majority (~80%) of experiments for this project and performed at least half data analysis (see significant results and major findings and PNAS paper).
Funding Support: UNM Cancer Center Support Grant (NIH, P30 CA118100) developmental funds.

Name: **Yanis Boumber, MD, PhD**
Project Role: PI
Nearest calendar month worked: 5
Researcher Identifier (e.g., ORCID ID): N/A
Contribution to Project: Dr. Boumber performed some (~5-10%) of the preliminary experiments for this project (see Significant results and major findings and PNAS paper) and supervised the project, key experiments, and wrote PNAS paper
Funding Support: Institutional Funds

Name: **Erica Golemis, PhD**
Project Role: PI
Nearest calendar month worked: 1
Researcher Identifier (e.g., ORCID ID): N/A
Contribution to Project: Dr. Golemis supervised the project, key experiments, and wrote PNAS paper
Funding Support: R21 CA181287 and R01 CA063366 (to EAG); NIH Core Grant CA006927 (to Fox Chase Cancer Center).

Name: **Alexander Deneka, MD**
Project Role: Graduate student
Researcher Identifier (e.g., ORCID ID): N/A
Nearest calendar month worked: 1
Contribution to Project: Dr. Deneka performed the several key (~15%) experiments for this project, including the majority of animal studies which have been completed, and also assisted with data analysis (see significant results and major findings of this report, and PNAS paper).
Funding Support: R21 CA181287 and R01 CA063366 (under EAG); and by the NIH Core Grant CA006927 (to Fox Chase Cancer Center). Russian Science Foundation project 15-15-20032 (to AD).

Name: **Anna Nikonova, PhD**
Project Role: Postdoctoral fellow
Researcher Identifier (e.g., ORCID ID): N/A
Nearest calendar month worked: 1
Contribution to Project: Dr. Nikonova some of the experiments (5%) and some data analysis for this project and also supervised Dr. Kudinov and Dr. Deneka in some key experiments, including animal experiments and Westerns
Funding Support: R21 CA181287 and R01 CA063366 (under EAG); and by the NIH Core Grant CA006927 (to Fox Chase Cancer Center).

Name: **Brian Egleston, PhD**
Project Role: Statistician
Researcher Identifier (e.g., ORCID ID): N/A
Nearest calendar month worked: 1
Contribution to Project: Dr. Egleston performed some key statistical analysis for this project, and supervised Dr. Kudinov and Dr. Deneka in data analysis (see Significant results section of this report and PNAS paper).
Funding Support: by the DOD CDA (current award), P30 CA006927 grant to Fox Chase Cancer Center biostatistics department, and by the NIH Core Grant CA006927 (to Fox Chase Cancer Center).

Name: **Helen Hathaway, PhD**
Project Role: Collaborator
Researcher Identifier (e.g., ORCID ID): N/A
Nearest calendar month worked: 1
Contribution to Project: Dr. Hathaway is a Director of Animal facility at UNMCC. She helped design and implement animal protocols and mice experiments (intra-thoracic injections, gavages) and supervised Laura Laidler, Alexander Kudinov and Helen Nordquist in ongoing animal experiments (some of these data are being analyzed).
Funding Support: NIH, P30 CA118100 UNM Cancer Center Core Grant – Animal Modeling Shared Resource

Name: **Laura Laidler, MS**
Project Role: technician, animal experiments
Researcher Identifier (e.g., ORCID ID): N/A

Nearest calendar month worked: 1
Contribution to Project: Dr. Laidler performed some key animal experiment for this project, including ongoing intra-thoracic injections, gavages, drug studies in mice, and supervised Dr. Kudinov and Ms. Nordquist animal work (some of these data are being analyzed).
Funding Support: NIH, P30 CA118100 UNM Cancer Center Core Grant – Animal Modeling Shared Resource

Name: **Helen Norquist, BS**
Project Role: undergraduate student, animal experiments assistant
Researcher Identifier (e.g., ORCID ID): N/A
Nearest calendar month worked: 4
Contribution to Project: Ms. Nordquist performed some animal experiment for this project, including assistance with intra-thoracic injections, gavages, drug studies in mice (some of these data are being analyzed).
Funding Support: Dr. Boumber's UNM Start-up funds.

Has there been a change in the active other support of the PD/PI(s) or senior/key personnel since the last reporting period?
Nothing to report

What other organizations were involved as partners?
Fox Chase Cancer Center – academic institution and a major cancer center
-provided statistical support, and overall guidance, collaboration and supervision for the project, computer and lab equipment

UNM Comprehensive Cancer Center – academic institution
-provided financial support and collaboration, computer and lab equipment

8. SPECIAL REPORTING REQUIREMENTS

None

9. REFERENCES

[1] Barretina J, Caponigro G, Stransky N, Venkatesan K, Margolin AA, Kim S, Wilson CJ, Lehar J, Kryukov GV, Sonkin D, Reddy A, Liu M, Murray L, Berger MF, Monahan JE, Morais P, Meltzer J, Korejwa A, Jane-Valbuena J, Mapa FA, Thibault J, Bric-Furlong E, Raman P, Shipway A, Engels IH, Cheng J, Yu GK, Yu J, Aspesi P, Jr., de Silva M, Jagtap K, Jones MD, Wang L, Hatton C, Palescandolo E, Gupta S, Mahan S, Sougnez C, Onofrio RC, Liefeld T, MacConaill L, Winckler W, Reich M, Li N, Mesirov JP, Gabriel SB, Getz G, Ardlie K, Chan V, Myer VE, Weber BL, Porter J, Warmuth M, Finan P, Harris JL, Meyerson M, Golub TR, Morrissey MP, Sellers WR, Schlegel R, Garraway LA: The Cancer Cell Line Encyclopedia enables predictive modelling of anticancer drug sensitivity. Nature 2012, 483:603-7.
[2] Kudinov AE, Deneka A, Nikonova AS, Beck TN, Ahn YH, Liu X, Martinez CF, Schultz FA, Reynolds S, Yang DH, Cai KQ, Yaghmour KM, Baker KA, Egleston BL, Nicolas E, Chikwem A, Andrianov G, Singh S, Borghaei H, Serebriiskii IG, Gibbons DL, Kurie JM, Golemis EA, Boumber Y: Musashi-2 (MSI2) supports TGF-beta signaling and inhibits claudins to promote non-small cell lung cancer (NSCLC) metastasis. Proc Natl Acad Sci U S A 2016, 113:6955-60.
[3] Park SM, Deering RP, Lu Y, Tivnan P, Lianoglou S, Al-Shahrour F, Ebert BL, Hacohen N, Leslie C, Daley GQ, Lengner CJ, Kharas MG: Musashi-2 controls cell fate, lineage bias, and TGF-beta signaling in HSCs. J Exp Med 2014, 211:71-87.
[4] Massague J: TGFbeta signalling in context. Nat Rev Mol Cell Biol 2012, 13:616-30.

[5] Ito T, Kwon HY, Zimdahl B, Congdon KL, Blum J, Lento WE, Zhao C, Lagoo A, Gerrard G, Foroni L, Goldman J, Goh H, Kim SH, Kim DW, Chuah C, Oehler VG, Radich JP, Jordan CT, Reya T: Regulation of myeloid leukaemia by the cell-fate determinant Musashi. Nature 2010, 466:765-8.
[6] Katz Y, Li F, Lambert NJ, Sokol ES, Tam WL, Cheng AW, Airoldi EM, Lengner CJ, Gupta PB, Yu Z, Jaenisch R, Burge CB: Musashi proteins are post-transcriptional regulators of the epithelial-luminal cell state. Elife 2014, 3:e03915.
[7] Lu Z, Ding L, Hong H, Hoggard J, Lu Q, Chen YH: Claudin-7 inhibits human lung cancer cell migration and invasion through ERK/MAPK signaling pathway. Exp Cell Res 2011, 317:1935-46.
[8] Prat A, Adamo B, Fan C, Peg V, Vidal M, Galvan P, Vivancos A, Nuciforo P, Palmer HG, Dawood S, Rodon J, Ramony Cajal S, Del Campo JM, Felip E, Tabernero J, Cortes J: Genomic analyses across six cancer types identify basal-like breast cancer as a unique molecular entity. Sci Rep 2013, 3:3544.
[9] Bruna A, Greenwood W, Le Quesne J, Teschendorff A, Miranda-Saavedra D, Rueda OM, Sandoval JL, Vidakovic AT, Saadi A, Pharoah P, Stingl J, Caldas C: TGFbeta induces the formation of tumour-initiating cells in claudinlow breast cancer. Nat Commun 2012, 3:1055.
[10] Liu W, Cheng S, Asa SL, Ezzat S: The melanoma-associated antigen A3 mediates fibronectin-controlled cancer progression and metastasis. Cancer Res 2008, 68:8104-12.
[11] Urtreger AJ, Werbajh SE, Verrecchia F, Mauviel A, Puricelli LI, Kornblihtt AR, Bal de Kier Joffe ED: Fibronectin is distinctly downregulated in murine mammary adenocarcinoma cells with high metastatic potential. Oncol Rep 2006, 16:1403-10.
[12] Zhang X, Liu S, Hu T, Liu S, He Y, Sun S: Up-regulated microRNA-143 transcribed by nuclear factor kappa B enhances hepatocarcinoma metastasis by repressing fibronectin expression. Hepatology 2009, 50:490-9.
[13] Yi M, Ruoslahti E: A fibronectin fragment inhibits tumor growth, angiogenesis, and metastasis. Proc Natl Acad Sci U S A 2001, 98:620-4.
[14] Kwon MJ: Emerging roles of claudins in human cancer. Int J Mol Sci 2013, 14:18148-80.
[15] Sakakibara S, Nakamura Y, Satoh H, Okano H: Rna-binding protein Musashi2: developmentally regulated expression in neural precursor cells and subpopulations of neurons in mammalian CNS. J Neurosci 2001, 21:8091-107.
[16] Rezza A, Skah S, Roche C, Nadjar J, Samarut J, Plateroti M: The overexpression of the putative gut stem cell marker Musashi-1 induces tumorigenesis through Wnt and Notch activation. J Cell Sci 2010, 123:3256-65.
[17] Wang S, Li N, Yousefi M, Nakauka-Ddamba A, Li F, Parada K, Rao S, Minuesa G, Katz Y, Gregory BD, Kharas MG, Yu Z, Lengner CJ: Transformation of the intestinal epithelium by the MSI2 RNA-binding protein. Nat Commun 2015, 6:6517.

10. APPENDICES

See attached: PNAS paper, AACR abstract and BioCentury Innovations

Musashi-2 (MSI2) supports TGF-β signaling and inhibits claudins to promote non-small cell lung cancer (NSCLC) metastasis

Alexander E. Kudinov[a,b], Alexander Deneka[a,c], Anna S. Nikonova[a], Tim N. Beck[a,d], Young-Ho Ahn[e,f], Xin Liu[e], Cathleen F. Martinez[g], Fred A. Schultz[g], Samuel Reynolds[g], Dong-Hua Yang[a,h], Kathy Q. Cai[a,b], Khaled M. Yaghmour[a], Karmel A. Baker[a], Brian L. Egleston[a], Emmanuelle Nicolas[a,h], Adaeze Chikwem[a,i], Gregory Andrianov[c], Shelly Singh[a], Hossein Borghaei[a,j], Ilya G. Serebriiskii[a,c], Don L. Gibbons[e], Jonathan M. Kurie[e], Erica A. Golemis[a,d,1], and Yanis Boumber[a,b,j,1]

[a]Molecular Therapeutics Program, Fox Chase Cancer Center, Philadelphia, PA, 19111; [b]Department of Medical Oncology, University of New Mexico Cancer Center, Albuquerque, NM 87131; [c]Kazan Federal University, 420000, Kazan, Russian Federation; [d]Program in Molecular and Cell Biology and Genetics, Drexel University College of Medicine, Philadelphia, PA 19111; [e]Department of Thoracic Head and Neck Medical Oncology, University of Texas MD Anderson Cancer Center, Houston, TX 77030; [f]Department of Molecular Medicine and Tissue Injury Defense Research Center, Ewha Womans University School of Medicine, 1071 Anyangcheon-ro, Yangcheon-gu, Seoul, Korea; [g]Department of Pathology, University of New Mexico School of Medicine, Albuquerque, NM 87131; [h]Genomics Facility, Fox Chase Cancer Center, Philadelphia, PA 19111; [i]Temple University School of Medicine, Philadelphia, PA 19140; and [j]Department of Medical Oncology, Fox Chase Cancer Center, Philadelphia, PA 19111

Edited by Trever G. Bivona, University of California, San Francisco, CA, and accepted by Editorial Board Member Peter K. Vogt May 2, 2016 (received for review July 10, 2015)

Non-small cell lung cancer (NSCLC) has a 5-y survival rate of ∼16%, with most deaths associated with uncontrolled metastasis. We screened for stem cell identity-related genes preferentially expressed in a panel of cell lines with high versus low metastatic potential, derived from NSCLC tumors of $Kras^{LA1/+}$;$p53^{R172H\Delta G/+}$ (KP) mice. The Musashi-2 (MSI2) protein, a regulator of mRNA translation, was consistently elevated in metastasis-competent cell lines. MSI2 was overexpressed in 123 human NSCLC tumor specimens versus normal lung, whereas higher expression was associated with disease progression in an independent set of matched normal/primary tumor/lymph node specimens. Depletion of MSI2 in multiple independent metastatic murine and human NSCLC cell lines reduced invasion and metastatic potential, independent of an effect on proliferation. MSI2 depletion significantly induced expression of proteins associated with epithelial identity, including tight junction proteins [claudin 3 (CLDN3), claudin 5 (CLDN5), and claudin 7 (CLDN7)] and down-regulated direct translational targets associated with epithelial–mesenchymal transition, including the TGF-β receptor 1 (TGFβR1), the small mothers against decapentaplegic homolog 3 (SMAD3), and the zinc finger proteins SNAI1 (SNAIL) and SNAI2 (SLUG). Overexpression of TGFβRI reversed the loss of invasion associated with MSI2 depletion, whereas overexpression of CLDN7 inhibited MSI2-dependent invasion. Unexpectedly, MSI2 depletion reduced E-cadherin expression, reflecting a mixed epithelial–mesenchymal phenotype. Based on this work, we propose that MSI2 provides essential support for TGFβR1/SMAD3 signaling and contributes to invasive adenocarcinoma of the lung and may serve as a predictive biomarker of NSCLC aggressiveness.

MSI2 | NSCLC | metastasis | lung cancer | claudins

Non-small cell lung cancer (NSCLC) is the leading cause of cancer-related deaths in the world (1). Approximately 7% of individuals born in the United States in 2013 will ultimately be diagnosed with lung cancer, and 160,000 die from this disease each year (1). The 5-y survival rate for lung cancer is around 16% of diagnosed cases (2). Much of the lethality of lung cancer is due to frequent diagnosis of the malignancy at the metastatic stage, when fundamental changes in tumor biology cause the disease to be refractory to many treatments. A better understanding of the biological processes that promote NSCLC metastasis promises to further improve clinical care of the patients.

$Kras^{LA1/+}$;$P53^{R172H\Delta G/+}$ (KP) mice provide a useful and well-validated model for the study of NSCLC metastasis. These mice combine a mutant *p53* allele ($p53^{R175H\Delta G}$) with an activating *KrasG12D* allele ($Kras^{LA1}$) (3), leading to development of adenocarcinomas resembling human NSCLC, which are often characterized by mutation of KRAS (∼30%) (4) and loss of TP53 (∼60%) (5). Many of the KP tumors metastasize to sites commonly seen in NSCLC patients (3). These features make the KP murine model a useful tool with which to evaluate factors that underlie NSCLC metastasis. Among the pathways activated in metastasis, a significant number are associated with tumor-initiating progenitor cell populations (6–12). In this study, using cell lines with high or low metastatic potential derived from multiple independent tumors arising in KP mice (13), we evaluated a set of genes associated with progenitor cell identity as candidate regulators of the invasive and metastatic properties of NSCLC tumors. As described later, this work for the first time, to our

Significance

The evolutionarily conserved RNA-binding protein Musashi-2 (MSI2) regulates mRNA translation and influences multiple biological processes, including maintenance of stem cell identity. This work for the first time, to our knowledge, identifies that more aggressive patient tumors have higher MSI2 levels. We define a critical role for MSI2 in supporting non-small cell lung cancer (NSCLC) invasiveness and further define claudins 3, 5, and 7 (CLDN3, CLDN5, and CLDN7), TGF-β receptor 1 (TGFβR1), and the small mothers against decapentaplegic homolog 3 (SMAD3) as targets through which MSI2 regulates this process. The observation that MSI2 expression is progressively elevated from an early stage in human NSCLC tumors suggests that this protein may play an essential role in the reprogramming of TGF-β signaling from growth-inhibiting to invasion-promoting during oncogenesis.

Author contributions: J.M.K., E.A.G., and Y.B. designed research; A.E.K., A.D., X.L., C.F.M., F.A.S., S.R., D.-H.Y., K.Q.C., K.M.Y., K.A.B., E.N., A.C., S.S., and Y.B. performed research; H.B., D.L.G., J.M.K., E.A.G., and Y.B. contributed new reagents/analytic tools; A.E.K., A.D., A.S.N., T.N.B., Y.-H.A., K.M.Y., K.A.B., B.L.E., E.N., G.A., I.G.S., D.L.G., J.M.K., E.A.G., and Y.B. analyzed data; and A.E.K., E.A.G., and Y.B. wrote the paper.

The authors declare no conflict of interest.

This article is a PNAS Direct Submission. T.G.B. is a guest editor invited by the Editorial Board.

Freely available online through the PNAS open access option.

[1]To whom correspondence may be addressed. Email: yboumber@gmail.com or Erica.Golemis@fccc.edu.

This article contains supporting information online at www.pnas.org/lookup/suppl/doi:10.1073/pnas.1513616113/-/DCSupplemental.

knowledge, identifies elevated expression of the Musashi-2 (MSI2) protein as a common driver of metastasis in NSCLC and defines its mechanism of action in this disease.

Results

Up-Regulation of MSI2 Accompanies Metastasis in Mouse NSCLC Cells and Human NSCLC Tumors. Using quantitative RT-PCR (qRT-PCR) (see *SI Appendix*, *SI Methods* and Table S1), we compared the mRNA expression of a candidate set of stem cell marker genes in a highly metastatic (344SQ) versus a nonmetastatic (393P) NSCLC cell line (*SI Appendix*, Fig. S1*A*), both derived from primary tumors that developed spontaneously in KP mice (13). Genes with a significant difference in expression between these two cell lines were further assessed in a panel of seven metastatic and seven nonmetastatic cell lines derived from additional independent KP tumors. Msi2 expression was consistently elevated in metastatic cell lines at both the mRNA and the protein level (Fig. 1 *A* and *B* and *SI Appendix*, Fig. S1*B*). Msi1, a paralogue of Msi2, also displayed a trend toward elevated expression in metastatic murine cell lines at the mRNA level, but this was not observed at the protein level (*SI Appendix*, Fig. S1 *C* and *D*).

To assess whether MSI2 overexpression is physiologically relevant in the context of human NSCLC, we first used Automated Quantitative Analysis to analyze the protein expression of MSI2 in tissue microarrays (TMAs) containing 123 primary human NSCLC tumors and normal lung tissue (*SI Appendix*, Table S2). This analysis indicated highly significant elevation of MSI2 in tumors compared with normal tissue (Fig. 1*C* and *SI Appendix*, Fig. S1*E*). In contrast, parallel assessment of MSI1 expression did not reveal differences in expression between normal lung tissue and primary NSCLC tumor specimens (*SI Appendix*, Fig. S1*F*). Independent analysis of 59 primary NSCLC tumors versus matching normal lung tissue data from The Cancer Genome Atlas (TCGA) Research Network (cancergenome.nih.gov/) indicated frequently elevated expression of MSI2 but not MSI1 mRNA levels in tumor specimens (Fig. 1*D*), whereas Kaplan–Meier plots analysis suggested higher levels of MSI2 were associated with reduced overall survival (*SI Appendix*, Fig. S1*G*). In addition, analysis of an independent cohort of matched NSCLC specimens containing normal lung, primary tumor, and tumor-positive lymph nodes from 14 individuals (*SI Appendix*, Table S3) demonstrated significant 2.4-fold elevation of MSI2 levels in the primary tumor and highly 4.5-fold elevation in the lymph nodes versus normal lung tissue (Fig. 1 *E* and *F*). The progressive increase in MSI2 expression as human lung tumors metastasized from the primary site, combined with data from the KP model, suggested a potential functional and clinical relevance for MSI2 in regulating tumor progression.

MSI2 Depletion in Metastatic NSCLC Cells Inhibits Invasion in Vitro and Tumor Dissemination in Vivo. Based on expression profiles of NSCLC cell lines available through the Cancer Cell Line Encyclopedia (14), we identified the human NSCLC cell lines A549 ($KRAS^{mut}$) and H358 ($KRAS^{mut}$;$TP53^{-/-}$) as metastasis-competent adenocarcinoma cell lines with high expression of MSI2 (*SI Appendix*, Fig. S1*H*). We used shRNA depletion of these and two metastatic murine NSCLC cell lines (344SQ and 531LN2) to further study the role of MSI2 in metastasis. Effective MSI2 mRNA and protein depletion were confirmed for four MSI2-depleted cell lines, in reference to matching scrambled shRNA control cell lines (Fig. 1*G* and *SI Appendix*, Fig. S1*I*). MSI2 depletion consistently and significantly reduced invasion through Matrigel for all lines (Fig. 1 *H* and *I* and *SI Appendix*, Fig. S1*J*). Similar results were obtained using transient siRNA transfections to deplete MSI2 (*SI Appendix*, Fig. S1 *K* and *L*). For three of the four cell

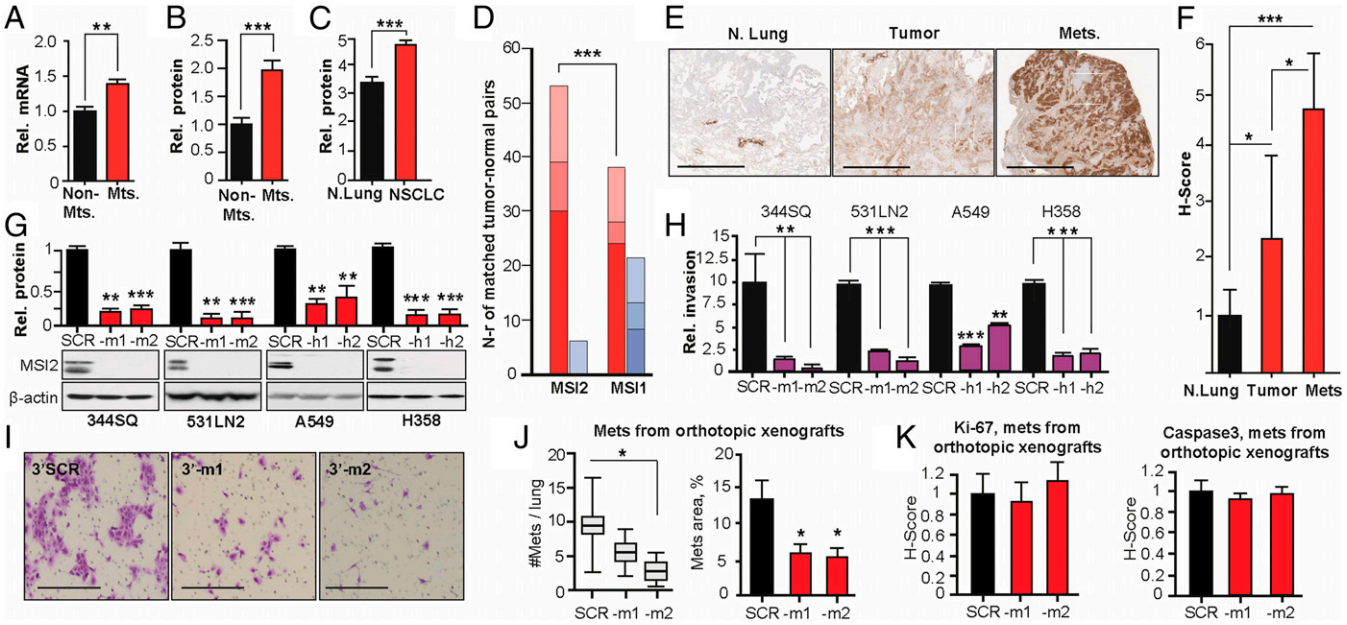

Fig. 1. Elevated MSI2 expression supports NSCLC invasion. (*A* and *B*) Averaged values from qRT-PCR (*A*) and Western blot (*B*) analysis of MSI2 mRNA and protein expression in seven metastatic versus seven nonmetastatic murine NSCLC cell lines. (*C*) Quantification of MSI2 expression in TMA of 22 normal and 123 NSCLC specimens; significance was determined by Mann–Whitney test. (*D*) Analysis of TCGA data for MSI2 and MSI1 mRNA in 59 NSCLC specimens versus paired normal lung samples. Dark red, percent of samples with tumor–up-regulated mRNA with a *z* score >3; red, up-regulation with a *z* score of 2–3; light red, up-regulation with a *z* score >1. Dark blue, percent of tumor samples with an mRNA down-regulation *z* score >3; blue, down-regulation with a *z* score of 2–3; light blue, down-regulation with a *z* score >1. (*E* and *F*) Immunohistochemical (IHC) assessment of MSI2 levels in normal lung, primary tumor, or lymph nodes, with representative data (*E*) and averaged H scores (*F*). (*G*) Western validation of MSI2 depletion with two independent shRNAs (–m1, –m2, –h1, and –h2) in indicated cell lines, referenced to control shRNA (SCR)-depleted cells. (*H* and *I*) Quantified (*H*) and representative (*I*; for 344SQ cells) data for Matrigel invasion for models shown in *J*. (*J*) Pathologist-quantified number of independent metastases per lung (*Left*) and relative area of lung metastases (*Right*) 28 d after injection of orthotopic 344SQ xenografts in 129Sv immunocompetent mice. (*K*) Quantification of K_i-67 (*Left*) and cleaved caspase (*Right*) in orthotopic xenografts; caspase levels were low in all specimens. For all graphs, $*P < 0.05$, $**P < 0.01$, and $***P < 0.001$ relative to controls.

lines (344SQ, A549, and H358), depletion of MSI2 had no effect on cell proliferation in vitro (*SI Appendix*, Fig. S1 *M* and *N*), and Msi2 depletion did not affect in vitro growth of 344SQ spheroids in the extracellular matrix (ECM) (*SI Appendix*, Fig. S2).

We next performed orthotopic lung injections of metastasis-competent 344SQ cells with shRNA vector control or shRNA targeting Msi2 into syngeneic, immunocompetent 129Sv mice. Msi2 depletion significantly reduced the burden of lung metastases following injection, predominantly affecting the total number of metastases and to a lesser extent the size of individual metastases (Fig. 1*J*), whereas no statistically significant difference in K_i-67 or cleaved caspase staining was observed (Fig. 1*K*). In a complementary experiment, an s.c. xenograft of 344SQ also indicated Msi2 depletion induced no statistically significant difference in the growth of primary xenografts or associated K_i-67 or cleaved caspase staining (*SI Appendix*, Fig. S3 *A* and *B*). However, there was a significantly higher metastatic burden in the lungs of mice bearing control versus Msi2-depleted tumors (*SI Appendix*, Fig. S3*D*). In this case, the difference in metastatic area predominantly reflected differences in numbers of metastatic foci, with K_i-67 and caspase staining comparable between control and MSI2-depletion groups (*SI Appendix*, Fig. S3 *E* and *F*). In a reciprocal approach, we overexpressed MSI2 in 393P non-metastatic cells, which have low endogenous levels of Msi2. MSI2 overexpression did not affect 393P proliferation (*SI Appendix*, Fig. S4*A*) but greatly increased invasion through Matrigel (*SI Appendix*, Fig. S4 *B* and *C*). In vivo analysis of orthotopic xenografts indicated a nonstatistically significant increase in metastasis in MSI2-overexpressing cells (*SI Appendix*, Fig. S4*D*). Finally, analysis of migration independent of invasion (*SI Appendix*, Fig. S4 *E* and *F*) showed limited effects of MSI2 depletion. We therefore focused subsequent analyses on mechanistic analysis of invasion signaling.

Unbiased and Candidate-Based Investigation of MSI2-Regulated Signaling. We used Reverse Protein Phase Array (RPPA) to query 171 total proteins and phosphoproteins for expression changes associated with Msi2 knockdown using control shRNA and Msi2-targeted shRNA derivatives of 344SQ cells (*SI Appendix*, Fig. S5). This work suggested a number of previously unidentified candidates associated with Msi2 expression and relevant to control of epithelial–mesenchymal transition (EMT) and invasion. Proteins with the greatest magnitude of response to Msi2 depletion that were subsequently validated by low throughput Western analysis included the tight junction (TJ)-associated protein claudin 7 (CLDN7) (15–17), elevated 19.4-fold, and the ECM protein fibronectin (FN1) (18–21), elevated 2.5-fold. Subsequent independent evaluation confirmed these RPPA results, as MSI2 depletion significantly elevated FN1 mRNA (4.0–9.4-fold) and protein (2.4–23 fold) in all four cell lines and elevated CLDN7 protein (2.5–28-fold) in three of the four cell lines (Fig. 2 *A* and *B* and *SI Appendix*, Fig. S6 *A* and *B*). Results were independently confirmed using transient siRNAs to deplete MSI2 (*SI Appendix*, Fig. S6*C*). Although RPPA data also suggested the neurogenic locus notch homolog protein 1 (NOTCH1) expression may be affected by MSI2 (*SI Appendix*, Fig. S5) and although some studies suggested expression of the NOTCH regulator NUMB is influenced by MSI1/2 (22, 23), we found no consistent and significant differences in NUMB in MSI2-depleted cells (*SI Appendix*, Fig. S6*D*), supporting the idea that regulation of NUMB by MSI1/2 may depend on cellular context (24, 25).

NSCLC cells have been shown to express multiple claudins with partially redundant function (26), most not represented in the RPPA panel. In direct testing, we found MSI2 depletion also induced CLDN3 and CLDN5 in all four cell lines at the protein level (3.8–22 fold for CLDN3 and 3.4–41 fold for CLDN5) (Fig. 2*B* and *SI Appendix*, Fig. S6 *E* and *F*), making restraint of claudin expression a consistent feature of MSI2 function. Studies of the MSI proteins (predominantly focused on MSI1) have defined these proteins as RNA-binding proteins that regulate mRNA translation (22, 24, 27). The induction of claudins may reflect a combination of transcriptional and posttranscriptional consequences of MSI2 depletion, as the mRNA level shows induction that is less marked than at the protein level (*SI Appendix*, Fig. S6 *A*, *B*, *E*, and *F*). However, the claudin mRNAs lack [(G/A)U(n)AGU (n = 1–3)] the consensus motifs for MSI2 binding described in Wang et al. (28), suggesting direct regulation of translation is not involved.

Direct MSI2 translational targets defined in other cell types that might be relevant to the invasiveness of NSCLC cells and tumors

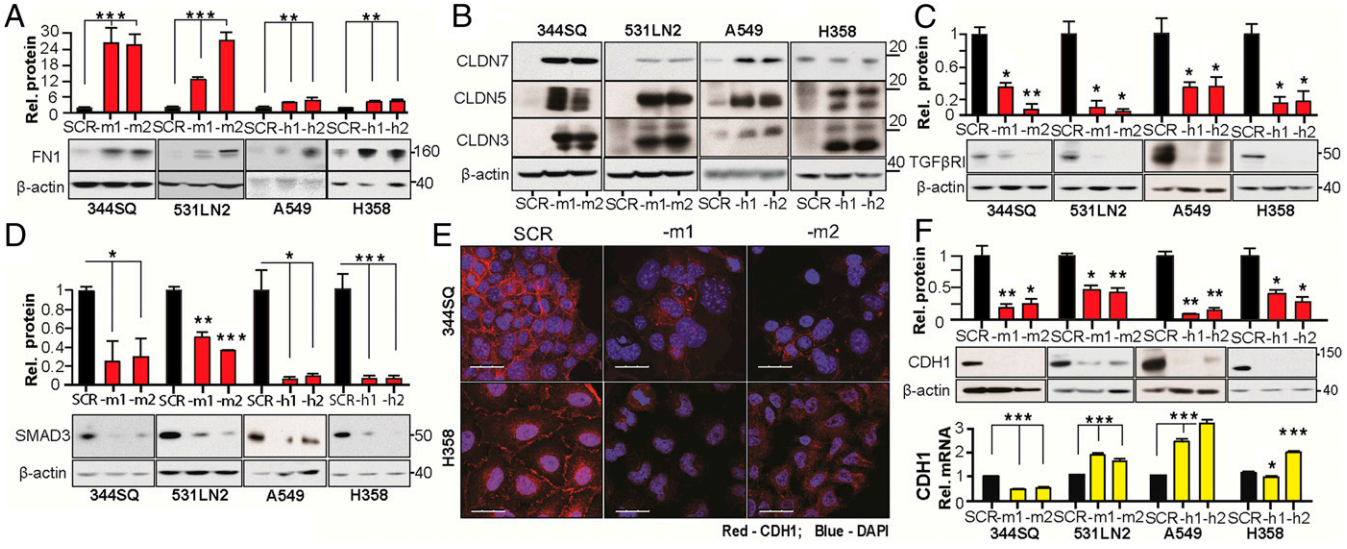

Fig. 2. MSI2 depletion controls the expression of indirect and direct targets relevant to invasion and EMT. (*A* and *B*) Western analysis of FN1 (*A*) and CLDN7, CLDN5, and CLDN3. (*B*) In murine and human NSCLC cell lines in the context of MSI2 depletion with independent targeting shRNAs (–m1/–m2, –h1/–h2). SCR, control scrambled shRNA. Graphs represent data from four independent runs. (*C* and *D*) Western analysis of expression of TGFβR1 (*C*) and SMAD3 (*D*) in murine and human NSCLC cell lines with stably depleted MSI2. Graphs represent data from three independent runs. For all graphs,*$P < 0.05$, **$P < 0.01$, and ***$P < 0.001$ relative to SCR (scrambled shRNA) controls. (*E*) Immunofluorescence analysis of E-Cadherin staining in 344SQ murine (*Top*) and H358 human (*Bottom*) NSCLC cell lines, with or without depleted MSI2. Blue, DAPI; red, E-Cadherin. (Scale bars, 30 μm.) (*F*) Western (*Top*) and qRT-PCR (*Bottom*) analysis of E-Cadherin expression in four NSCLC cell line models with or without depleted MSI2. Graphs represent data from three independent runs. For all graphs, *$P < 0.05$, **$P < 0.01$, and ***$P < 0.001$ relative to SCR (scrambled shRNA) controls.

include the TGF-β receptor (TGFβR1) and its effector, the small mothers against decapentaplegic homolog 3 (SMAD3) (24), which promote EMT by down-regulating E-cadherin (CDH1) and inducing other transcriptional changes (29). We found that stable or transient MSI2 knockdown caused strong down-regulation of TGFβR1 and SMAD3, predominantly at the protein level, in all four models (Fig. 2 *C* and *D* and *SI Appendix*, Fig. S6 *G* and *H*). Reciprocally, exogenous overexpression of MSI2 induced TGFβR1 and SMAD3 expression and caused loss of CLDN3, CLDN5, and CLDN7 expression in the 393P cell line (*SI Appendix*, Fig. S6 *I* and *J*).

Depletion of MSI2 Affects the Composition of Cell–Cell Junctions and Causes Partial EMT. Based on the action of MSI2 in supporting the expression of TGFβR1 and SMAD3, while repressing CLDN3, CLDN5, CLDN7, and FN1, we hypothesized that the reduced invasiveness of MSI2-depleted cells might reflect changes involving TJs and reduced EMT, associated with elevated E-cadherin (CDH1). Unexpectedly, immunofluorescence analysis demonstrated that expression of epithelial protein E-cadherin at cell–cell junctions was much reduced by MSI2 depletion (Fig. 2*E*), as was total E-cadherin protein expression, whereas mRNA levels were not consistently affected (Fig. 2*F*). In contrast, there was a significant increase in CLDN3 and CLDN7 staining at cell–cell contact points, whereas TJP1 (ZO-1), which localizes to the cytoplasmic surface of TJs, was unaffected (*SI Appendix*, Fig. S7). We examined expression of additional proteins associated with mesenchymal identity (*SI Appendix*, Fig. S8 *A* and *B*). MSI2 depletion up-regulated the pro-EMT factors ZEB1, ZEB2, and FOXC2 but down-regulated VIM (vimentin) and the zinc finger proteins SNAI1 (SNAIL) and SNAI2 (SLUG). Conversely, MSI2 overexpression induced CDH1, VIM, SNAIL, and SLUG (*SI Appendix*, Fig. S8 *C* and *D*). Collectively, these data indicated a mixed effect of MSI2 depletion on EMT.

MSI2 Regulation of Invasion via TGFβR1, SMAD3, and CLDN7. To assess the functional interaction between MSI2, its direct targets TGFβR1 and SMAD3, and claudins, we depleted SMAD3 or TGFβR1 in MSI2-depleted versus control cell lines. SMAD3 knockdown reduced CDH1 expression levels in both parental and MSI2-depleted lines (Fig. 3*A*). By contrast, the relationship between TGFβR1 and CDH1 expression was modulated by MSI2 status, with the TGFβR1 knockdown elevating CDH1 expression in the parental cell lines but reducing it in MSI2-depleted cell lines (Fig. 3*B*). MSI2 also influenced the response of cells growing as spheroids to treatment with TGF-β (*SI Appendix*, Fig. S2), with control scrambled shRNA (SCR)-depleted cells responding by increasing sphere size but MSI2-depleted cells showing little proliferative response and instead responding by showing a greater phenotype of collective migration. Importantly, depletion of TGFβR1 or SMAD3 caused a statistically significant decrease in invasion in SCR-depleted NSCLC cell lines but not in those with depleted MSI2 (Fig. 3*C*). Conversely, overexpression of TGFβR1 partially but incompletely rescued the decrease in invasion seen in MSI2-depleted cells (*SI Appendix*, Fig. S9), suggesting other contributing factors.

The profile of mixed pro- and anti-EMT changes, and incomplete rescue by TGFβR1 overexpression, suggested a possible important role for claudin-associated TJs in limiting NSCLC invasion induced by MSI2-dependent TGFβR1/SMAD3 signaling. Exploring the relationship between these proteins, we found that siRNA depletion of TGFβR1 or SMAD3 did not significantly affect the expression of CLDN3, CLDN7, or MSI2. This indicated that MSI2 regulates CLDN3/CLDN7 expression independently of TGFβR1 and SMAD3 (Fig. 3 *A* and *B* and *SI Appendix*, Fig. S10 *A* and *B*). Functionally, overexpression of CLDN7 significantly decreased invasion in cells expressing high levels of endogenous MSI2 (Fig. 4 *A*–*D*). Conversely, siRNA depletion of CDLN7 significantly increased invasion in 344SQ cells with depleted MSI2 but had no effect in cells with significant endogenous MSI2 (Fig. 4 *E*–*G*). Taken together, we conclude that MSI2 stimulates invasion in lung cancer in part by sustaining TGFβR1 signaling and suppressing the expression of CLDN7 and potentially other claudins.

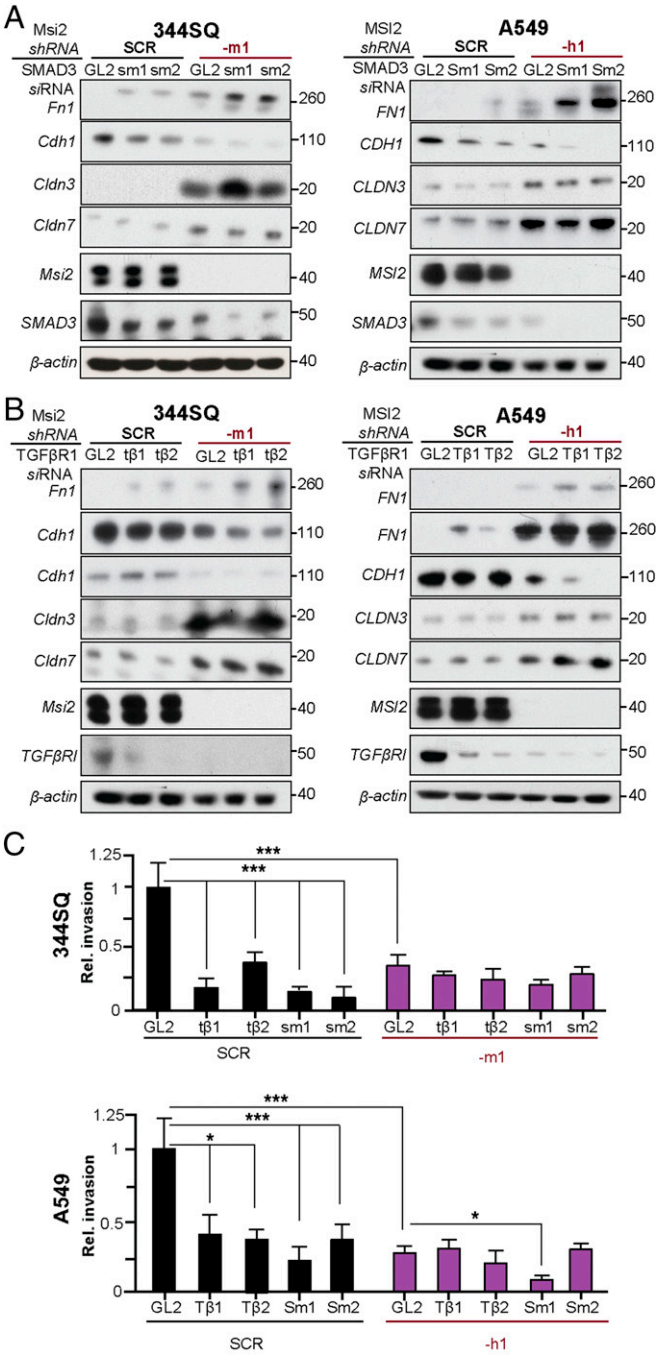

Fig. 3. Functional interaction of MSI2 with TGFβR1, SMAD3, FN1, E-Cadherin, and CLDN3 and CLDN7. (*A*) Western analysis for expression of indicated proteins in the 344SQ and A549 cell lines with (–m1 and –h1) or without (SCR) shRNA depletion of MSI2, and with (–sm1, –sm2, and –Sm1, –Sm2) or without (GL2) siRNA depletion of SMAD3. (*B*) Western analysis for expression of indicated proteins in the 344SQ and A549 cell lines with (m1 and h1) or without (SCR) shRNA depletion of MSI2, and with TGFβR1 (–tβ1, –tβ2 and –Tβ1, –Tβ2) or without (GL2) siRNA depletion of TGFβR1. (*C*) Quantification of results from three independent Matrigel invasion assays for 344SQ and A549 with (–m1 and –h1) or without (SCR) shRNA depletion of MSI2, in the context of additional siRNA depletion of TGFβR1 (–tβ1, –tβ2 and –Tβ1, –Tβ2) or SMAD3 (–sm1, –sm2 and –Sm1, –Sm2) versus siRNA negative control (GL2). $*P < 0.05$ and $***P < 0.001$ relative to controls.

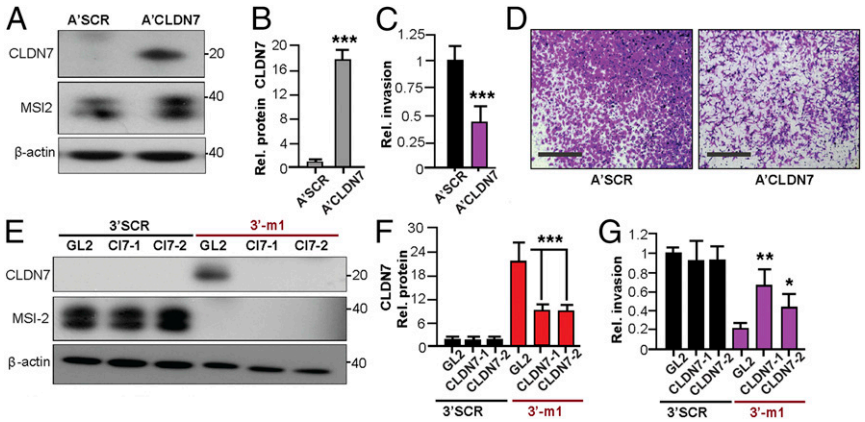

Fig. 4. CLDN7 regulation of invasion. (*A* and *B*) Representative Western blot analysis of indicated proteins (*A*) and quantification of CLDN7 expression (*B*) in negative control A'SCR and A'CLDN7 stably transfected A549 cells. (*C* and *D*) Quantification (*C*) and representative images (*D*) of Matrigel invasion for A'SCR and A'CLDN7 stably transfected A549 cells. (*E* and *F*) Western blot analysis (*E*) and quantification of CLDN7 expression (*F*) in 344SQ cells expressing MSI2 (SCR) or stably MSI2-depleted (–m1) and transiently transfected with GL2 control or CI7 siRNAs (CI7-1, CI7-2). (*G*) Quantification of Matrigel invasion assay for cells in *E* and *F*, based on three experiments. For all graphs, $*P \leq 0.05$, $*P \leq 0.01$, and $***P \leq 0.001$ relative to controls.

Discussion

In summary, our study for the first time, to our knowledge, shows that elevation of MSI2 expression progressing NSCLC supports tumor cell invasion and metastasis by modulating TGF-β–dependent EMT and repressing claudin expression (Fig. 5). Although a number of studies have previously identified a role for the MSI2 paralogue MSI1 as oncogenic in a number of cancer types (30–32), MSI2 has attracted much less scrutiny. However, MSI2 has been shown to be oncogenic in a mouse model of colon cancer (28); MSI2 expression is induced by loss of the adenomatous polyposis coli (APC) gene, and overexpression of MSI2 phenocopies APC loss (28). MSI2 is also overexpressed and oncogenic in human leukemias. Elevated MSI2 expression is associated with poor survival in leukemia, and MSI2 knockdown or genetic deletion reduced engraftment and caused a defect in hematopoietic stem cell maintenance in vivo as a result of decreased proliferation (23, 24, 33), in part due to a loss of sensitivity to TGF-β–mediated expansion and compromised TGFβR1 and SMAD3 signaling. Our data confirm the relevance of TGFβR1 and SMAD3 to some MSI2 activities in NSCLC but also establish for the first time, to our knowledge, that MSI2 status conditions TGFBβR1 regulation of E-cadherin/CDH1 as well as the ability of TGFβR1 and SMAD3 to influence cell invasion. These results coupled with our evidence showing rising levels of MSI2 as tumors become increasingly metastatic in mouse models or human specimens suggest that MSI2 expression status may be relevant to the change in TGF-β signaling from prodifferentiation to proinvasive during tumor progression (29). Full understanding of the functional role of MSI2 in NSCLC metastasis will require additional studies, such as clinical correlative analysis.

Importantly, our data suggest that, in NSCLC, proliferation is a much less important target of MSI2 regulation than control of invasion, in a marked difference from leukemia models. Analysis of MSI proteins in breast cancer has led to the suggestion that these proteins may be required to support an epithelial luminal cell identity (25). However, our findings point to a more complex mode of action, with MSI2 supporting expression of CDH1, VIM, SLUG, and SNAIL but suppressing that of Zeb1/2, FOXC2, and multiple claudins. TGF-β has previously been shown to directly support expression of SNAIL but not ZEB1/2 in an NSCLC cell model (34), suggesting these downstream effects of MSI2 include both TGF-β–dependent and –independent outputs. Together with MSI2-dependent expression of CDH1, these results are compatible with a model in which MSI2 creates conditions that favor collective migration (35), an idea bearing further investigation.

Although essentially unaddressed in lung cancer, a claudin-low phenotype has been linked to EMT, stemness, and chemotherapy resistance in breast and bladder cancer (36–38). CLDN7 is known to inhibit human lung cancer invasion (15), and low expression of CLDN7 is linked to poor prognosis in NSCLC (39). Our data for the first time, to our knowledge, indicate that MSI2 represses the expression of multiple claudins, with at least CLDN7 functionally important for MSI2-dependent invasion. Although technical issues limit simultaneous targeting of multiple claudins, it is likely that control of this suite of proteins significantly influences NSCLC metastasis, particularly given the mixed EMT phenotype of modulating MSI2 expression.

Finally, given their role as noncatalytic RNA-binding proteins, it is likely to be difficult to develop effective small molecule inhibitors targeting MSI1 or MSI2. However, several recent therapeutic strategies to improve NSCLC treatment focus on TGF-β (40–42), and activity of such compounds could be strongly influenced by MSI2 status in tumors, with invasive or metastatic NSCLC expressing higher levels of MSI2 having a differential response. In addition, the EMT process itself has been shown to influence cellular resistance to a number of drugs of relevance to NSCLC treatment (7). Further study of MSI2 function in normal lung development, cellular transformation, and NSCLC drug resistance is clearly warranted.

Methods

Also see the extended methods in *SI Appendix, SI Methods*.

Cell Culture. Mouse cell lines (344SQ, 531LN2, others) from $p53^{R172H\Delta g/+}$*K-ras*$^{LA1/+}$ mice were derived from tumor tissues at necropsy from different mice as

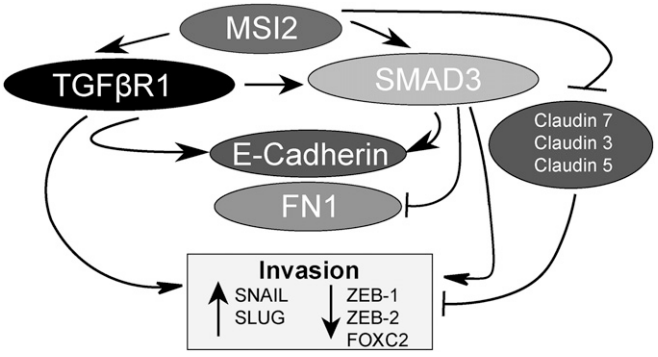

Fig. 5. Model for MSI2 action in coordinating EMT and invasion potential. See *Discussion* for details.

previously described (13). Human alveolar basal epithelial adenocarcinoma cell lines A549, H358, H322, and H226 were obtained from the American Type Culture Collection (ATCC). All cells were grown in RPMI 1640 with 10% FBS (50 mL FBS/450 mL RPMI). The 344SQ-m1/2, 531LN2-m1/2, A549-h1/h2, and H358-h1/h2 MSI2-knockdown cell lines were created by transfection with the pLKO.1 system-based shRNA lentivirus (SIGMA) (*SI Appendix, SI Methods*).

Cell Proliferation and Invasion Assays. Cell growth was measured by CellTiterBlue and water-soluble tetrazolium salts assays and by direct quantitation of DAPI-stained nuclei. Invasion assays were performed using standard Matrigel invasion assays. Details of protocols and statistical analyses are provided in detail in *SI Appendix, SI Methods*.

In Vivo Analysis of Tumor Growth and Metastasis. All animal experiments were reviewed and approved by the Institutional Animal Care and Use Committees at the MD Anderson Cancer Center and at the Fox Chase Cancer Center. Orthotopic and s.c. xenograft studies were performed to study the proliferation and metastatic potential of NSCLC cell lines with overexpressed or depleted MSI2. Detailed protocols are provided in *SI Appendix, SI Methods*.

RPPA Reverse-Phase Protein Analysis. The 344SQ-SCR, 344SQ-m1, and 344SQ-m2 mouse cells were lysed and prepared according to MD Anderson Core Facility instructions, as previously described, and RPPA was performed at the facility (43–45). Data were visualized using the MultiExperiment Viewer program (www.tm4.org/mev.html) (46).

Protein Expression Analysis by Western Blotting. Lysates were prepared for analysis, and Western blotting and analysis were performed using standard protocols. Quantified data were averaged from at least three independent runs for all experiments. See *SI Appendix, SI Methods* for the specific antibody reagents used.

siRNA Transfection. SMARTpool siRNAs targeting human/mouse TGFβR1/TgfβR1, SMAD3/Smad3, and CLDN7/Cldn7 (*SI Appendix*, Table S4) and nonspecific control pool siRNA were purchased from Dharmacon. NSCLC cells at 50% confluence were transfected with siRNA at final concentrations of 50 nmol/L using the LipofectAMINE 2000 transfection reagent (Thermo Fisher Scientific) according to the manufacturer's instructions.

ACKNOWLEDGMENTS. We thank Drs. Jamie Rodriguez and Ignacio Wistuba for preparing tester blocks for immunohistochemistry. We thank Cara Dubyk for technical assistance with TMA staining, Dr. Margret Einarson for assistance with high throughput analyses, Dr. Marcos Estécio for advice, Dr. Waun Ki Hong for general support, and Vladislav Korobeynikov for assistance with the Vectra Imaging System. The authors and the work were supported by the NCI Core Grant P30 CA006927 (to Fox Chase Cancer Center); NCI P30 Core Grant CA016672 (to MD Anderson Cancer Center); a Conquer Cancer Foundation (ASCO) Young Investigator Award, American Cancer Society IRG Pilot Grant, Lung Cancer Research Foundation (LCRF), AHEPA Foundation grant, and DOD Career Development Award LC140074 (to Y.B.); UNM Core Funding (C.F.M., F.A.S., and S.R.); NCI Grants CA181287 and R21CA191425 (to E.A.G.); a Ruth L. Kirschstein NRSA F30 fellowship (F30 CA180607) from the NIH (to T.N.B.); NIH Grant K08 CA151651 and the MD Anderson Physician-Scientist Award (to D.L.G.); and NIH Grant R01 CA157450 (to J.M.K.). This research was also supported by the Basic Science Research Program through the National Research Foundation of Korea (NRF) funded by the Ministry of Science, ICT & Future Planning (NRF 2010-0027945; to Y.-H.A.). Bioinformatics analysis for this work was supported by Russian Science Foundation Grant 15-15-20032.

1. Siegel R, Naishadham D, Jemal A (2013) Cancer statistics, 2013. *CA Cancer J Clin* 63(1):11–30.
2. Howlader NNA, et al. (2013) *SEER Cancer Statistics Review, 1975-2010*, ed Cronin KA (National Cancer Institute, Bethesda).
3. Zheng S, El-Naggar AK, Kim ES, Kurie JM, Lozano G (2007) A genetic mouse model for metastatic lung cancer with gender differences in survival. *Oncogene* 26(48):6896–6904.
4. Mitsudomi T, et al. (1991) Mutations of ras genes distinguish a subset of non-small-cell lung cancer cell lines from small-cell lung cancer cell lines. *Oncogene* 6(8):1353–1362.
5. Takahashi T, et al. (1989) p53: A frequent target for genetic abnormalities in lung cancer. *Science* 246(4929):491–494.
6. Bertolini G, et al. (2009) Highly tumorigenic lung cancer CD133+ cells display stem-like features and are spared by cisplatin treatment. *Proc Natl Acad Sci USA* 106(38):16281–16286.
7. Singh A, Settleman J (2010) EMT, cancer stem cells and drug resistance: An emerging axis of evil in the war on cancer. *Oncogene* 29(34):4741–4751.
8. Licciulli S, et al. (2013) Notch1 is required for Kras-induced lung adenocarcinoma and controls tumor cell survival via p53. *Cancer Res* 73(19):5974–5984.
9. Arasada RR, Amann JM, Rahman MA, Huppert SS, Carbone DP (2014) EGFR blockade enriches for lung cancer stem-like cells through Notch3-dependent signaling. *Cancer Res* 74(19):5572–5584.
10. Hassan KA, et al. (2013) Notch pathway activity identifies cells with cancer stem cell-like properties and correlates with worse survival in lung adenocarcinoma. *Clin Cancer Res* 19(8):1972–1980.
11. Tirino V, et al. (2013) TGF-β1 exposure induces epithelial to mesenchymal transition both in CSCs and non-CSCs of the A549 cell line, leading to an increase of migration ability in the CD133+ A549 cell fraction. *Cell Death Dis* 4:e620.
12. Beck TN, Chikwem AJ, Solanki NR, Golemis EA (2014) Bioinformatic approaches to augment study of epithelial-to-mesenchymal transition in lung cancer. *Physiol Genomics* 46(19):699–724.
13. Gibbons DL, et al. (2009) Contextual extracellular cues promote tumor cell EMT and metastasis by regulating miR-200 family expression. *Genes Dev* 23(18):2140–2151.
14. Barretina J, et al. (2012) The Cancer Cell Line Encyclopedia enables predictive modelling of anticancer drug sensitivity. *Nature* 483(7391):603–607.
15. Lu Z, et al. (2011) Claudin-7 inhibits human lung cancer cell migration and invasion through ERK/MAPK signaling pathway. *Exp Cell Res* 317(13):1935–1946.
16. Prat A, et al. (2013) Genomic analyses across six cancer types identify basal-like breast cancer as a unique molecular entity. *Sci Rep* 3:3544.
17. Bruna A, et al. (2012) TGFβ induces the formation of tumour-initiating cells in claudinlow breast cancer. *Nat Commun* 3:1055.
18. Liu W, Cheng S, Asa SL, Ezzat S (2008) The melanoma-associated antigen A3 mediates fibronectin-controlled cancer progression and metastasis. *Cancer Res* 68(19):8104–8112.
19. Urtreger AJ, et al. (2006) Fibronectin is distinctly downregulated in murine mammary adenocarcinoma cells with high metastatic potential. *Oncol Rep* 16(6):1403–1410.
20. Zhang X, et al. (2009) Up-regulated microRNA-143 transcribed by nuclear factor kappa B enhances hepatocarcinoma metastasis by repressing fibronectin expression. *Hepatology* 50(2):490–499.
21. Yi M, Ruoslahti E (2001) A fibronectin fragment inhibits tumor growth, angiogenesis, and metastasis. *Proc Natl Acad Sci USA* 98(2):620–624.
22. Rezza A, et al. (2010) The overexpression of the putative gut stem cell marker Musashi-1 induces tumorigenesis through Wnt and Notch activation. *J Cell Sci* 123(Pt 19):3256–3265.
23. Ito T, et al. (2010) Regulation of myeloid leukaemia by the cell-fate determinant Musashi. *Nature* 466(7307):765–768.
24. Park SM, et al. (2014) Musashi-2 controls cell fate, lineage bias, and TGF-β signaling in HSCs. *J Exp Med* 211(1):71–87.
25. Katz Y, et al. (2014) Musashi proteins are post-transcriptional regulators of the epithelial-luminal cell state. *eLife* 3:e03915.
26. Kwon MJ (2013) Emerging roles of claudins in human cancer. *Int J Mol Sci* 14(9):18148–18180.
27. Sakakibara S, Nakamura Y, Satoh H, Okano H (2001) Rna-binding protein Musashi2: Developmentally regulated expression in neural precursor cells and subpopulations of neurons in mammalian CNS. *J Neurosci* 21(20):8091–8107.
28. Wang S, et al. (2015) Transformation of the intestinal epithelium by the MSI2 RNA-binding protein. *Nat Commun* 6:6517.
29. Massagué J (2012) TGFβ signalling in context. *Nat Rev Mol Cell Biol* 13(10):616–630.
30. Sureban SM, et al. (2008) Knockdown of RNA binding protein musashi-1 leads to tumor regression in vivo. *Gastroenterology* 134(5):1448–1458.
31. Li D, et al. (2011) Msi-1 is a predictor of survival and a novel therapeutic target in colon cancer. *Ann Surg Oncol* 18(7):2074–2083.
32. Oskarsson T, et al. (2011) Breast cancer cells produce tenascin C as a metastatic niche component to colonize the lungs. *Nat Med* 17(7):867–874.
33. Kharas MG, et al. (2010) Musashi-2 regulates normal hematopoiesis and promotes aggressive myeloid leukemia. *Nat Med* 16(8):903–908.
34. Liu J, et al. (2013) Suppression of SCARA5 by Snail1 is essential for EMT-associated cell migration of A549 cells. *Oncogenesis* 2:e73.
35. Shamir ER, Ewald AJ (2015) Adhesion in mammary development: Novel roles for E-cadherin in individual and collective cell migration. *Curr Top Dev Biol* 112:353–382.
36. Creighton CJ, et al. (2009) Residual breast cancers after conventional therapy display mesenchymal as well as tumor-initiating features. *Proc Natl Acad Sci USA* 106(33):13820–13825.
37. Hennessy BT, et al. (2009) Characterization of a naturally occurring breast cancer subset enriched in epithelial-to-mesenchymal transition and stem cell characteristics. *Cancer Res* 69(10):4116–4124.
38. Choi W, et al. (2014) Intrinsic basal and luminal subtypes of muscle-invasive bladder cancer. *Nat Rev Urol* 11(7):400–410.
39. Yamamoto T, et al. (2010) Reduced expression of claudin-7 is associated with poor outcome in non-small cell lung cancer. *Oncol Lett* 1(3):501–505.
40. Akhurst RJ, Hata A (2012) Targeting the TGFβ signalling pathway in disease. *Nat Rev Drug Discov* 11(10):790–811.
41. Dituri F, et al. (2013) Differential inhibition of the TGF-β signaling pathway in HCC cells using the small molecule inhibitor LY2157299 and the D10 monoclonal antibody against TGF-β receptor type II. *PLoS One* 8(6):e67109.
42. Park CY, et al. (2014) An novel inhibitor of TGF-β type I receptor, IN-1130, blocks breast cancer lung metastasis through inhibition of epithelial-mesenchymal transition. *Cancer Lett* 351(1):72–80.
43. Iadevaia S, Lu Y, Morales FC, Mills GB, Ram PT (2010) Identification of optimal drug combinations targeting cellular networks: Integrating phospho-proteomics and computational network analysis. *Cancer Res* 70(17):6704–6714.
44. Kornblau SM, et al. (2009) Functional proteomic profiling of AML predicts response and survival. *Blood* 113(1):154–164.
45. Tibes R, et al. (2006) Reverse phase protein array: Validation of a novel proteomic technology and utility for analysis of primary leukemia specimens and hematopoietic stem cells. *Mol Cancer Ther* 5(10):2512–2521.
46. Saeed AI, et al. (2003) TM4: A free, open-source system for microarray data management and analysis. *Biotechniques* 34(2):374–378.

SUPPLEMENTAL MATERIALS.

1. Supplemental Figures and Tables.

Figure S1. A. Genes assessed for differential expression in 344SQ versus 393P cell lines; graphs show quantification of qRT-CPR data. **B.** Western blot of MSI2 protein expression in 7 non-invasive versus 7 metastatic murine cell lines. **C.** Quantification of MSI1 mRNA and protein data in in 7 non-invasive versus 7 metastatic murine cell lines. **D.** Western blot of Msi1 protein expression in 7 non-invasive versus 7 metastatic murine cell lines. **E**. Representative AQUA images of MSI2 expression from analysis of TMAs containing 22 normal and 123 NSCLC specimens. Blue - DAPI; Green -cytokeratin; Red - MSI2. Scale bars: 100 μm **F.** Quantification of MSI1 expression in TMA of 19 normal and 120 NSCLC specimens was not significant, as determined by Mann-Whitney test. **G**. KM Plots (http://kmplot.com/) analysis of overall survival in non-small cell lung cancer expressing high versus low MSI2. **H.** Western confirmation of higher expression of MSI2 human NSCLC A549 and H358 cell lines versus H226 and H322. **I**. qRT-PCR indicates effective stable knockdown of MSI2 in 344SQ, 531LN2 murine and MSI2 in A549, H358 human cell lines by independent shRNA depleting MSI2 (- m1, -m2, -h1, -h2) or a control shRNA (SCR). **J.** Representative images of crystal violet-stained cells from Matrigel invasion assay for the 531LN2, A549, and H358 cell lines. **K.** Western blot of MSI2 expression following transfection of siRNAs targeting Msi2 in 344SQ murine and A549 and H358 human NSCLC cell lines, using 2 independent siRNAs. **L.** Quantification of Matrigel invasion assay for 344SQ and A549 cells, transfected by GL2 control or Msi2/MSI2 –targeting SiRNAs, based on three independent assays. **M., N.** Quantification of viability assay calculated by CellTiterBlue (CTB) (**M**) or direct count of DAPI-stained nuclei (**N**). P values reflect data on final day of experiment. All graphs: *, p≤0.05; *, p≤0.01; ***, p≤0.001 relative to controls.

Figure S2. MSI2 depletion decreases response of murine 344SQ and human H358 cells to TGF-beta stimulation of ECM matrix sphere formation. Images (**A**) and quantitation **(B)** of control (SCR) and MSI2-depleted (-m1, -m2) 344SQ cells grown on ECM Matrix for 5 days in the presence of 0, 10, or 100 ng/ml TGFβ. All cells were imaged by confocal microscopy. Scale bar, 50 mm. All graphs: *, p≤0.05; **, p≤0.01; ***, p≤0.001 relative to indicated controls.

Figure S3. Primary and metastatic 344SQ Tumor Growth in Subcutaneous Xenografts. A. Gross tumor volume measurement of subcutaneous (S.C.) tumor growth of control (SCR) and MSI2-depleted (-m1, -m2) 344SQ xenografts. **B., C.** IHC assessment for (**B**) Ki-67 proliferation marker and (**C**) cleaved caspase apoptotic marker in 344SQ primary subcutaneous xenograft tumors using H-score, quantified by Vectra. **D.** Left, graph represents metastatic burden in lung of the mice with 344SQ subcutaneous xenografts analyzed in (**A**), expressed as ratio of metastatic area / total lung, quantified from three section levels per lung. Right, representative images of metastatic burden of SCID mice with 344SQ control (SCR) and MSI2 depleted (-m1/-m2) subcutaneous xenografts. Arrows indicate metastatic nodules in the lungs. **E, F**. Analysis of the same metastases shown in (D) for expression of Ki-67 (E) and cleaved caspase (F); H-score quantitation performed as in (**B, C**) Scale bars: shown on images respectively. All graphs: values shown are not significant between comparison groups, except ****, p≤0.0001 for **D**.

Figure S4. MSI2 overexpression, and MSI2 phenotype in migration control. A. Quantification of CellTiterBlue (CTB) proliferation assays of 393p/M2a and 393p/M2b MSI2-overexpressing clones versus 393p/cDNA control cell lines. **B**., **C**. Quantification (**B**) and representative image (**C**) of Matrigel invasion analysis of 393p/cDNA control and 393p/M2a and 393p/M2b MSI2 overexpressing cell lines. **D.** Gross pathological assessment of lung metastases of 393p xenografts (393p/cDNA, 393p/M2a and 393p/M2b). **E.** Quantification of cell migration for indicated cell lines with control (SCR) or MSI2-targeting shRNAs, based on a wound healing assay. **F.** Quantified migration for the SCR control and MSI2-depleted cells 531LN2 cell line in a transwell invasion assay. Statistical differences were calculated for each time point using Excel software, t-test. All graphs: *, p≤0.05; **, p≤0.01; ***, p≤0.001 relative to controls.

Figure S5. Reverse phase protein array (RPPA) analysis heatmap representing relative expression of 171 proteins or phosphoproteins. Comparison groups are two independent 344SQ derivatives with MSI2 knockdown (-m1 and –m2) and negative control. Three biological repeats were used for each cell line. 344SQ-SCR, 344SQ-m1 344SQ-m2 murine cells were lysed and prepared according to MD Anderson Core Facility instructions as previously described, and RPPA performed at the facility (48-50). Data were analyzed to establish significant differences in expression using the MultiExperiment Viewer (MeV, v4.9) program (www.tm4.org/mev/) (51). Scale bar represents ln values from fold change. Note, some hits scoring as positive in this assay were not validated in subsequent probe of MSI2 depletion in the 4 independent cell line models used in this study, including notably NOTCH-1.

Figure S6. Stable and transient depletion or overexpression of MSI2. A. qRT-PCR comparing expression of mRNA for FN1 and CLDN7 in 4 model NSCLC cell lines (MSI2-depleted -m1/-h1, -m2/-h2) and SCR, control scrambled shRNA. Graphs represent data from four independent runs. **B.** Western blot analysis quantification of CLDN7 protein expression in 4 model NSCLC cell lines (-m1,-m2,-h1,-h2 MSI2-depleted) and SCR, control scrambled shRNA. Graphs represent data from four independent runs. **C.** Western blot analysis of indicated proteins in 344SQ, A549 and H358 cell lines, transfected by GL2 control or MSI2-depleting (-m1, -m2,-h1, -h2) siRNAs. **D**. Western blot analysis of NUMB expression in murine and human cell lines. **E.**, **F**. qRT-PCR (**E**) and Western (**F**) quantification of expression of mRNA for CLDN5 and CLDN3 in 4 NSCLC cell lines expressing control shRNA (SCR) or MSI2-depleting shRNA (-m1,-m2,-h1,-h2). Graphs represent data from four independent experiments. **G.** qRT-PCR comparing expression of TGFβRI and SMAD3 in 4 model NSCLC cell lines expressing control shRNA (SCR) or MSI2-depleting shRNA (-m1,-m2,-h1,-h2). Graphs represent data from four independent experiments. **H.** Western blot of indicated proteins in 3 model cell lines, transfected by GL2 control or two independent MSI2-depleting siRNAs. **I.,** J. Western blot analysis of indicated proteins in the 393P cell line, overexpressing MSI2 (393p/M2a and 393p/M2b versus the 393p/cDNA control cell line). All graphs: *, p≤0.05; *, p≤0.01; ***, p≤0.001 relative to controls.

Figure S7. MSI2 controls expression of CLDN7 at cell-cell junctions. A., **B**. Immuofluorescence analysis of CLDN7 co-stained with the tight junction marker ZO-1 in murine 344SQ (**A**) and 531LN2 (**B**) NSCLC cell lines, with or without MSI2 stable knockdowns. Green, CLDN7; Red, ZO-1; Blue, DAPI. Scale bars are 30μm.

Figure S8. Western blot analysis of EMT markers in MSI2 overexpressing or depleted cells. A., B. Western blot analysis (**A**) and quantification (**B**) of MSI2, ZEB-1, ZEB-2, FOXC2, SNAIL, SLUG, VMN (vimentin) versus β-actin loading control in 344SQ, A549 and H358 cell lines expressing MSI2 (SCR) or depleted of MSI2 (-m1, -m2, -h1, -h2). **C., D.** Western blot analysis (C) and quantification (D) of MSI2, E- Cadherin, vimentin, SLUG and SNAIL protein expression 393p/cDNA control and 393p/M2a and 393p/M2b MSI2 overexpressing cell lines. All graphs: *, p≤0.05; *, p≤0.01; ***, p≤0.001 relative to controls.

Figure S9. Invasion by TGFβR1/SMAD3-overexpressing NSCLC 3NSCLC cell lines. A., B. Representative Western blot (**A**) and quantitation of TGFβR1 (**B**) in 344SQ (left) or A549 (right) cells expressing control (SCR) or MSI2-depleting shRNA (m1, h1), after introduction of TGFβR1 (TβR1). **C., D.** Quantified (**C**) and representative (**D**) data for invasion through Matrigel for the cell models shown in **A, B**. **D.** All graphs: *, p≤0.05; *, p≤0.01; ***, p≤0.001.

Figure S10. Quantification of Western blots of control and MSI2-depleted mouse NSCLC cells, transiently depleted of TGFβRI or SMAD3. A., B. Quantified data for Western blots shown in Figure 3A, B. for 344SQ (**A**) and A549 (**B**) cells with (-m1 and -h1) or without (SCR) shRNA depletion of MSI2, and with depletion of TGFβR1 (-tβ1, -tβ2, -Tβ1 and -Tβ2), SMAD3 (-sm1, -sm2, -Sm1 and -Sm2) or neither (GL2) by siRNA depletion of TGFβR1. All graphs: *, p≤0.05; *, p≤0.01; ***, p≤0.001 relative to controls based on t-test.

Figure S11. CLDN7 regulation of invasion. A., B. Representative Western blot analysis of indicated proteins (A) and quantification of CLDN7 expression (**B**) in pCMV6-control/SCR and pCLDN7/SCR stably transfected

A549 cells. **C**., **D**. Quantification (**C**) and representative images (**D**) of Matrigel invasion for pCMV-control/SCR and pCLDN7/SCR stably transfected A549 cells. **E., F.** Western blot analysis (**E**) and quantification of CLDN7 expression (**F**) in 344SQ cells expressing MSI2 (SCR) or stably MSI2-depleted (-m1) transiently transfected with GL2 control or CLDN7 siRNAs. **G.** Quantification of Matrigel invasion assay for cells in **E, F**., based on three experiments. All graphs: *, p≤0.05; *, p≤0.01; ***, p≤0.001 relative to controls.

Table S1. Primers used in RT-QPCR analysis. Expression of genes noted in left column were analyzed by Taqman or SYBR Green assays, using primers indicated in columns 2-4 as noted.

Table S2. Patient characteristics for the primary NSCLC tumors arrayed in tissue microarray (TMA).

Table S3. Patient characteristics for the analyzed grouped NSCLC samples (normal, primary tumor and lymph node metastasis).

Table S4. Sequences of siRNA mixtures and shRNA used in gene knockdowns. Data represent siRNA pools (two independent siRNAs/pool) used for depletion of the genes indicated, for function testing experiments.

Table S5. Antibodies used for RPPA analysis. A list of antibodies used with corresponding catalog numbers, validation status (2013), provided by MD Anderson Cancer Center RPPA Facility.

2. Supplemental Methods.

Quantitative RT–PCR analysis. Total RNA was isolated using a Qiagen AllPrep DNA/RNA Mini Kit (#80204) and tested for quality on a Bioanalyzer (Agilent Technologies, Santa Clara, CA). RNA concentrations were determined with a NanoDrop spectrophotometer (Thermo Fisher Scientific, Waltham, MA). RNA was reverse transcribed using Moloney murine leukemia virus reverse transcriptase (Ambion-Thermo Fisher Scientific, Waltham, MA) and a mixture of anchored oligo-dT and random decamers (Integrated DNA Technologies, Coralville, IA). Two reverse-transcription reactions were performed for each sample using either 100 or 25 ng of input RNA. Aliquots of the cDNA were used to measure the expression levels of the genes using the primers listed in Supplmentary Table S1. The assays were from Applied Biosystems (Thermo Fisher Scientific Waltham, MA) or designed with Primer Express as indicated in Table S1. They were used in combination with Taqman Universal Master mix or Power SYBR Green master mix (Applied Biosystems, Thermo Fisher Scientific Waltham, MA) and run on a 7900 HT sequence detection system (Applied Biosystems, Thermo Fisher Scientific Waltham, MA). Cycling conditions were 95°C, 15 min, followed by 40 (two-step) cycles (95°C, 15 s; 60°C, 60 s). Ct (cycle threshold) values were converted to quantities (in arbitrary units) using a standard curve (four points, four fold dilutions) established with a calibrator sample. Ppib and POLR2F were used as normalizers. For each sample, the values were averaged and standard deviation of data derived from two independent PCR experiments.

siRNA Targeting Sequences: Small interfering RNAs (siRNAs) were obtained from GE Dharmacon (Lafayette, CO). See Supplementary Table S4 for sequences used.

shRNA Targeting Sequences and lentivirus production: Short hairpin RNAs (shRNAs) were obtained from SIGMA-ALDRICH (St Louis, MO). See Supplementary Table S4 for sequences used. To prepare lentivirus for introduction of shRNAs into NSCLC cells, HEK-293T cells were transfected with shRNA lentivirus prepared in the pLKO.1 system (Addgene, Cambridge, MA), with the psPAX2 and pMD2.G packaging plasmids. Media containing lentiviral particles was collected on day 4. Subsequently, lung cancer cells were infected with lentivirus and selected by growth in RPMI 1640 with 10% FBS and puromycin, using standard methods.

***cDNA ORF Sequences*.** cDNA ORF inserts were obtained from OriGene (Rockville, MD). See Supplementary Table S4 for sequences used.

***TCGA Analysis*.** The Cancer Genome Atlas (TCGA) results shown in this study are based upon provisional data generated by the TCGA Research Network (http://cancergenome.nih.gov/). Expression data for the 59 tumor-normal paired samples for the lung adenocarcinoma study were downloaded from https://tcga-data.nci.nih.gov/. Z-score corresponds to the mRNA expression of the tumor sample minus the mean expression in the reference sample divided by the standard deviation of expression in the reference sample.

Kaplan-Meier analysis for overall survival (OS). Was performed using http://kmplot.com online software with JetSet option for the optimal MSI2 probe, auto select for the best cutoff and censore at threshold settings applied (5).

***Mouse models for tumor growth*.** All experiments involving mice were performed according to protocols approved by Institutional Animal Care and Use Committees (IACUCs) at M.D. Anderson Cancer Center or the Fox Chase Cancer Center. Orthotopic xenograft experiments were performed in syngeneic wild type 129Sv mice of at least 6 weeks of age. Intrathoracic injections of 10^6 cells into the left lung in single-cell suspension were placed in a volume of 100 µl of complete media as previously described (1). Animals were monitored regularly and euthanized on day 28. Necropsies were performed to quantify the number of metastases to mediastinal lymph nodes, chest wall and distant extrathoracic sites.

For sub-cutaneous xenografts, immunocompromised eight week-old C.B17 SCID mice were inoculated

subcutaneously with shRNA-transfected derivatives of 344SQ syngeneic lung cancer cells into the left and right flank subcutaneously using a 27G needle, 100 ul volume. Mice were palpated twice a week after tumor cells implantation to assess tumor onset. Tumor volume was determined by external caliper twice a week (body weight also was monitored twice weekly), the greatest longitudinal diameter (length) and the greatest transverse diameter (width) were determined. Tumor volumes based on caliper measurements were calculated by the modified ellipsoidal formula: *Tumor volume = 1/2(length × width^2).* After three weeks mice were euthanized and tumors and lungs were collected.

***Tissue preparation, Histology, Quantitative Analysis*.** Lungs and tumors were collected. Tissues were collected and fixed in 10% phosphate-buffered formaldehyde (formalin) 24-48 hrs, dehydrated and embedded in paraffin. Tissues were processed by dehydration in a series through ethanol followed by xylene (70% ethanol, 3 hr; 95% ethanol, 2 hr; 100% ethanol, 2 hr; ethanol-xylene, 1hr; xylene, 3hr) then immersed in paraffin. Paraffin blocks were cut into 5 µm sections, mounted on microscope slides, and stored at room temperature until used. Prepared specimens were analyzed by hematoxylin and eosin (H&E) staining (Sigma-Aldrich, St. Louis, MO). Tumor sections were immunostained with antibodies to Ki-67 (DAKO, Carpinteria, CA) to allow quantitation of proliferation, and with antibodies to cleaved caspase (Cell Signaling, #9661) to allow quantitation of apoptosis. Immunohistochemistry and H&E were performed by standard protocols. Immunostained slides were scanned using an Aperio ScanScope CS scanner (Aperio, Vista, CA) and Vectra Automated Quantitative Pathology Imaging System (Perkin Elmer, Waltham, MA). Scanned images then were viewed with Aperio's image viewer software (ImageScope). Selected regions of interest were outlined manually by a pathologist (KQ Cai). Expression levels of the proliferative index marker Ki-67 or the cleaved caspase indicator of apoptosis were quantified using Vectra Automated Quantitative Pathology Imaging System specific protocols and algorithms. H-score was calculated as follows: the percentage of cells at each staining intensity level was calculated, and an H-score was assigned and calculated for each slide using the following formula: [1 × (% cells 1+) + 2 × (% cells 2+) + 3 × (% cells 3+)](2, 3). H-scores were subsequently used for results analysis. The area of lung metastases was assessed using the Vectra automated multispectral slide analysis system, using specific protocols and algorithms designed for the identification of tumor tissue.

Tissue Microarrays (TMAs) Non-small cell lung cancer surgical specimens resected from 1997 to 2012 from the Fox Chase Cancer Center (FCCC) Biosample Repository Facility were used to construct tissue microarrays (TMA). Tissue from each tumor was placed in two unique spots on each TMA. All samples were obtained from primary tumors and/or nodal metastases at the time of initial resection. Clinical information (Supplementary Table S3) was available from the repository database and abstracted from clinical databases in an anonymized fashion. At the time of tissue acquisition, patients provided Institutional Review Board (IRB)–approved informed consent for storing tissue and reviewing de-identified clinical data. For TMAs, automated image capture was performed by the HistoRx PM-2000 (HistoRx) (New Haven, CT), using the AQUAsition software. High-resolution monochromatic digital images of the cytokeratin staining visualized with AF555, DAPI, and target staining with Cy5 were captured and saved for each tumor histospot. Tumor mask was created from the cytokeratin image of each histospot, representing areas of the epithelial tumor. Histospots were excluded if the tumor mask represented less than 5% of the total histospot area. DAPI immunoreactivity defined the nuclear compartment. Images were visually inspected and cropped for unfavorable factors such as “out of focus,” debris, or damaged specimen before automatic analysis. An AQUA score was generated by dividing the sum of target signals within the tumor mask. AQUA scores were normalized to the exposure times and bit depth at which the images were captured, allowing scores collected at different exposure times to be compared directly. The nuclear scores from two non-overlapping images were averaged for each case.

***Paired Analysis of NSCLC specimens*.** Non-small cell lung cancer surgical specimens from the University of New Mexico Human Tissue Repository Facility (HTR) were used to conduct IHC. All samples were obtained from normal lung, primary tumors and/or nodal or distant metastasis at the time of initial resection. Clinical information (Supplementary Table S3) was available from the repository database and

abstracted from clinical databases in an anonymized fashion. At the time of tissue acquisition, patients provided Institutional Review Board (IRB)–approved informed consent for storing tissue and reviewing de-identified clinical data. IHC slides stained for MSI2 were analyzed using APERIO Spectrum scanner (Leica Biosystems, Buffalo Grove, USA).

***SDS-PAGE and Western Blots*.** For Western blotting, cells were disrupted in CelLytic M lysis buffer (Sigma-Aldrich, St. Louis, MO) supplemented with protease and phosphatase inhibitor cocktails (Roche, Basel, Switzerland). Whole cell lysates were used directly for SDS–PAGE and Western blotting, using standard procedures. Primary antibodies included rabbit anti-MSI2 (Abcam #ab76148), anti-MSI1 (Abcam #ab52865), anti-NUMB (Abcam #ab14140), anti–FN1 (Abcam #ab6328), anti-TGFβR1 (Cell Signaling #3712), anti-SMAD3 (Cell Signaling #9523) and anti-SMAD3p (Cell Signaling #9520), Claudin-7 (Novus #67525), Claudin-3 (Abcam #ab15102), Claudin-5 (Abcam, #ab15106), FN1 (Abcam #ab6328), anti-E-Cadherin (Cell Signaling #3195), anti-β-Actin (Abcam #ab49900), anti-ZEB1(Cell Signaling #3396), anti-ZEB2 (Santa Cruz #271984), anti-FOXC2 (Abcam #65141), anti-SNAIL(Abcam #180714), anti-SLUG(Abcam #51772), anti-VMN (Cell Signaling #5741)*.* Secondary anti-mouse and anti-rabbit horseradish peroxidase–conjugated antibodies (GE Healthcare, Little Chalfont, UK) were used at a dilution of 1:10,000 for visualization of Western blots and blots developed by chemiluminescence using the West-Pico system (Pierce, Waltham, MA). Image analysis was done using ImageJ (National Institutes of Health, Bethesda, MD), with signal intensity normalized to β-actin or total level of detected proteins. Data was analyzed in Excel by paired t-test to determine statistical significance.

***Immunofluorescence*.** Cells were fixed with 4% paraformaldehyde (10 min) and then cold methanol (5 min), permeabilized with 1% Triton X-100 in PBS and blocked with 3–5% BSA in PBS. Samples were then incubated with the primary antibodies overnight at 4°C. Primary antibodies were: anti-Claudin-7 (Novus #67525), anti-Claudin-3 (Abcam #ab15102) and anti E-Cadherin (BD Transductions 610182). Following rinse in PBS + 0.01% Tween, samples were incubated for 1 hour with an Alexafluor 488, 568 or 647 tagged donkey anti-rabbit, mouse, or goat secondary antibody (Life Technologies, Eugene, OR), and counterstained with a 2 μmol/L 4′, 6-diamidino-2-phenylindole (DAPI) (Life Technologies, #1652731, Eugene, OR) solution. Samples were imaged using a Nikon C1 Spectral confocal microscope (Nikon, Melville, NY) equipped with a numerical aperture (NA) 1.40, oil immersion, 63x Plan Apo objective (Nikon). Images were acquired at room temperature using EZ-C1 3.8 (Nikon) software and analyzed with MetaMorph (Molecular Devices, Union City, CA).

***Analysis of cell migration*.** Time-lapse multifield experiments were performed in phase contrast on an automated inverted Nikon Eclipse TE300 microscope equipped with thermal and CO_2 regulation (Nikon, Melville, NY). 2 x10^6 cells of each clone were plated on a 6 well plate a day prior to imaging. The next morning cells were "scratched" with a p200 pipet tip. Immediately after, the cells were imaged at 15 minute intervals with a 100× objective and a CCD camera (EZ CoolSnap, Roper) and then "stacked" into movies using Metamorph (Universal Imaging) software. The videos were analyzed using the ImageJ public domain software (http://imagej.nih.gov/ij/docs/guide/146.html). Visual fields were divided into different coordinates and the distance between the invasion fronts of the cells was measured at each of the assigned longitudes at 0, 1, 3, 6, 9 and 12 hour time points. The distance was then converted from pixels into millimeters using a premeasured scale bar (1mm= 406,001 pixels) and normalized to 0 hour being 1 for each video. Statistical differences were calculated for each time point using Excel software, t-test.

As a second approach, the upper chambers of migration chambers (3465-024-K Trevigen, Gaithersburg, MD) were seeded with serum-starved cells (1 × 10^5 cells per well) in triplicate wells. Medium (RPMI 1640/DMEM), with 10% FBS, was placed in the lower and upper chambers, respectively. Mitomycin C at a concentration of 10 μg/ml was added to the upper chamber to inhibit cell proliferation. Cells were incubated at 37°C for 24 hours. After incubation, the cells remaining on the upper surface of the membrane were removed with cotton swabs. The cells on the lower surface of the membrane were fixed and stained with crystal violet and visualized under a Nikon Eclipse TE 2000-U microscope at 20X magnification and CRI Nuance Multispectral Imaging System. Four visual fields were photographed and counted per chamber, and

the results were analyzed with Image J and Excel expressed as the mean relative cell count number per visual field ± SEM with two-tailed t-test showing statistical significance.

Cell proliferation assays. Cells (1-2 × 10^3 cells/well) were plated in quadruplicate in RPMI1640 media with 10% FBS in 96-well cell culture plates for 5 days. On days 1-5, *CellTiter-Blue*® (Promega, Fitchburg, WI) or WST-1 Sigma-Aldrich (St. Louis, MO) reagent (for the 393P cell line) were added to each well; after 2 hours incubation at 37°C, optical density readings were made in the 570 – 600 and 420-480 nm wave-length range, responsively, using *Perkin*-Elmer ProXpress Visible-UV-fluorescence 16 bit scanner (Perkin-Elmer, Waltham, MA). As a second approach to measuring proliferation 1-2 x 10^3 cells for each model of interest were plated in 96-well plates, and wells fixed and stained with DAPI at 24 hour intervals from days 1-5 after plating, then scored by automated microscope (ImageXpress Micro, Downingtown, PA).

Cell invasion assay. The upper chambers of growth factor–reduced Matrigel invasion chambers (354483; BD Biosciences, Franklin Lakes, NJ or 3483-024-01, Trevigen, Gaithersburg, MD) were seeded with cells (1 × 10^5 cells per well) in triplicate wells. Medium (RPMI 1640), with or without 10% FBS, was placed in the lower and upper chambers, respectively. Mitomycin C at a concentration of 10 µg/ml was added to the upper chamber to inhibit cell proliferation. Cells were incubated at 37°C for 24 hours. Cells that had invaded through Matrigel were visualized with crystal violet. Three microscopic fields (original magnification, 10X) were photographed and counted per chamber, and the results were expressed as the mean ± SEM of invaded cells from replicate wells and multiple independent experiments. Data was analyzed in Excel by paired t-test to determine statistical significance.

Spheroidal growth assay: A 3D culture sphere assay was run using the Cultrex 3D Spheroid BME Cell Invasion Assay kit (Trevigen, catalog # 3500-096-K) by the standart protocol. 344SQ and A549 were plated 1000 per well in the Spheroid Formation Extracellular Matrix with or without TGF-β at 10 or 100 ng/ml concentration and grown for 3 days. Then the invasion matrix was added on top. On day 5 pictures were taken with the NIKON Eclipse TE 2000U microscope and CRI Nuance Multispectral Imaging System FX and then analyzed with Image J to measure the spheres' size.

Overexpression studies. For overexpression of MSI2, a full-length cDNA encoding MSI2 (for sequence information, please refer to NM_138962.2) or empty vector was obtained from the human ORFeome collection and transferred to the following viral vectors via Gateway recombination and virus production following manufacturer's recommendations: pLenti63/V5 DEST (Thermo Fisher Scientific, Waltham, MA)(4). All overexpression studies were performed using newly transduced stable cell lines generated by single clone selection. In brief, MSI2 cDNA cloned into pLenti63/V5 DEST plasmid or was empty pLenti63/V5 DEST plasmid were transfected into 393p cells. Subsequently, lung cancer cells were selected by growth in RPMI 1640 with 10% FBS and selected in blasticidin. Individual clones were picked and validated for MSI2 overexpression by Western blot. For overexpression of claudin 7 (CLDN7), a lentiviral plasmid containing a full length ORF insert encoding human CLDN7, transcript variant 1(RC200530L1) was acquired from OriGene (Rockville, MD) and expressed in A549 NCLC cells using pLKO.1 system from Addgene (Cambridge, MA). Subsequently, lung cancer cells were selected by growth in RPMI 1640 with 10% FBS with puromycin and A'lenti CLDN7 cell line was validated for CLDN7 overexpression by Western blot. For overexpression of TGFβR1, the previously generated MSI2 shRNA depleted human and mouse NSCLC A559 and 344SQ cells were transfected with lentivirally expressed ORF TGFβR1, transcript variant 1 (CW301688, a modification of RC219514L1) from Origene, using the Addgene pLKO.1 system and selected in DMEM and RPMI 1640 with 10% FBS and blasticidin. Effectiveness of targeted gene expression in 3'-m1/TβR1 and A-h1/TβR1 cell lines was confirmed by Western blot analysis.

3. Supplementary References.

1. Onn A*, et al.* (2003) Development of an orthotopic model to study the biology and therapy of primary human lung cancer in nude mice. *Clin Cancer Res* 9(15):5532-5539.
2. Hirsch FR*, et al.* (2003) Epidermal growth factor receptor in non-small-cell lung carcinomas: correlation between gene copy number and protein expression and impact on prognosis. *J Clin Oncol* 21(20):3798-3807.
3. John T, Liu G, & Tsao MS (2009) Overview of molecular testing in non-small-cell lung cancer: mutational analysis, gene copy number, protein expression and other biomarkers of EGFR for the prediction of response to tyrosine kinase inhibitors. *Oncogene* 28 Suppl 1:S14-23.
4. Meerbrey KL*, et al.* (2011) The pINDUCER lentiviral toolkit for inducible RNA interference in vitro and in vivo. *Proc Natl Acad Sci U S A* 108(9):3665-3670.
5. Gyorffy B, *et al.* (2013) Online survival analysis software to assess the prognostic value of biomarkers using transcriptomic data in non-small-cell lung cancer, PLoSOne 18;8(12):e82241.

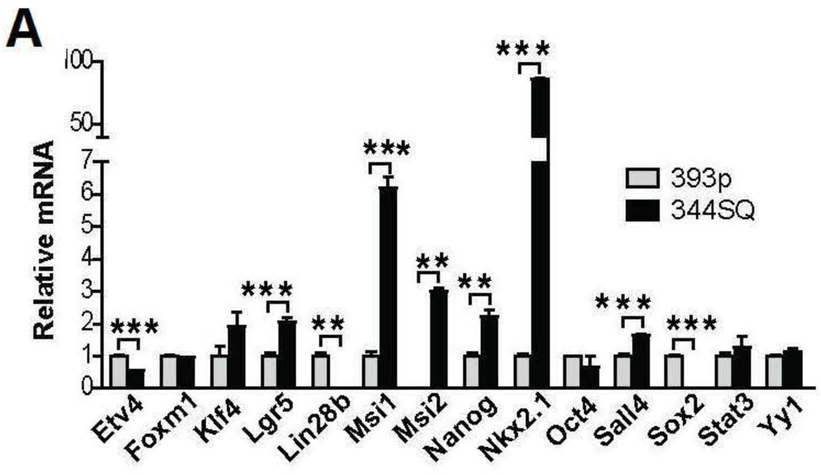

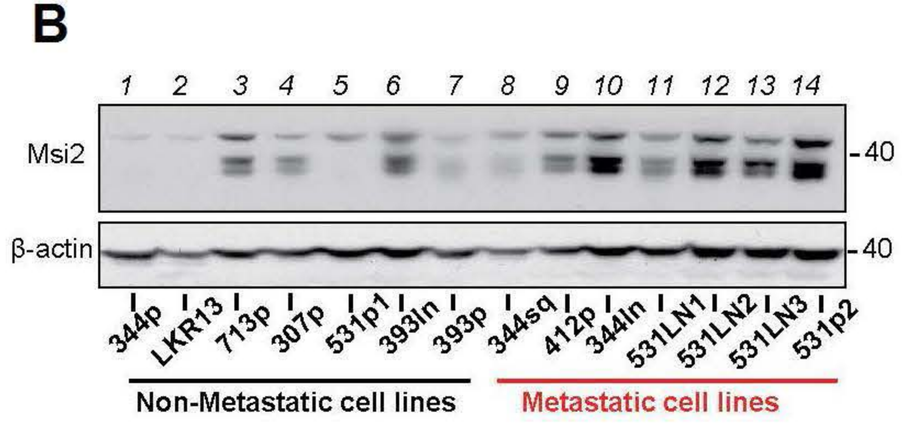

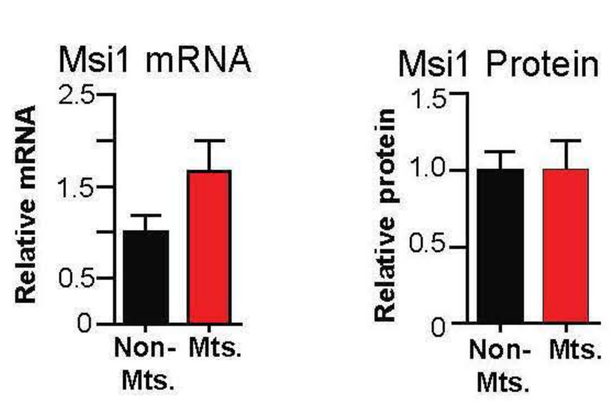

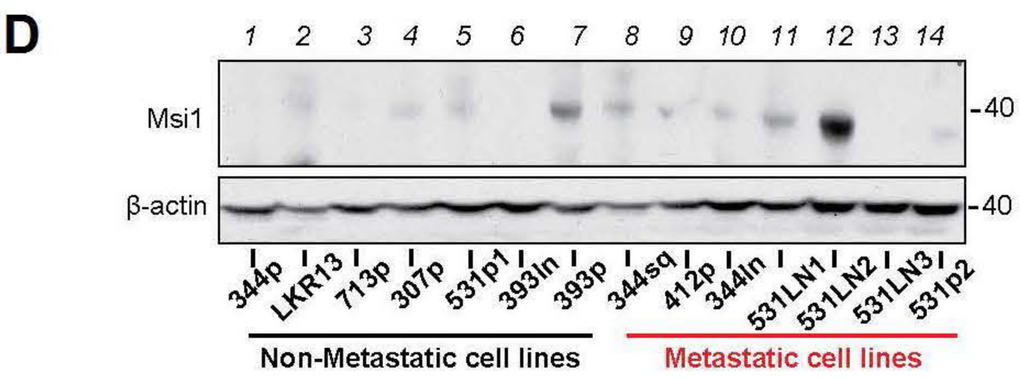

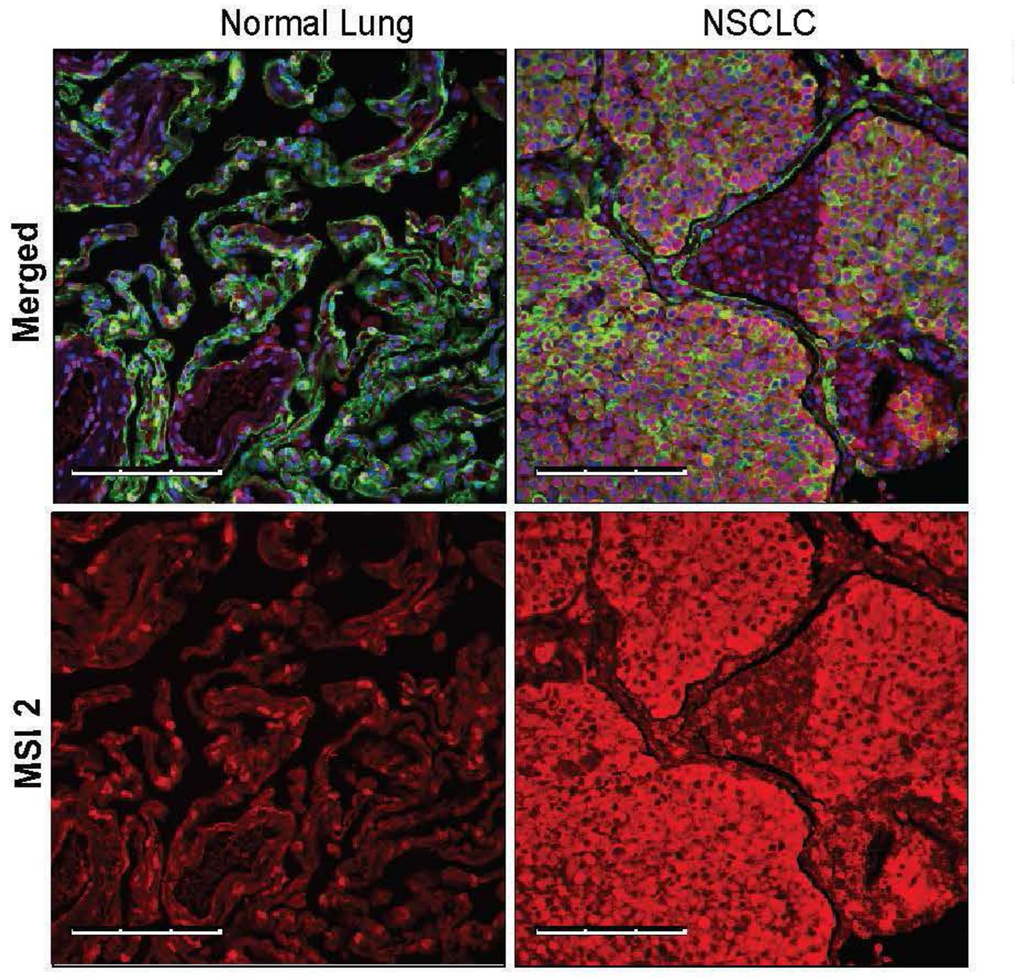

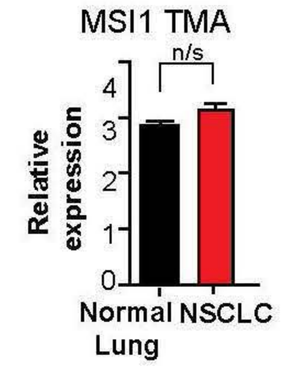

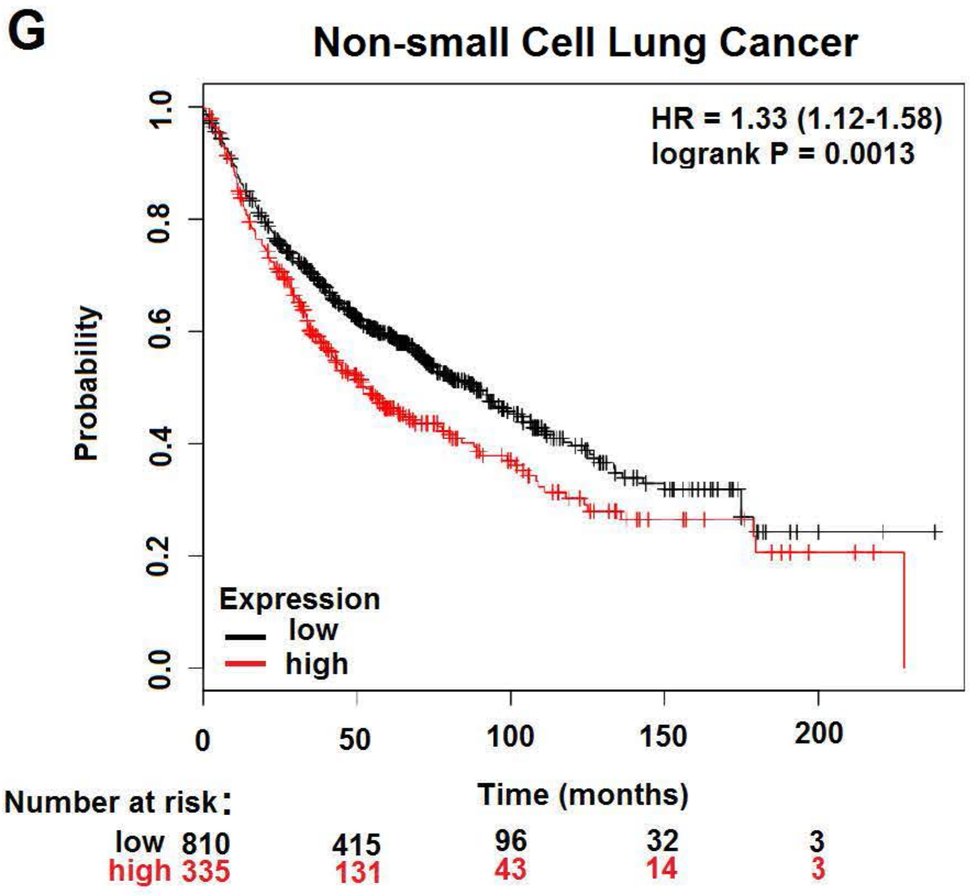

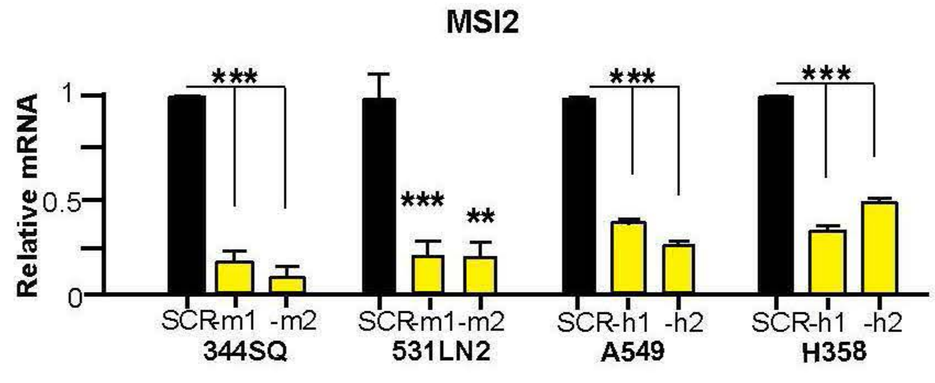

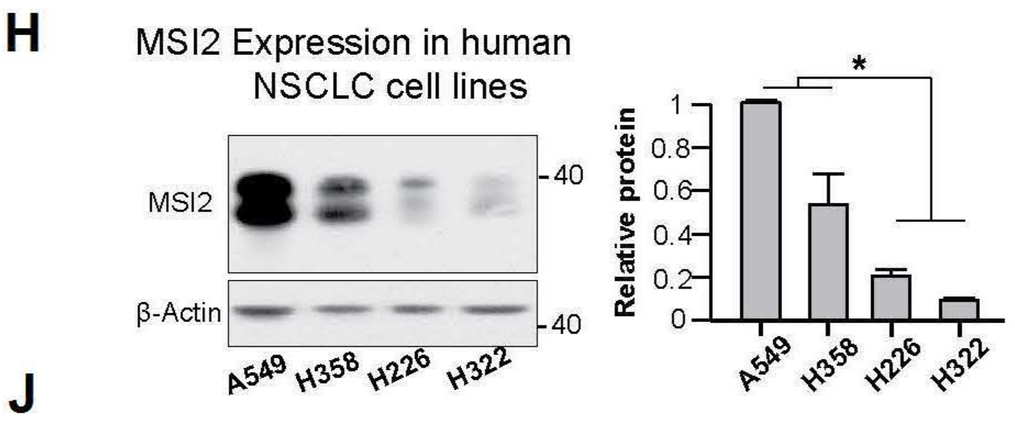

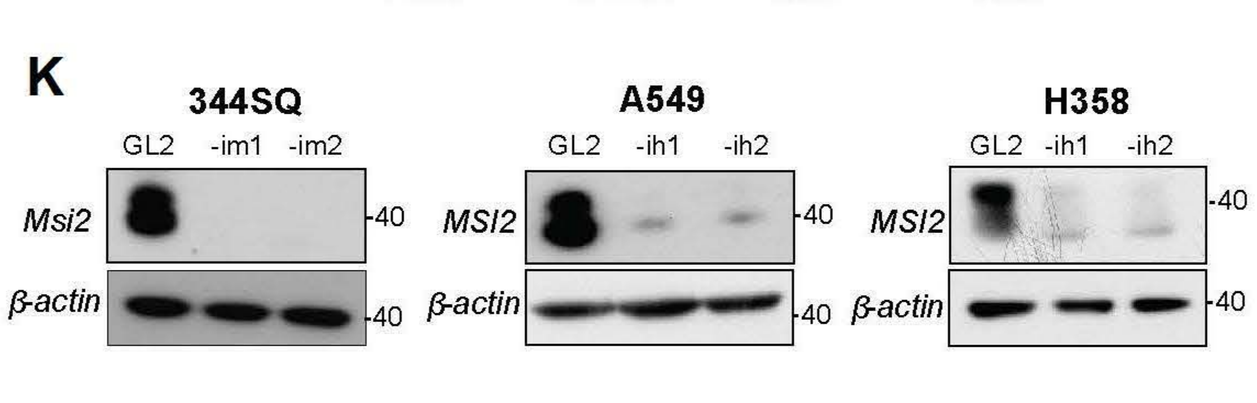

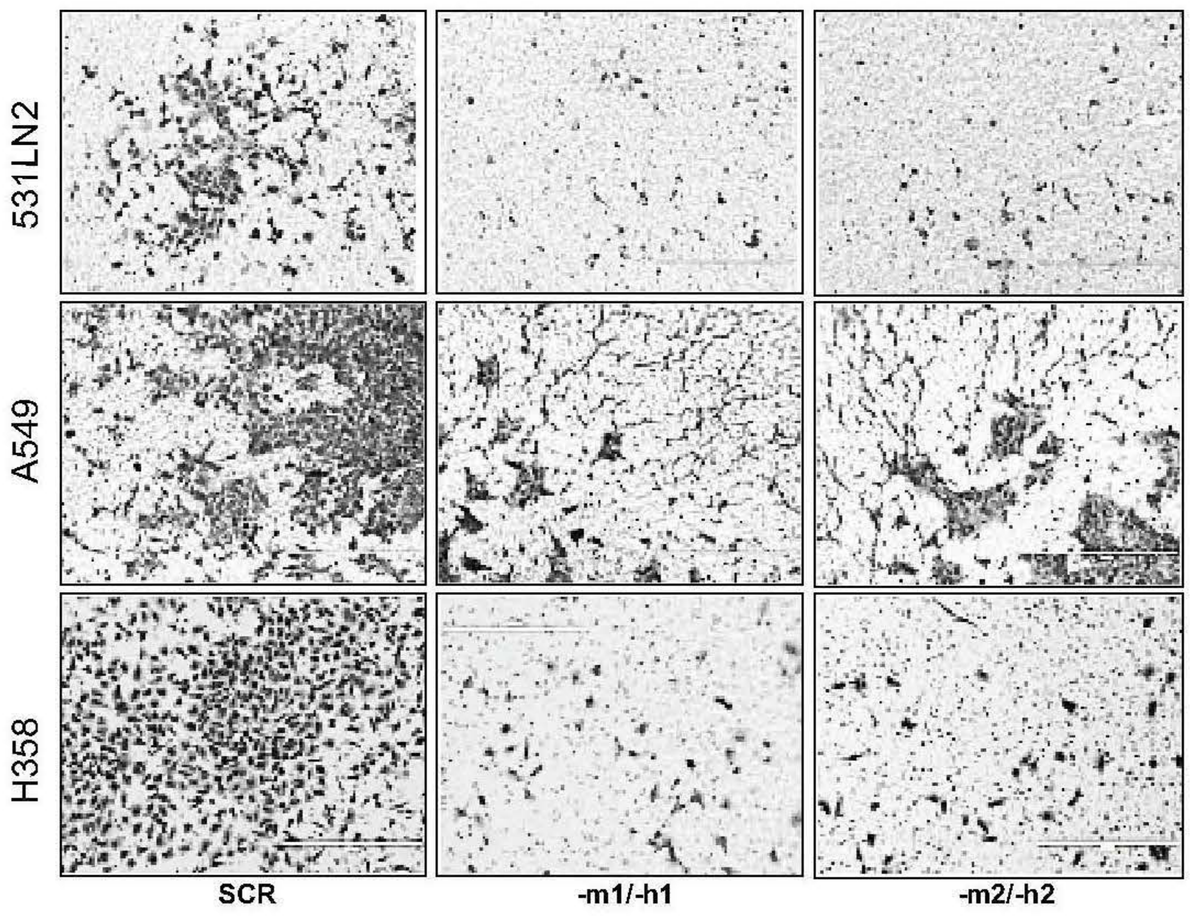

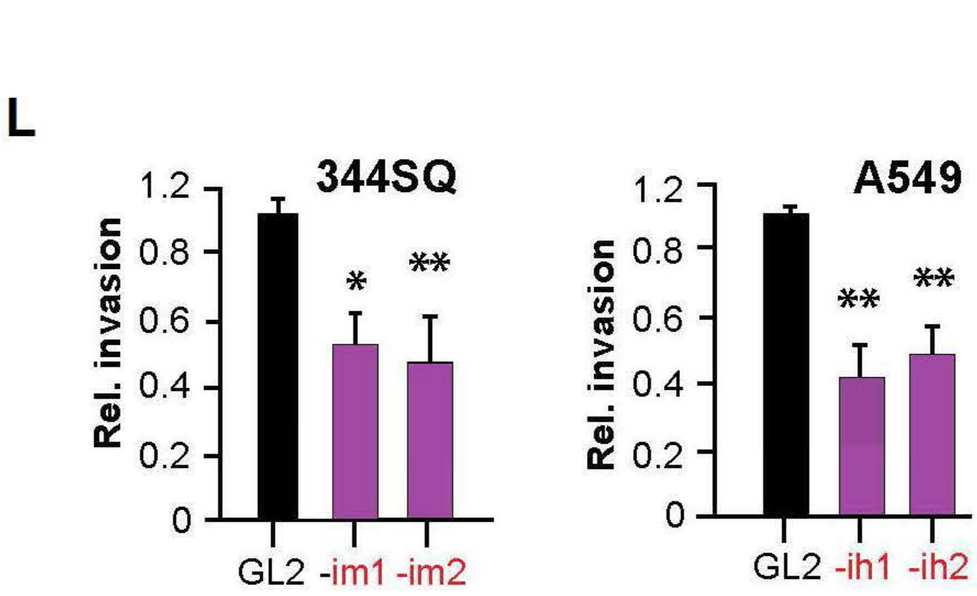

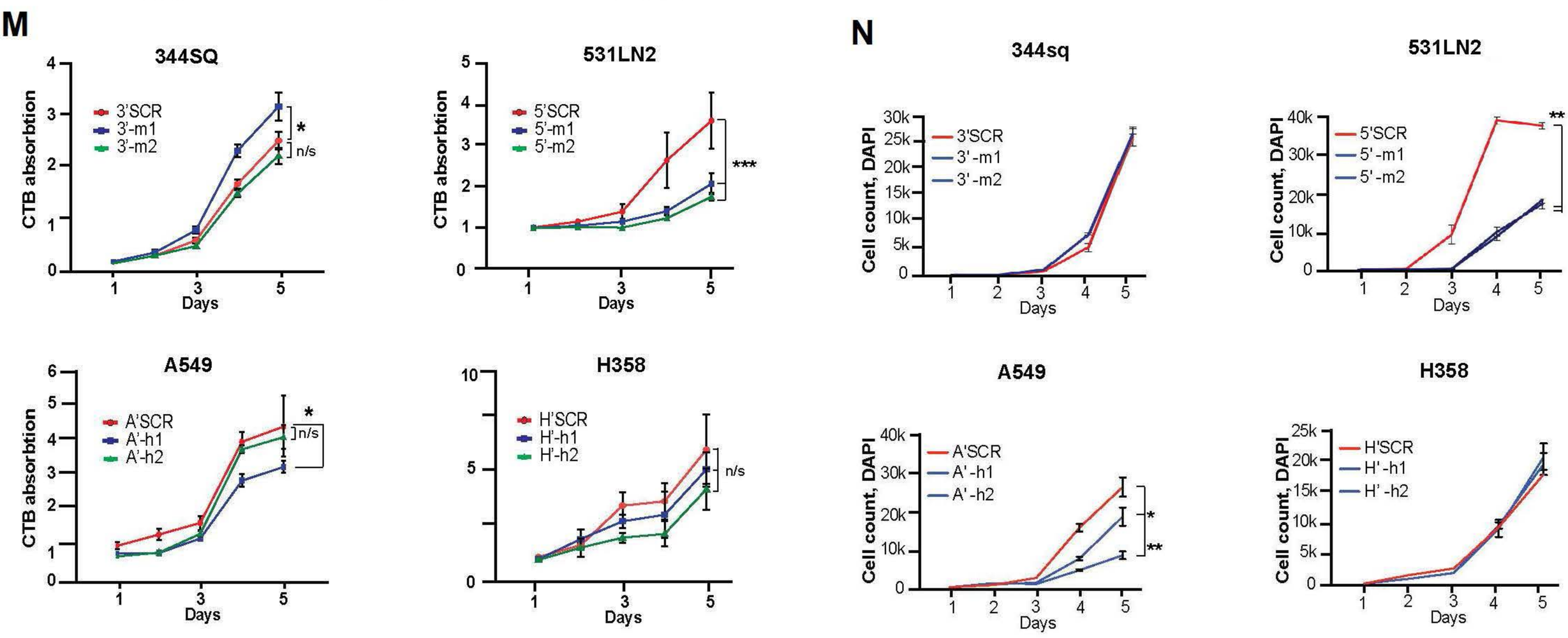

Kudinov et al, Figure S1.

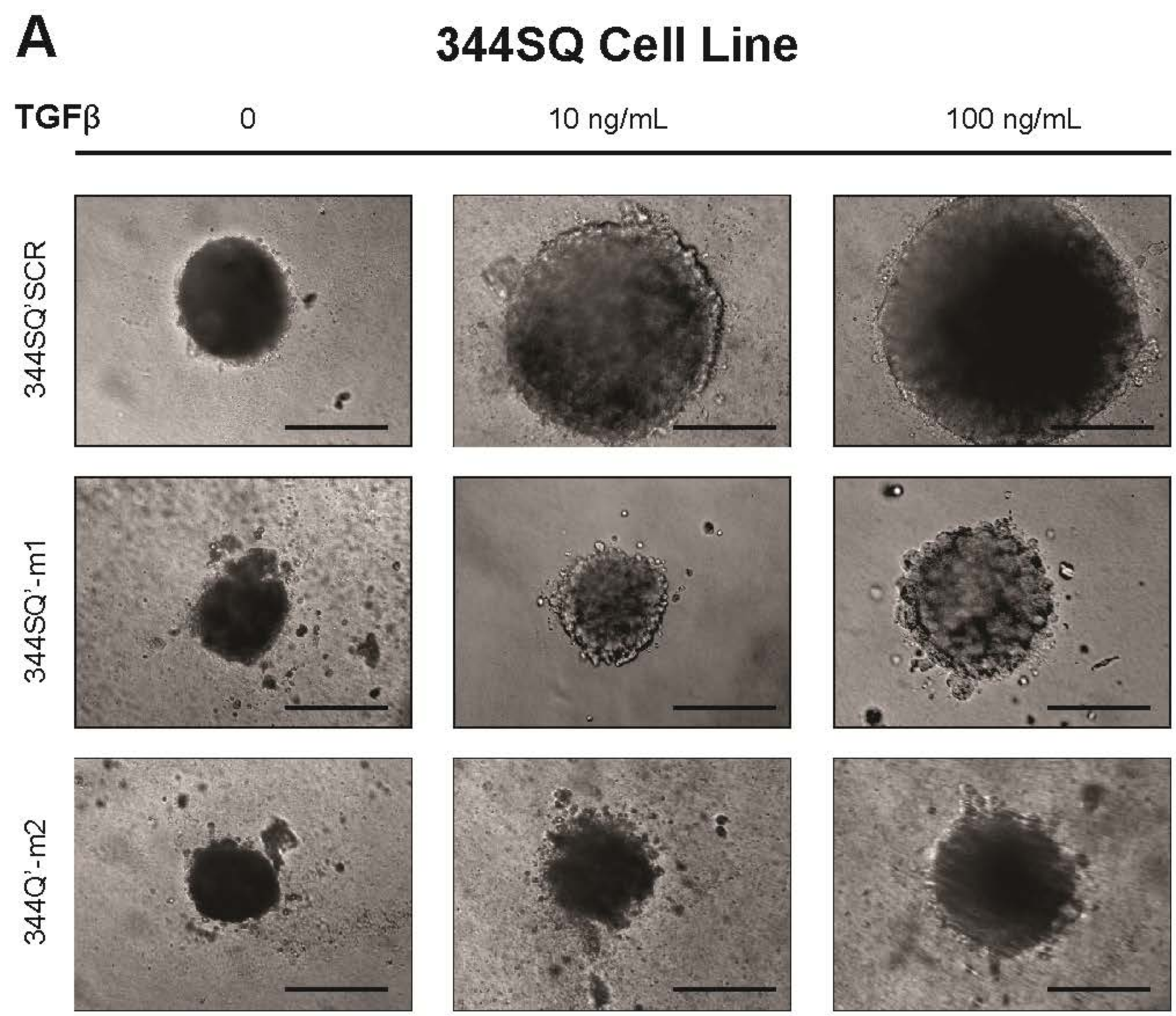

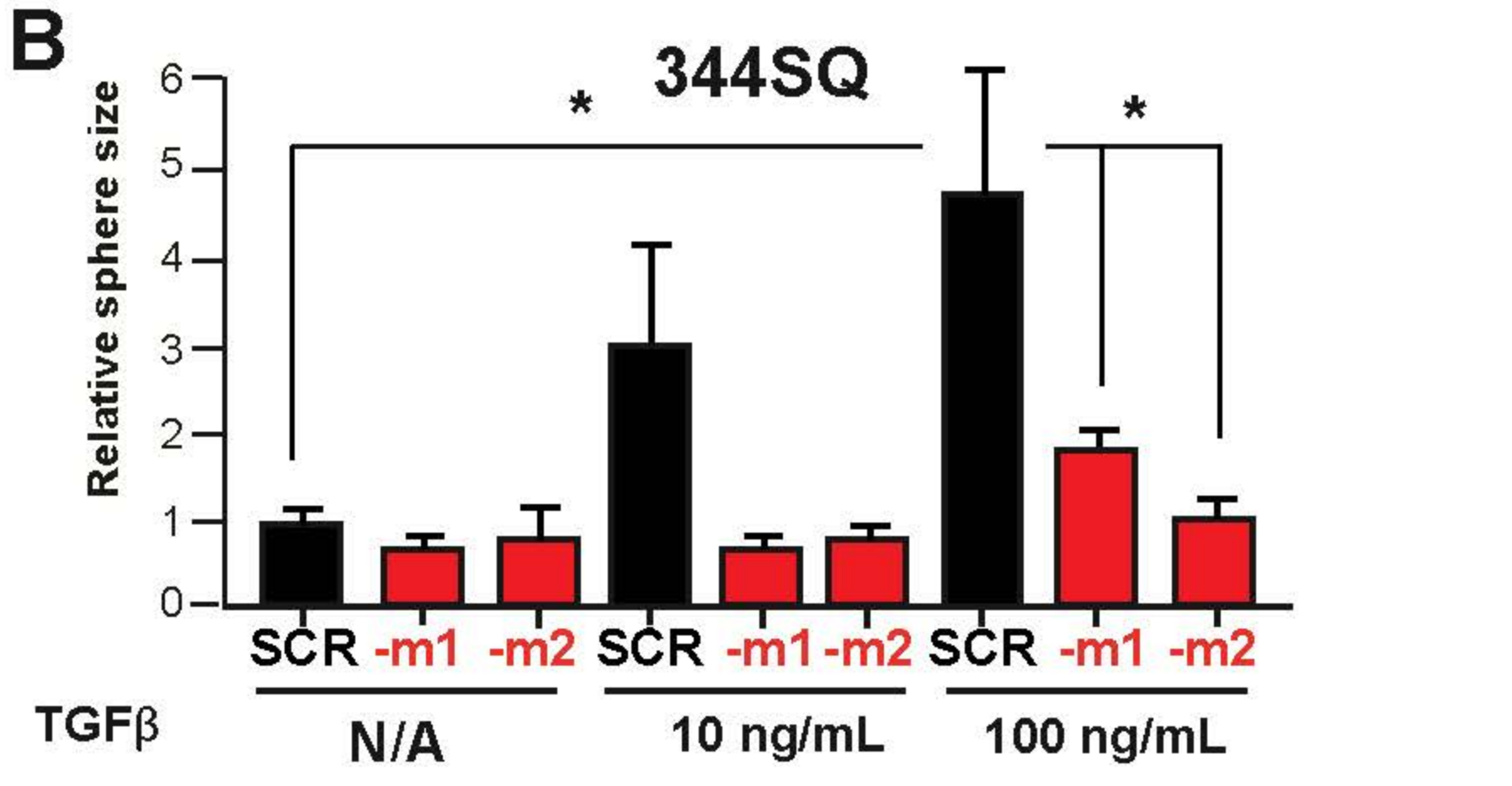

Kudinov et al, Figure S2

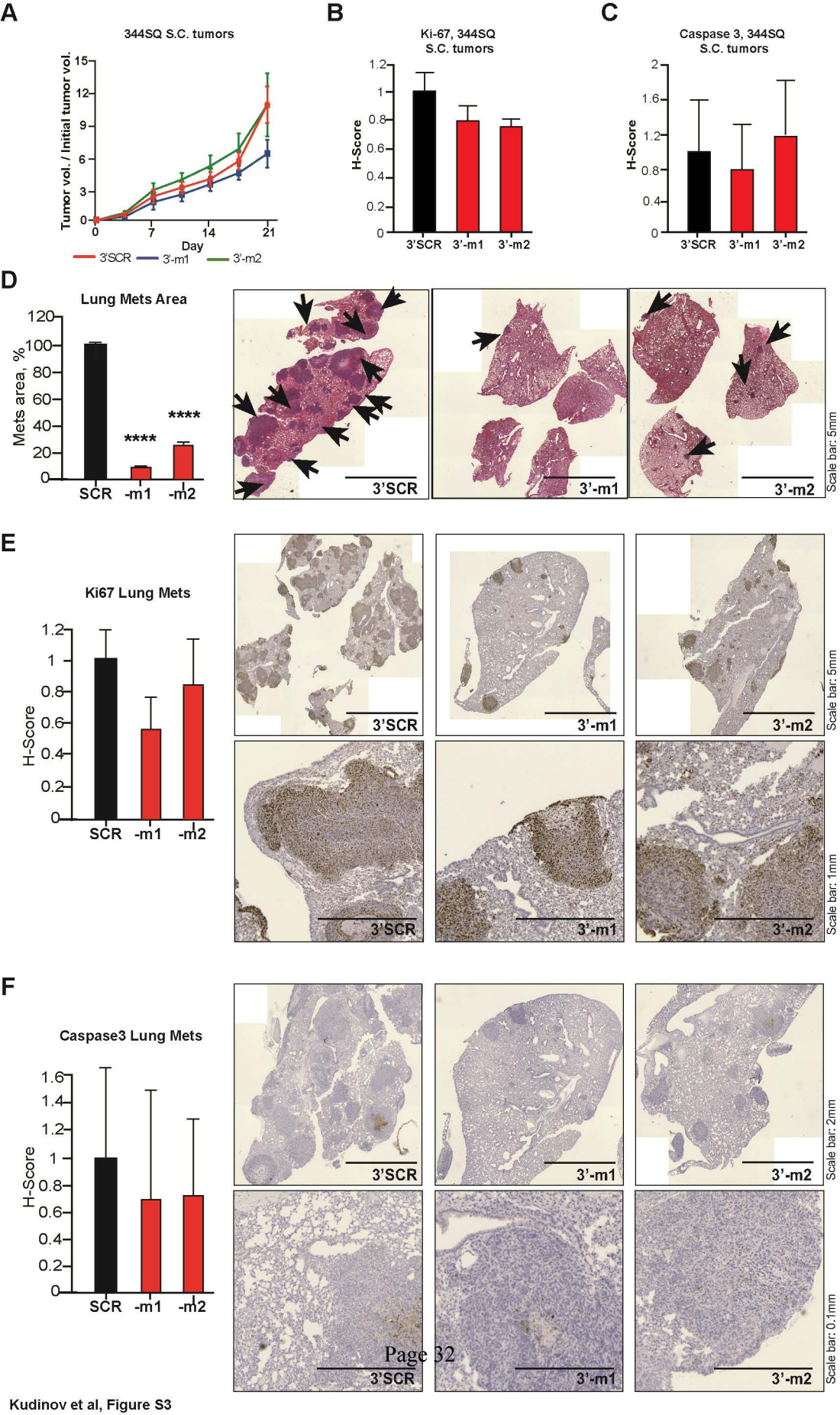

Kudinov et al, Figure S3

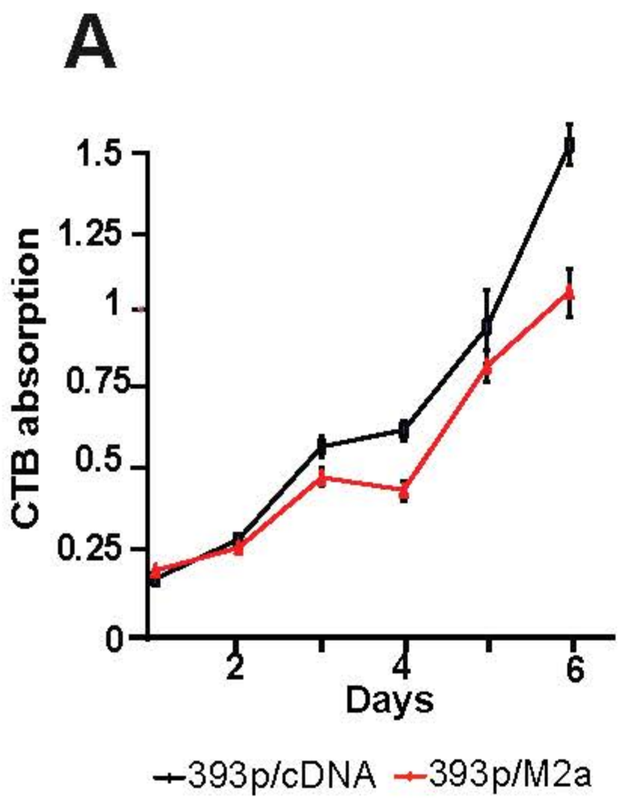

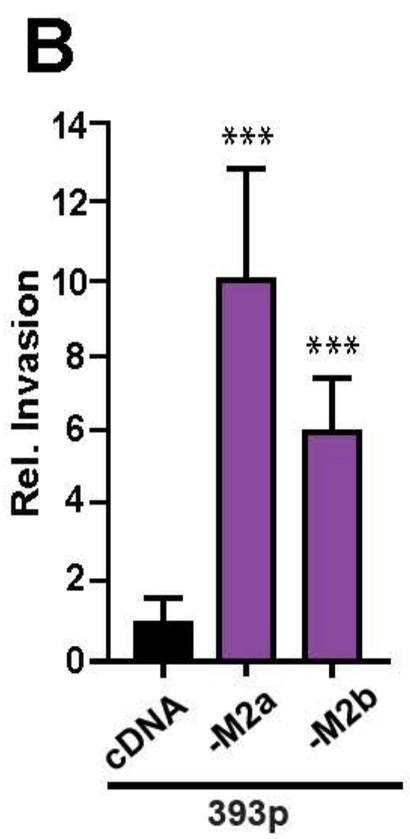

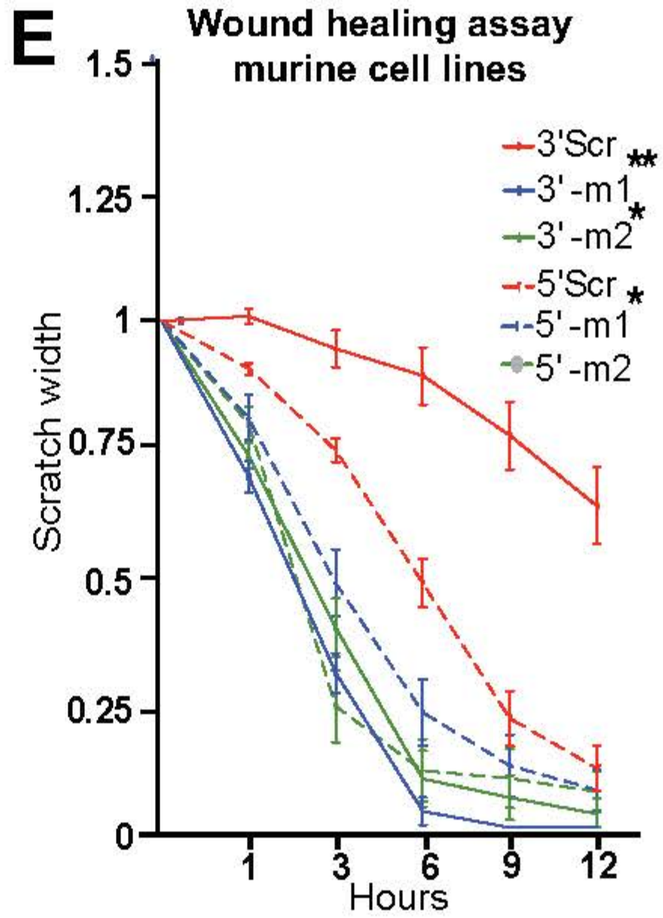

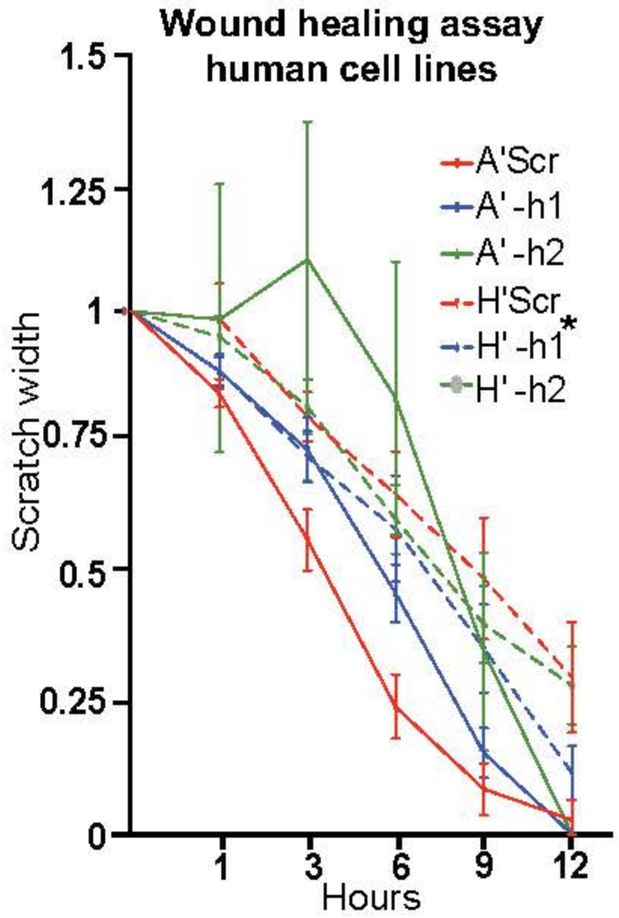

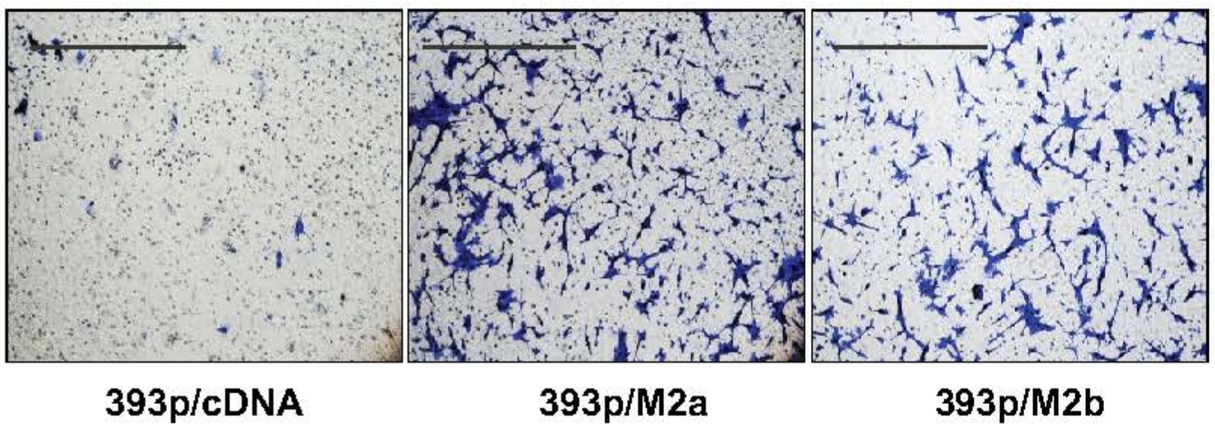

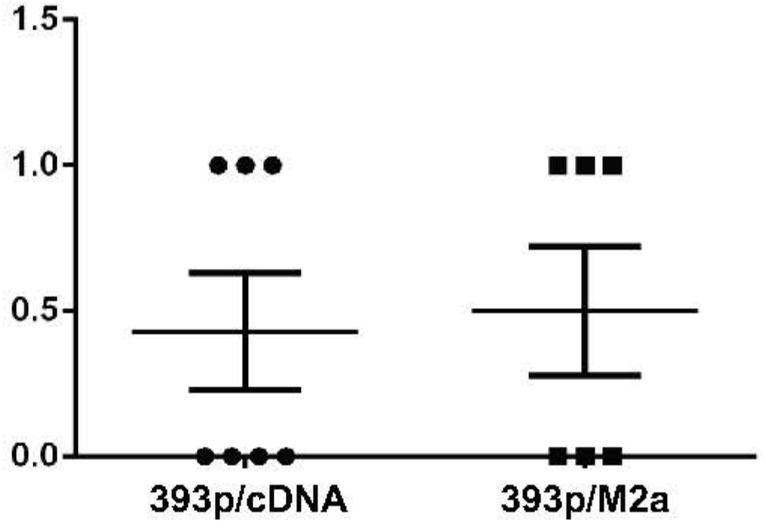

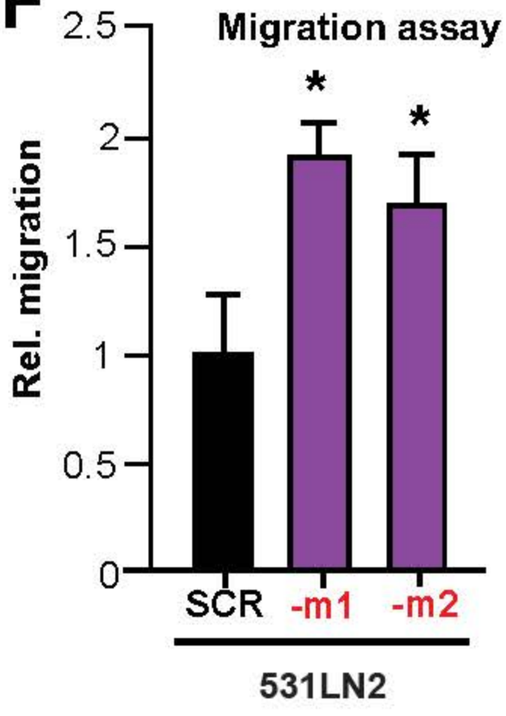

Kudinov et al, Figure S4.

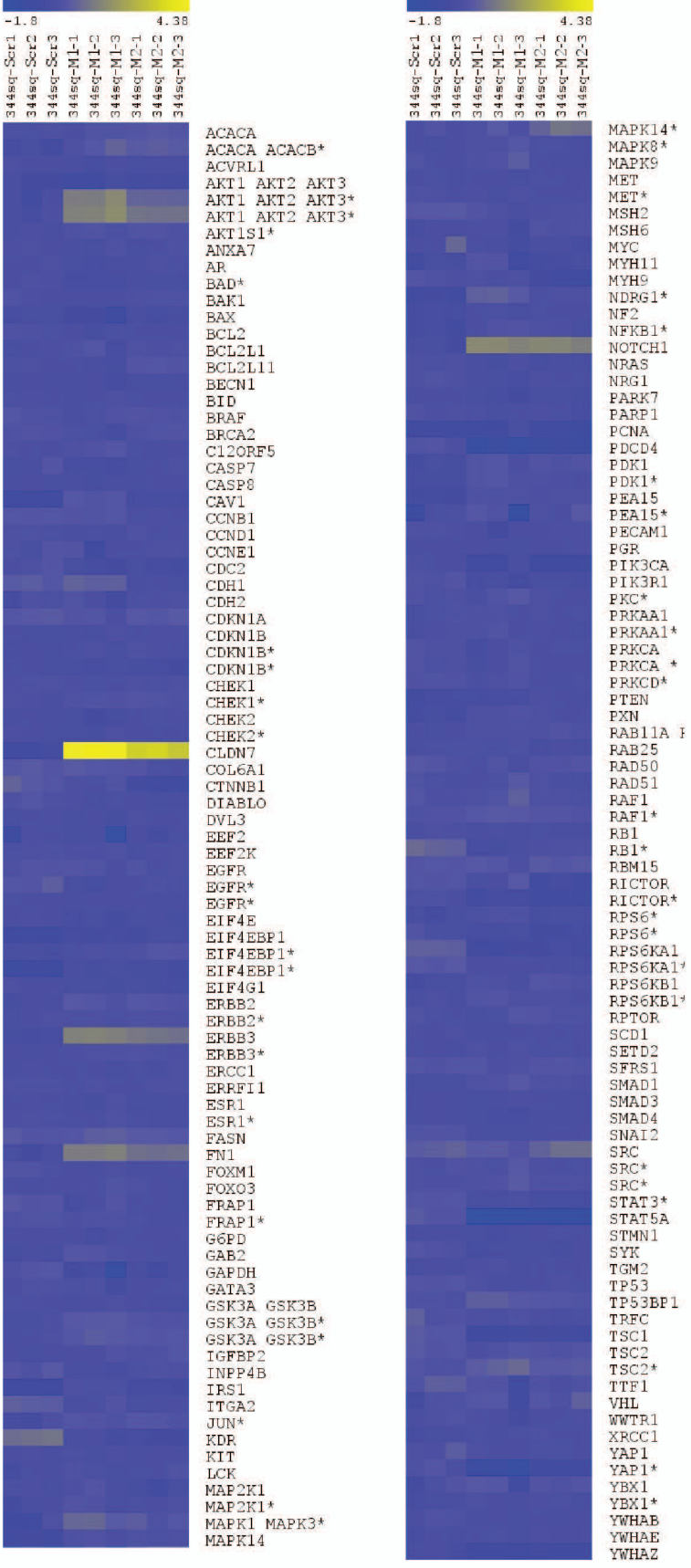

Kudinov et al, Figure S5.

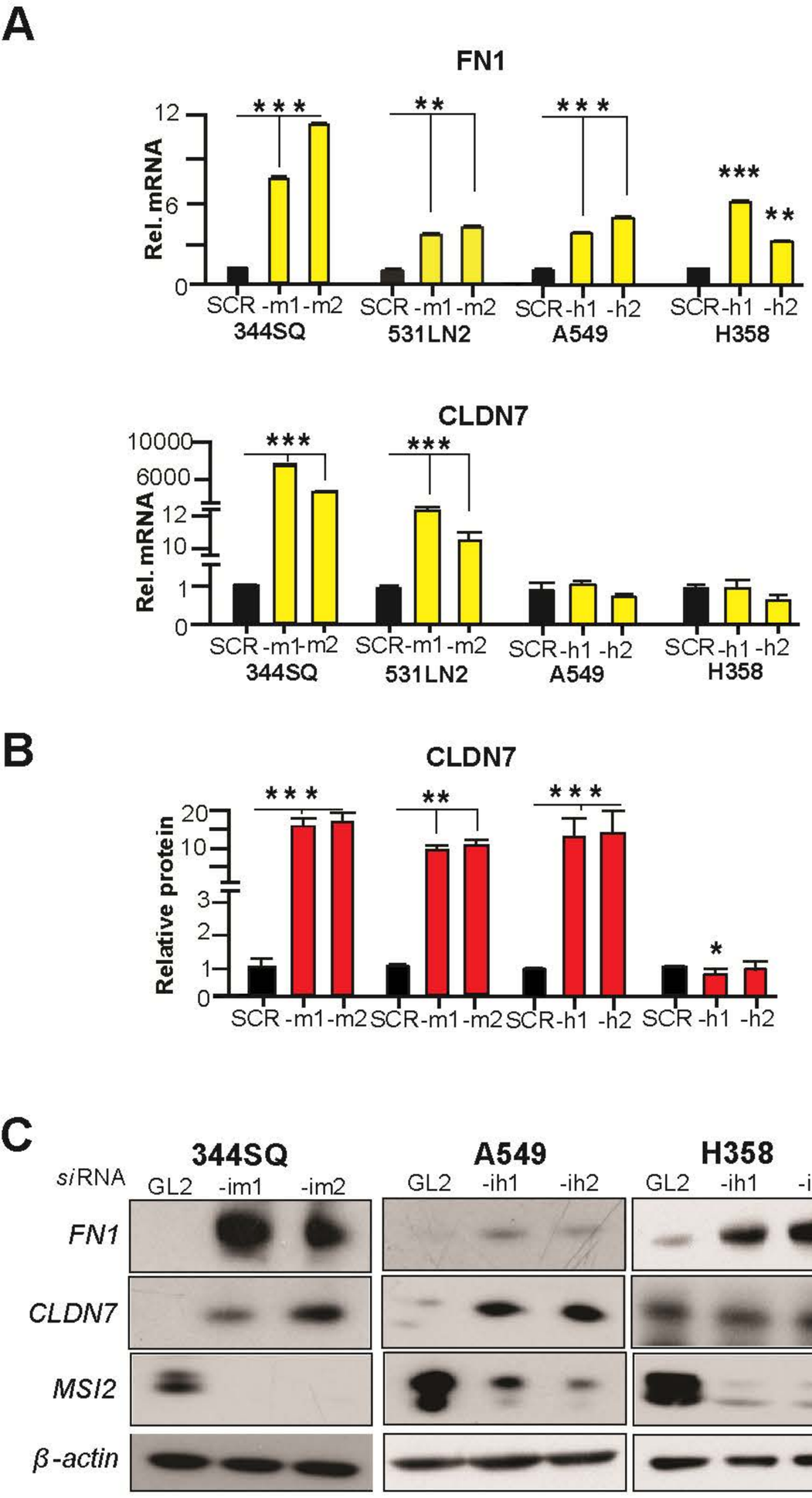

Kudinov et al, Figure S6.

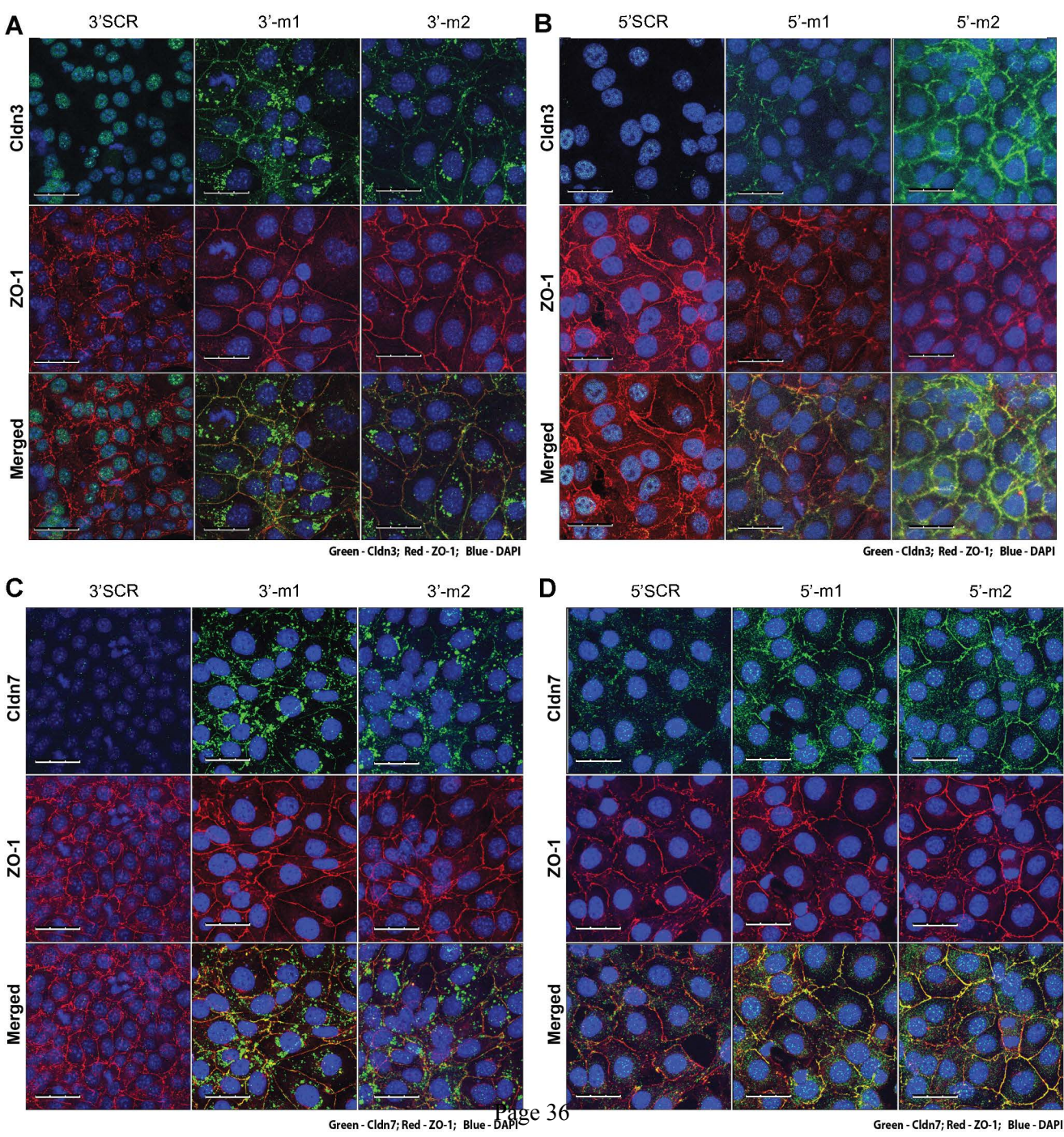

Kudinov et al, Figure S7.

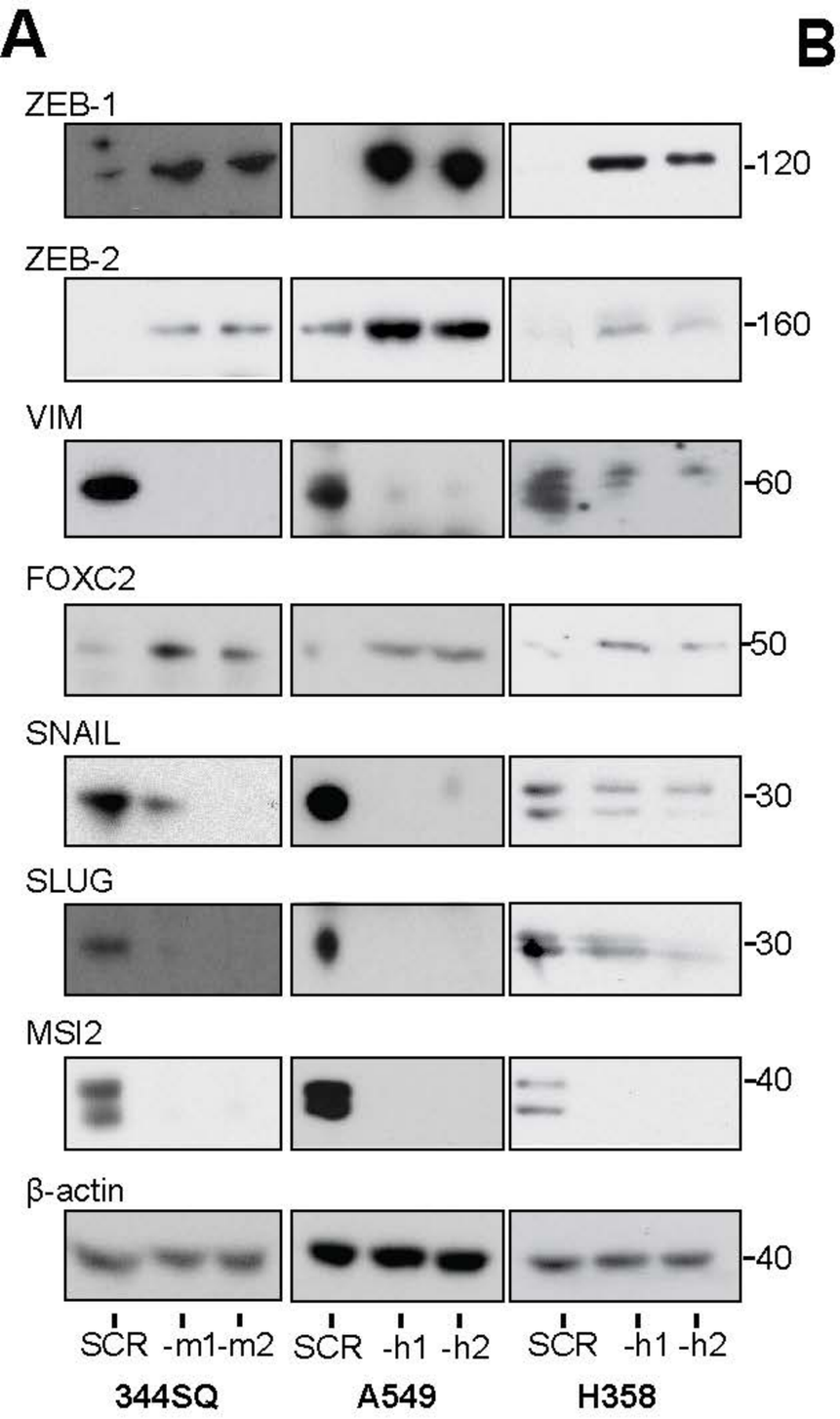
A
ZEB-1
ZEB-2
VIM
FOXC2
SNAIL
SLUG
MSI2
β-actin
-120
-160
-60
-50
-30
-30
-40
-40
SCR -m1-m2 SCR -h1 -h2 SCR -h1 -h2
344SQ A549 H358

B
ZEB-1
VIM
ZEB-2
FOXC2
SNAIL
SLUG
Rel. protein
SCR-m1-m2 SCR -h1-h2 SCR -h1-h2
344SQ A549 H358

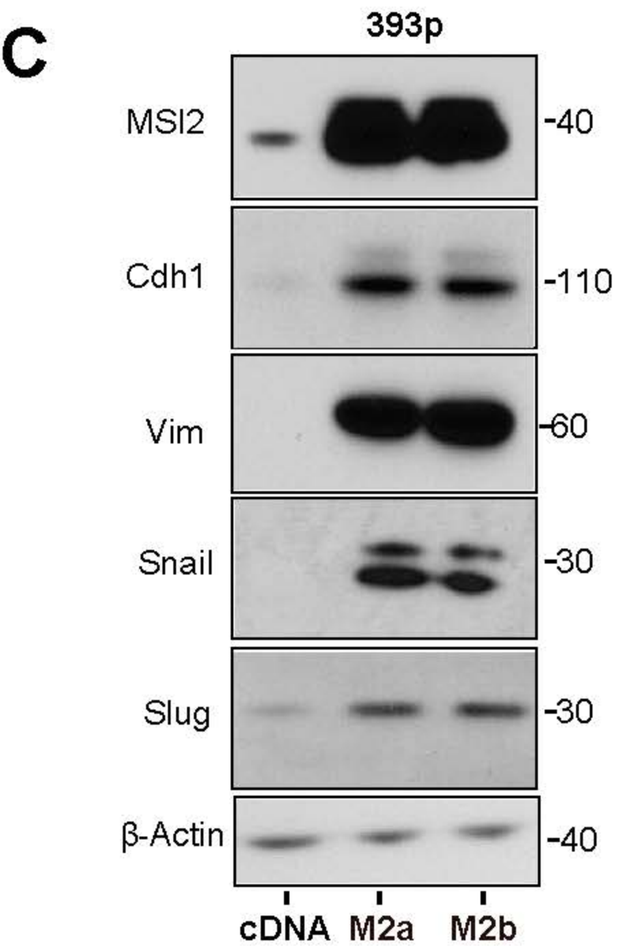
C
393p
MSI2
Cdh1
Vim
Snail
Slug
β-Actin
-40
-110
-60
-30
-30
-40
cDNA M2a M2b

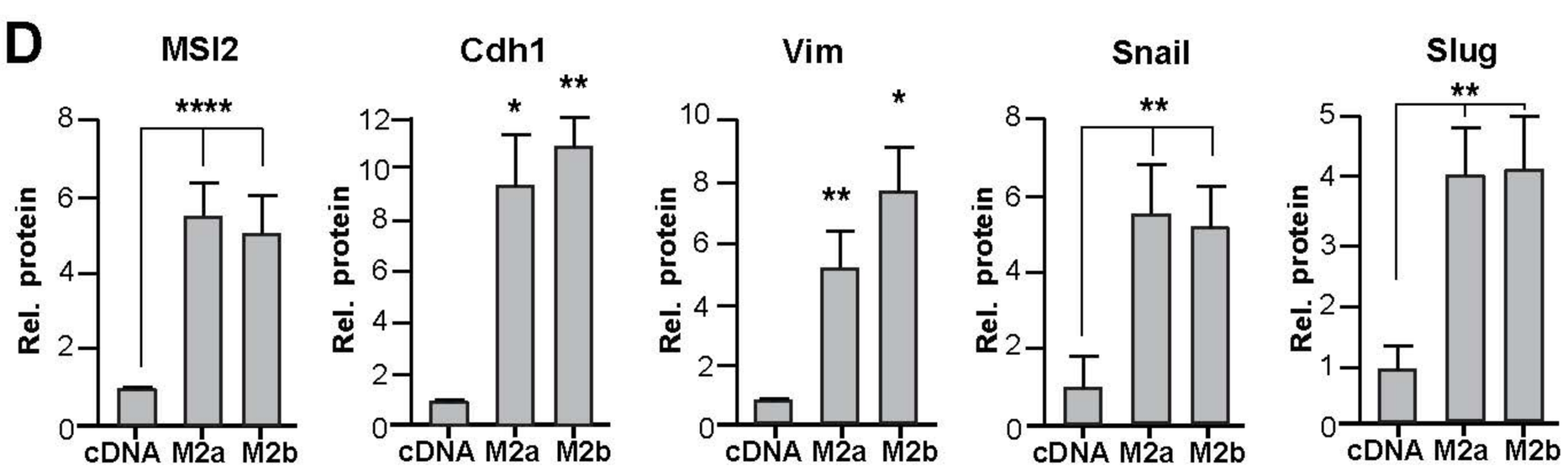
D
MSI2
Cdh1
Vim
Snail
Slug
Rel. protein
cDNA M2a M2b

A

344SQ Cell Line

A549 Cell Line

3'SCR 3'-m1 3'-m1/TβR1

A'SCR A'-h1 A'-h1/TβR1

TGFβR1

MSI2

β-actin

50

40

40

50

40

40

B

Rel. protein TGFβRI

1.6
1.4
1.2
1
0.8
0.6
0.4
0.2
0

**

3'SCR 3'-m1 3'-m1/TβR1

1.4
1.2
1
0.8
0.6
0.4
0.2
0

*

A'SCR A'-h1 A'-h1/TβR1

C

Rel. Invasion

1.2
1
0.8
0.6
0.4
0.2
0

***

3'SCR 3'-m1 3'-m1/TβR1

5
4
3
2
1
0

*

A'SCR A'-h1 A'-h1/TβR1

D

3'SCR

3'-m1

3'-m1/TβR1

A'SCR

A'-h1

A'-h1/TβR1

Kudinov et al, Figure S9

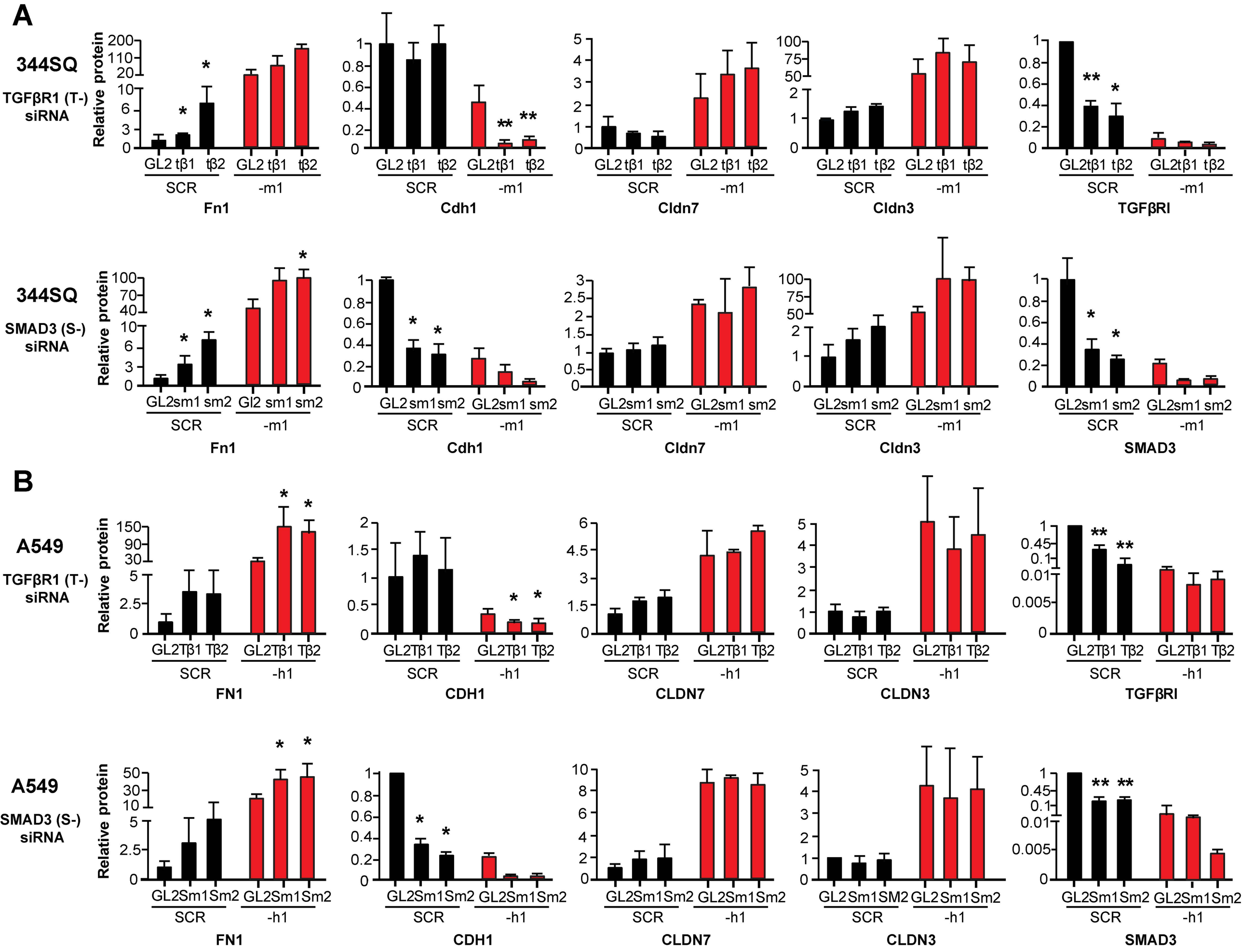

Kudinov et al, Figure S10.

Table S1. Primers used in RT-QPCR analysis.

	Taqman assays from Life Technologies	Taqman assays designed with Primer Express	SYBR Green assays designed with Primer Express
Mouse			
Msi2			F:AGCAGTATTTCGAGCAGTTTGGCA R:TGTCGAACATCAGCATCGCATCC
Fn1	Mm01256744_m1		
Cldn7			F: AGAGCACCGGCATGATGAG R:GGCGACAAACATGGCTAAGAA
Tgfbr1	Mm00436964_m1		
Smad3	Mm01170760_m1		
Cldn3	Mm00515499_s1		
Cldn5	Mm00727012_s1		
Cdh1 (E-Cad)	Mm00486918_m1		
Ppib	Mm00478295_m1		
HUMAN			
MSI2			F:GGTCATGAGAGATCCCACTACG R:TCTACACTTGCTGGGTCTGC
FN1		F:ATGCCGACCAGAAGTTTGG R:AATGCGGTACATGACCCCTT P:6fam-CCCCATGGCTGCCCACGAG-bhq1	
CLDN7	Hs00600772_m1		
TGFBR1	Hs00610320_m1		
SMAD3	Hs00232222_m1		
CLDN3	Hs00265816_s1		
CLDN5			
CDH1	Hs00170423_m1		
POLR2F		F:TGCCATGAAGGAACTCAAGG R:TCATAGCTCCCATCTGGCAG P:6fam-CCCCATCATCATTCGCCGTTACC-bhq1	

F, forward; R, reverse; P, probe.

Table S2. Patient characteristics for the primary NSCLC tumors arrayed in tissue microarray (TMA).

Gender	
Male	48%
Female	52%
Age at diagnosis	Years
Mean	66.0
Min	41.0
Max	83.0
SD	9.1
Histology	%
Acinar cell carcinoma	12.0
Squamous cell carcinoma, NOS	23.0
Adenocarcinoma, NOS	44.0
Non-small cell carcinoma	4.0
Bronchiolo-alveolar adenocarcinoma, NOS	7.0
Papillary adenocarcinoma, NOS	4.0
Adenosquamous carcinoma	6.0
Overall stage	%
1A	7
1B	12
2B	2
3A	55
3B	13
4	12
T stage	%
1	19
2	53
3	13
4	15
Lymph nodes	%
0	22
X	78
M stage	%
0	88
X	12
Grade	%
Well differentiated	2.3
Moderately differentiated	46.6
Poor differentiated	48.8
Undifferentiated	2.4

TMAs contained specimens from 123 patients with characteristics noted in the table and for 22 normal lungs

Table S3. Patient characteristics for the analyzed grouped NSCLC samples (normal, primary tumor and lymph node metastasis).

Normal-Lung Cancer-Metastatic Matched Cases

Patient	Age at DOS	M/F	Diagnosis	Grade	Stage (pathologic)	Type of Metastasis
001	46	M	adenocarcinoma (mucinous features)	G2	T1 N1 MX (IIA)	Lymph node
002	64	F	adenocarcinoma	G2	T2 N1 MX (IIB)	Lymph node
003	68	F	adenocarcinoma	G3	T0 N2 MX (IIIA)	Lymph node
004	63	M	adenocarcinoma (conventional)	G2	T1a N1 MX (IIA)	Lymph node
005	64	M	adenocarcinoma (mixed: mucinous 80%, fetal 10%, acinar 5%, solid 5%)	G2	T2a N2 MX (IIIA)	Lymph node
006	73	M	adenocarcinoma	G2	T2a N1 MX (IIB)	Lymph node
007	70	F	invasive squamous cell with focal adenocarcinoma (nodal mets appear squamous in differentiation)	G2	T4 N2 MX (IIIB)	Lymph node
008	78	F	squamous cell carcinoma	G2	T3 N1 MX (IIIA)	Lymph node
009	54	M	squamous cell (keratinizing) carcinoma	G2	T2a N1 MX (IIB)	Lymph node
010	73	F	adenocarcinoma	G2-3 (Moderately to poorly)	T1a N2 MX (IIIA)	Lymph node
011	61	F	squamous cell carcinoma (minor component of glandular differentiation <5%)	G2	T1b N1 MX (IIA)	Lymph node
012	52	F	adenocarcinoma (predominantly solid pattern)	G3	T2a N1 MX (IIB)	Lymph node
013	65	M	adenocarcinoma	G3	T2N2MX	Lymph node
014	55	F	squamous cell carcinoma	G3	T1N2MX (IIIA)	Lymph node

Table S4. Sequences of siRNA mixtures and shRNA used in gene knockdowns.

LP_4873								
G-CUSTOM-117757								
Supplier	**Well**	**Pool Catalog Number**	**Duplex Catalog Number**	**Gene Symbol**	**GENE ID**	**Gene Accession**	**GI Number**	**Sequence**
Dharmacon	B02	J-003929-09	J-003929-09	Human TGFBR1 "Tβ1" (Mixture 1)	7046	NM_004612	66346739	GAGAAGAACGUUCGUGGUU and UGCGAGAACUAUUGUGUUA
Dharmacon	B04	J-003929-11	J-003929-11	Human TGFBR1 "Tβ2" (Mixture 2)	7046	NM_004612	66346739	GACCACAGACAAAGUUAUA and CGAGAUAGGCCGUUUGUAU
Dharmacon	B07	J-040617-05	J-040617-05	Mouse Tgfbr1 "tβ1" (Mixture 1)	21812	NM_009370	40254607	GGGCAGUUACUACAACAUA and CUAGAUCGCCCUUUCAUUU
Dharmacon	B09	J-040617-07	J-040617-07	Mouse Tgfbr1 "tβ2" (Mixture 2)	21812	NM_009370	40254607	GCGAAGGCAUUACAGUGUU and UGACAGCUUUGCGAAUUAA
Dharmacon	C02	J-020067-05	J-020067-05	Human SMAD3 "Sm1" (Mixture 1)	4088	NM_005902	52352808	CAACAGGAAUGCAGCAGUG and GAGUUCGCCUUCAAUAUGA
Dharmacon	C04	J-020067-07	J-020067-07	Human SMAD3 "Sm2" (Mixture 2)	4088	NM_005902	52352808	GGACGCAGGUUCUCCAAAC and UUAGAGACAUCAAGUAUGG
Dharmacon	C07	J-040706-05	J-040706-05	Mouse Smad3 "sm1" (Mixture 1)	17127	NM_016769	31543221	GAACUUACAAGGCGACACA and GGACGCAGGUUCUCCAAAC
Dharmacon	C09	J-040706-07	J-040706-07	Mouse Smad3 "sm2" (Mixture 2)	17127	NM_016769	31543221	CCAUGGAGCUCUGUGAGUU and GGAUUGAGCUACACCUGAA
Dhamrmacon	=D07	J-060672-09	J-060672-09	Mouse Cldn7 "Cl7-1" (Mixture 1)	53624	NM_016887	31560439	CCAUGAACGUUAAGUACGA and GGGAGAUGACAAAGCGAAG
Dhamrmacon	D09	J-060672-11	J-060672-11	Mouse Cldn7 "Cl7-2" (Mixture 2)	53624	NM_016887	31560439	CCGAAUAGCUAUGACUGGA and CUGGAUUGGUCAUCAGAUU
Qiagen		SI04236652 and SI04285834		Human MSI2 "-ih1" (Mixture 2)	124540		31560439	ATGAGAGATCCCACTACGAAA and CUGGAUUGGUCAUCAGAUU
Qiagen		SI04312665 and SI04375847		Human MSI2 "-h2" (Mixture 1)	124540		31560439	TCCCAACTTCGTGGCGACCTA and CCAGATAGCCTTAGAGACTAT
Qiagen		SI04465426 and SI04958079		Mouse Msi2 "-m1" (Mixture 2)	76626		31560439	TTCCAAGACGATTGACCCAAA and GCAAGTGTAGATAAAGTATTA
Qiagen		SI04958086 and SI04958093		Mouse Msi2 "-m2" (Mixture 1)	76626		31560439	ATGAGAGATCCCACAACGAAA and CCAGATAGCCTTAGAGACTAT

shRNA Targeting Sequences

Mouse Msi2-m1: CCGGCCCAACTTTGTGGCAACCTATCTCGAGATAGGTTGCCACAAAGTTGGGTTTTTG

Mouse Msi2-m2: CCGGCGTAGGAGGATTGTCTGCAAACTCGAGTTTGCAGACAATCCTCCTACGTTTTTG

Human MSI2-h1: CCGGGTGGAAGATGTAAAGCAATATCTCGAGATATTGCTTTACATCTTCCACTTTTTG

Human MSI2-h2: CCGGCCCAACTTCGTGGCGACCTATCTCGAGATAGGTCGCCACGAAGTTGGGTTTTTG

cDNA ORF Sequences used for rescue experiments

Human CLDN7:
ATGGCCAATTCGGGCCTGCAGTTGCTGGGCTTCTCCATGGCCCTGCTGGGCTGGGTGGGTCTGGTGGCCTGCACCGCCATCCCGCAGTGGCAGATGAGCTCCTATGCGGGT
GACAACATCATCACGGCCCAGGCCATGTACAAGGGGCTGTGGATGGACTGCGTCACGCAGAGCACGGGGATGATGAGCTGCAAAATGTACGACTCGGTGCTCGCCCTGTCCG
CGGCCTTGCAGGCCACTCGAGCCCTAATGGTGGTCTCCCTGGTGCTGGGCTTCCTGGCCATGTTTGTGGCCACGATGGGCATGAAGTGCACGCGCTGTGGGGGAGACGACA
AAGTGAAGAAGGCCCGTATAGCCATGGGTGGAGGCATAATTTTCATCGTGGCAGGTCTTGCCACCTTGGTAGCTTGCTCCTGGTATGGCCATCAGATTGTCACAGACTTTTATA
ACCCTTTGATCCCTACCAACATTAAGTATGAGTTTGGCCCTGCCATCTTTATTGGCTGGGCAGGGTCTGCCCTAGTCATCCTGGGAGGTGCACTGCTCTCCTGTTCCTGTCCTG
GGAATGAGAGCAAGGCTGGGTACCGTGCACCCCGCTCTTACCCTAAGTCCAACTCTTCCAAGGAGTATGTG

Human TGFβR1:
ATGGAGGCGGCGGTCGCTGCTCCGCGTCCCCGGCTGCTCCTCCTCGTGCTGGCGGCGGCGGCGGCGGCGGCGGCGCTGCTCCCGGGGGCGACGGCGTTACAGTGTTTCTGCCA
CCTCTGTACAAAAGACAATTTTACTTGTGTGACAGATGGGCTCTGCTTTGTCTCTGTCACAGAGACCACAGACAAAGTTATACACAACAGCATGTGTATAGCTGAAATTGACTTAATTCCTCG
AGATAGGCCGTTTGTATGTGCACCCTCTTCAAAAACTGGGTCTGTGACTACAACATATTGCTGCAATCAGGACCATTGCAATAAAATAGAACTTCCAACTACTGTAAAGTCATCACCTGGC
CTTGGTCCTGTGGAACTGGCAGCTGTCATTGCTGGACCAGTGTGCTTCGTCTGCATCTCACTCATGTTGATGGTCTATATCTGCCACAACCGCACTGTCATTCACCATCGAGTGC
CAAATGAAGAGGACCCTTCATTAGATCGCCCTTTTATTTCAGAGGGTACTACGTTGAAAGACTTAATTTATGATATGACAACGTCAGGTTCTGGCTCAGGTTTACCATTGCTTGTTCAGAGAA
CAATTGCGAGAACTATTGTGTTACAAGAAAGCATTGGCAAAGGTCGATTTGGAGAAGTTTGGAGAGGAAAGTGGCGGGGAGAAGAAGTTGCTGTTAAGATATTCTCCTCTAGAGAAGAACG
TTCGTGGTTCCGTGAGGCAGAGATTTATCAAACTGTAATGTTACGTCATGAAAACATCCTGGGATTTATAGCAGCAGACAATAAAGACAATGGTACTTGGACTCAGCTCTGGTTGGTGTCAG
ATTATCATGAGCATGGATCCCTTTTTGATTACTTAAACAGATACACAGTTACTGTGGAAGGAATGATAAAACTTGCTCTGTCCACGGCGAGCGGTCTTGCCCATCTTCACATGGAGATTGTT
GGTACCCAAGGAAAGCCAGCCATTGCTCATAGAGATTTGAAATCAAAGAATATCTTGGTAAAGAAGAATGGAACTTGCTGTATTGCAGACTTAGGACTGGCAGTAAGACATGATTCAGCCA
CAGATACCATTGATATTGCTCCAAACCACAGAGTGGGAACAAAAAGGTACATGGCCCCTGAAGTTCTCGATGATTCCATAAATATGAAACATTTTGAATCCTTCAAACGTGCTGACATCTAT
GCAATGGGCTTAGTATTCTGGGAAATTGCTCGACGATGTTCCATTGGTGGAATTCATGAAGATTACCAACTGCCTTATTATGATCTTGTACCTTCTGACCCATCAGTTGAAGAAATGAG
AAAAGTTGTTTGTGAACAGAAGTTAAGGCCAAATATCCCAAACAGATGGCAGAGCTGTGAAGCCTTGAGAGTAATGGCTAAAATTATGAGAGAATGTTGGTATGCCAATGGAGCAGC
TAGGCTTACAGCATTGCGGATTAAGAAAACATTATCGCAACTCAGTCAACAGGAAGGCATCAAAATG

Table S5. Antibodies used for RPPA analysis.

Ab Name	Gene Name	Company	Catalog #	Ab ID	Species	Validation Status*
14-3-3_beta	YWHAB	Santa Cruz	sc-628	882.	Rabbit	Validated
14-3-3_epsilon	YWHAE	Santa Cruz	sc-23957	913.1	Mouse	Use with Caution
14-3-3_zeta	YWHAZ	Santa Cruz	sc-1019	883.	Rabbit	Validated
4E-BP1	EIF4EBP1	CST	9452	2.8	Rabbit	Validated
4E-BP1_pS65	EIF4EBP1	CST	9456	3.1	Rabbit	Validated
4E-BP1_pT37_T46	EIF4EBP1	CST	9459	6.4	Rabbit	Validated
53BP1	TP53BP1	CST	4937	985.1	Rabbit	Validated
ACC_pS79	ACACA ACACB	CST	3661	13.4	Rabbit	Validated
ACC1	ACACA	Epitomics	1768-1	14.1	Rabbit	Under evaluation
ACVRL1	ACVRL1	Epitomics	2940-1	1086.10	Rabbit	Use with Caution
Akt	AKT1 AKT2 AKT3	CST	4691	1084.11	Rabbit	Validated
Akt_pS473	AKT1 AKT2 AKT3	CST	9271	23.10	Rabbit	Validated
Akt_pT308	AKT1 AKT2 AKT3	CST	2965	1154	Rabbit	Validated
AMPK_alpha	PRKAA1	CST	2532	39.4	Rabbit	Use with Caution
AMPK_pT172	PRKAA1	CST	2535	40.6	Rabbit	Validated
Annexin_VII	ANXA7	BD Biosciences	610668	1142.1	Mouse	Validated
AR	AR	Epitomics	1852-1	756.1	Rabbit	Validated
Bad_pS112	BAD	CST	9291	63.7	Rabbit	Validated
Bak	BAK1	Epitomics	1542-1	71.2	Rabbit	Use with Caution
Bax	BAX	CST	2772	73.5	Rabbit	Validated
Bcl-2	BCL2	Dako	Dako M0887	80.1	Mouse	Validated
Bcl-xL	BCL2L1	CST	2762	85.5	Rabbit	Validated
Beclin	BECN1	Santa Cruz	sc-10086	87.1	Goat	Use with Caution
beta-Catenin	CTNNB1	CST	9562	75.3	Rabbit	Validated
Bid	BID	Epitomics	1008-1	88.1	Rabbit	Use with Caution
Bim	BCL2L11	Epitomics	1036-1	90.1	Rabbit	Validated
B-Raf	BRAF	Santa Cruz	sc-5284	96.2	Mouse	Use with Caution
BRCA2	BRCA2	CST	9012	761.1	Rabbit	Use with Caution
Caspase-7_cleavedD198	CASP7	CST	9491	109.6	Rabbit	Use with Caution
Caveolin-1	CAV1	CST	3238	114.1	Rabbit	Validated
CD31	PECAM1	Dako	M0823	127.1	Mouse	Validated
CD49b	ITGA2	BD Biosciences	611016	937.1	Mouse	Validated
CDK1	CDC2	CST	9112	1007.5	Rabbit	Validated
Chk1	CHEK1	CST	2360	1203.3	Mouse	Use with caution
Chk1_pS345	CHEK1	CST	2348	903.7	Rabbit	Use with caution
Chk2	CHEK2	CST	3440	146.1	Mouse	Validated
Chk2_pT68	CHEK2	CST	2197	147.2	Rabbit	Use with Caution
cIAP	BIRC2	Millipore	07-759	930.1	Rabbit	Caution
c-Jun_pS73	JUN	CST	9164	155.5	Rabbit	Validated
c-Kit	KIT	Epitomics	1522	157	Rabbit	Validated
Claudin-7	CLDN7	Novus	NB100-91714	852.1	Rabbit	Validated
c-Met_pY1235	MET	CST	3129	727.5	Rabbit	Validated

c-Myc	MYC	Santa Cruz	sc-764	1143.1	Rabbit	Use with Caution
Collagen_VI	COL6A1	Santa Cruz	SC-20649	171.1	Rabbit	Validated
C-Raf	RAF1	Millipore	05-739	803	Rabbit	Validated
C-Raf_pS338	RAF1	CST	9427	179.4	Rabbit	Validated
Cyclin_B1	CCNB1	Epitomics	1495-1	192.1	Rabbit	Validated
Cyclin_D1	CCND1	Santa Cruz	SC-718	194.1	Rabbit	Validated
Cyclin_E1	CCNE1	Santa Cruz	SC-247	201.1	Mouse	Validated
DJ-1	PARK7	Abcam	ab76008	891.1	Rabbit	Validated
Dvl3	DVL3	CST	3218	940.1	Rabbit	Validated
E-Cadherin	CDH1	CST	3195	1099.10	Rabbit	Validated
eEF2	EEF2	CST	2332	1060.3	Rabbit	Use with Caution
eEF2K	EEF2K	CST	3692	1061.2	Rabbit	Validated
EGFR	EGFR	CST	2232	1120.15	Rabbit	Validated
EGFR_pY1068	EGFR	CST	2234	217.13	Rabbit	Use with caution; also sees pHer2
EGFR_pY1173	EGFR	Epitomics	1124	221.3	Rabbit	Validated
eIF4E	EIF4E	CST	9742	722.3	Rabbit	Validated
eIF4G	EIF4G1	CST	2498	1124.3	Rabbit	Use with Caution
ER-alpha	ESR1	Lab Vision	RM-9101-S	238.6	Rabbit	Validated
ER-alpha_pS118	ESR1	Epitomics	1091-1	241.1	Rabbit	Validated
FASN	FASN	Cell Signaling	3180	1156.00	Rabbit	Validated
Fibronectin	FN1	Epitomics	1574-1	262.1	Rabbit	Validated
FOX03a	FOXO3	CST	2497	1122.6	Rabbit	Use with Caution
FOXO3a_pS318_S321	FOXO3	CST	9465	270.1	Rabbit	Use with Caution
FoxM1	FOXM1	CST	5436	1123.1	Rabbit	Validated
G6PD	G6PD	Santa Cruz	sc-373887	1155	Mouse	Validated
Gab2	GAB2	CST	3239	943.1	Rabbit	Validated
GAPDH	GAPDH	Ambion	AM4300	274.11	Mouse	Caution
GATA3	GATA3	BD Biosciences	558686	764.1	Mouse	Validated
GSK3_pS9	GSK3A GSK3B	CST	9336	1082.12	Rabbit	Validated
GSK3-alpha-beta	GSK3A GSK3B	Santa Cruz	SC-7291	284.2	Mouse	Validated
GSK3-alpha-beta_pS21_S9	GSK3A GSK3B	CST	9331	285.12	Rabbit	Validated
HER2	ERBB2	Lab Vision	MS-325-P1	1038.2	Mouse	Validated
HER2_pY1248	ERBB2	R&D Systems	AF1768	1075.1	Rabbit	Use with caution; likely sees pEGFR
HER3	ERBB3	Santa Cruz	sc-285	911.1	Rabbit	Validated
HER3_pY1289	ERBB3	CST	4791	728.12	Rabbit	Use with Caution
Heregulin	NRG1	CST	2573	890.1	Rabbit	Validated
IGFBP2	IGFBP2	CST	3922	335.1	Rabbit	Validated
INPP4B	INPP4B	CST	4039	1065.1	Rabbit	Validated
IRS1	IRS1	Upstate (Millipore)	06-248	802.1	Rabbit	Validated
JNK_pT183_pY185	MAPK8	CST	4668	888.5	Rabbit	Validated
JNK2	MAPK9	CST	4672	380.1	Rabbit	Use with Caution
Lck	LCK	CST	2752	397.2	Rabbit	Validated
MAPK_pT202_Y204	MAPK1 MAPK3	CST	4377	405.3	Rabbit	Validated
MEK1	MAP2K1	Epitomics	1235-1	417.1	Rabbit	Validated
MEK1_pS217_S221	MAP2K1	CST	9154	1076.3	Rabbit	Validated
MIG-6	ERRFI1	Sigma	WH0054206M1	1062.1	Mouse	Validated
mTOR	FRAP1	CST	2983	444.3	Rabbit	Validated
mTOR_pS2448	FRAP1	CST	2971	446.14	Rabbit	Use with caution
MYH11	MYH11	SDI / Novus	21370002	1139.1	Rabbit	Validated
Myosin IIa pS1943	MYH9	CST	5026	1160	Rabbit	Validated

N-Cadherin	CDH2	CST	4061	452.1	Rabbit	Validated
NDRG1_pT346	NDRG1	CST	3217	1126	Rabbit	Validated
NF2	NF2	SDI	2271.00.02	1046.1	Rabbit	Use with Caution
NF-kB-p65_pS536	NFKB1	CST	3033	457.4	Rabbit	Use with Caution
Notch1	NOTCH1	CST	3268	1064.1	Rabbit	Validated
N-Ras	NRAS	Santa Cruz	sc-31	1136.1	Mouse	Validated
p21	CDKN1A	Santa Cruz	SC-397	470.1	Rabbit	Validated
p27	CDKN1B	Epitomics	1591-1	897.1	Rabbit	Validated
p27_pT157	CDKN1B	R&D	AF1555	842.1	Rabbit	Use with Caution
p27_pT198	CDKN1B	Abcam	ab64949	878.1	Rabbit	Validated
p38_MAPK	MAPK14	CST	9212	478.10	Rabbit	Validated
p38_pT180_Y182	MAPK14	CST	9211	479.15	Rabbit	Validated
p53	TP53	CST	9282	481.3	Rabbit	Under evaluation
p70S6K	RPS6KB1	Epitomics	1494-1	493.1	Rabbit	Validated
p70S6K_pT389	RPS6KB1	CST	9205	494.7	Rabbit	Validated
p90RSK	RPS6KA1	CST	9347	759.5	Rabbit	Caution
p90RSK_pT359_S363	RPS6KA1	CST	9344	770.2	Rabbit	Use with Caution
Paxillin	PXN	Epitomics	1500-1	505.1	Rabbit	Caution
PCNA	PCNA	Abcam	ab29	511.1	Mouse	Caution
PDCD4	PDCD4	Rockland	600-401-965	816.1	Rabbit	Use with Caution
PDK1	PDK1	CST	3062	515.5	Rabbit	Validated
PDK1_pS241	PDK1	CST	3061	516.7	Rabbit	Validated
PEA15	PEA15	CST	2780	1017.2	Rabbit	Validated
PEA15_pS116	PEA15	Invitrogen	44-836G	1018.1	Rabbit	Validated
PI3K-p110-alpha	PIK3CA	CST	4255	808.1	Rabbit	Use with Caution
PI3K-p85	PIK3R1	Upstate (Millipore)	06-195	523.3 or 523.4	Rabbit	Validated
PKC-alpha	PRKCA	Upstate (Millipore)	05-154	529.1	Mouse	Validated
PKC-alpha_pS657	PRKCA	Upstate (Millipore)	06-822	530.2	Rabbit	Use with caution
PKC-delta_pS664	PRKCD	Upstate (Millipore)	07-875	932.1	Rabbit	Validated
PKC-pan_BetaII_pS660	PKC	CST	9371	1137.	Rabbit	Validated
PR	PGR	Epitomics	1483-1	549.1	Rabbit	Validated
PRAS40_pT246	AKT1S1	Biosource	441100G	739.1	Rabbit	Validated
PTEN	PTEN	CST	9552	566.3	Rabbit	Validated
Rab11	RAB11A RAB11B	CST	3539	1083.3	Rabbit	Under evaluation
Rab25	RAB25	CST	4314	1150.1	Rabbit	Validated
Rad50	RAD50	Millipore	05-525	987.1	mouse	Validated
Rad51	RAD51	Chem Biotech	na 71	579.3	Mouse	Under evaluation
Raptor	RPTOR	CST	2280	1128.8	Rabbit	Validated
Rb_pS807_S811	RB1	CST	9308	557.9	Rabbit	Validated
RBM15	RBM15	SDI / Novus	21390002	1138.1	Rabbit	Validated
Rictor	RICTOR	CST	2114	1129.4	Rabbit	Use with Caution
Rictor_pT1135	RICTOR	CST	3806	1130.4	Rabbit	Validated
S6_pS235_S236	RPS6	CST	2211	600.8	Rabbit	Validated
S6_pS240_S244	RPS6	CST	2215	601.4	Rabbit	Validated
SCD1	SCD1	Santa Cruz	sc-58420	1127.1	Mouse	Validated
SF2	SFRS1	Invitrogen	32-4500	1131.1	Mouse	Validated
Smad1	SMAD1	Epitomics	1649-1	922.2	Rabbit	Validated
Smad3	SMAD3	Epitomics	1735-1	796.1	Rabbit	Validated
Smad4	SMAD4	Santa Cruz	sc-7966	920.1	Mouse	Validated
Src	SRC	Upstate (Millipore)	05-184	621.2	Mouse	Validated

Src_pY416	SRC	CST	2101	623.18	Rabbit	Use with caution
Src_pY527	SRC	CST	2105	626.5	Rabbit	Validated
STAT3_pY705	STAT3	CST	9131	637.6	Rabbit	Validated
STAT5-alpha	STAT5A	Epitomics	1289-1	638.1	Rabbit	Validated
Stathmin	STMN1	Epitomics	1972-1	718.1	Rabbit	Validated
Syk	SYK	Santa Cruz	sc-1240	1033.1	Mouse	Validated
TAZ	WWTR1	CST	2149	777.1	Rabbit	Validated
TIGAR	C12ORF5	Epitomics	S1711	1107.1	Rabbit	Validated
Transglutaminase	TGM2	Lab Vision	MS-224-P1	908.2	Mouse	Validated
TRFC	TRFC	SDI / Novus	22500002	1140.1	Rabbit	Validated
TSC1	TSC1	CST	4906	1125.1	Rabbit	Use with Caution
TTF1	TTF1	Epitomics	2044-1	1081.1	Rabbit	Validated
Tuberin	TSC2	Epitomics	1613-1	670.30	Rabbit	Validated
Tuberin_pT1462	TSC2	CST	3617	671.2	Rabbit	Validated
VEGFR2	KDR	CST	2479	688.4	Rabbit	Validated
VHL	VHL	BD Biosciences	556347	693.1	Mouse	Use with Caution
XRCC1	XRCC1	CST	2735	906.1	Rabbit	Under evaluation
YAP	YAP1	Santa Cruz	sc-15407	780.3	Rabbit	Under evaluation
YAP_pS127	YAP1	CST	4911	782.1	Rabbit	Under evaluation
YB-1	YBX1	SDI	1725.00.02	700.1	Rabbit	Validated
YB-1_pS102	YBX1	CST	2900	835.1	Rabbit	Validated

Validation Status*

VALID=RPPA and WB correlation > 0.7

Use with Caution=RPPA and WB correlation < 0.7

Under Evaluation=Antibody has given mixed results and / or evaluated by another lab; we are in the process of (re)validating.

Print this Page

Presentation Abstract

Abstract Number:	1584
Presentation Title:	Musashi-2 (MSI2) drives TGFBR1/SMAD3 dependent partial EMT and supports VEGFR2 expression and metastasis of human and mouse NSCLC cells
Presentation Time:	Monday, Apr 18, 2016, 8:00 AM -12:00 PM
Location:	Section 30
Poster Board Number:	1
Author Block:	Alexander Kudinov[1], Alexander Deneka[2], Anna Nikonova[2], Ilya Serebriiskii[2], Tim N. Beck[2], Qi Cai[2], Brian L. Egleston[2], Emmanuelle Nicolas[2], Hossein Borghaei[2], Don Gibbons[3], Jonathan Kurie[3], Erica A. Golemis[2], Yanis Boumber[1]. [1]University of New Mexico Cancer Center, Albuquerque, NM; [2]Fox Chase Cancer Center, Philadelphia, PA; [3]The University of Texas: MD Anderson Cancer Center, Houston, TX
Abstract Body:	About 221,200 new patients will be diagnosed with lung cancer and ~158,040 will succumb to this disease in the United States in 2015. Non-small cell lung cancer (NSCLC) has a 17.4% overall 5-year survival, with metastasis contributing to the vast majority of deaths. Analyzing NSCLC tumors spontaneously arising in $Kras^{LA1/+}$; $P53^{R172HG/+}$ (KP) mice, we identified Musashi-2 (MSI2) protein, a stem cell-associated factor that is regulates mRNA translation, as upregulated in the metastasis-competent mouse cell lines. Importantly, MSI2 shRNA depletion in either mouse or human NSCLC cells decreased invasion in Matrigel in vitro and decreased metastasis upon orthotopic injection 129Sv immunocompetent mice in vivo. Mechanistically, by both overexpressing Msi2 cDNA in 393p murine NSCLC and shRNA depleting MSI2 in four independent mouse and human NSCLC cell lines, we defined MSI2 as a driver of a partial epithelial-mesenchymal transition (EMT) program in NSCLC cells. In support of EMT, MSI2 increases the expression of the Snail and Slug pro-EMT transcription factors, as well as the mesenchymal protein vimentin (VMN). MSI2 also downregulates expression of the extracellular matrix component fibronectin (FN1) and tight junction proteins Claudin-3, 5 and 7. However, MSI2 also inhibits protein expression of Zeb-1 and Zeb-2, while sustaining expression of E-cadherin (E-Cad), associated with epithelial identity. Moreover, MSI2 represses NOTCH-1 and upregulates VEGFR2 at the mRNA and protein levels. This is of interest, as NOTCH-1 has been shown to regulate VEGFR2 in angiogenic signaling. We found that knockdown of NOTCH-1 in MSI2-depleted mouse and human NSCLC cells rescued the loss of VEGFR2 expression, suggesting MSI2 increases VEGFR2 expression in a NOTCH-1 dependent manner. Additionally, siRNA of VEGFR2 in the highly metastatic NSCLC cell line 344sq significantly decreased Matrigel invasion, but had only a limited effect in 344sq derivative lines with stable depletion of MSI2, and human NSCLC experiments are ongoing. Together, these results indicate a possible role of MSI2/NOTCH-1/VEGFR2 axis in NSCLC, and suggest that MSI2 connects cancer cell stemness, EMT, and angiogenesis in lung cancer metastasis.

American Association for Cancer Research
615 Chestnut St. 17th Floor
Philadelphia, PA 19106

BIOCENTURY
Innovations
FROM IDEA TO IND

JUNE 23, 2016

TOOLS & TECHNIQUES

WHAT GWAS WILL BE

By Karen Tkach, Staff Writer

Genome-wide association studies (GWAS) identify thousands of genetic variants that are linked to disease, without distinguishing the alleles that cause the phenotype from variants that are co-inherited but not causal. Two groups from the Broad Institute of MIT and Harvard have shown a high throughput assay can help pinpoint the variants that actually impact gene expression, which could uncover targets and mechanisms for a wide range of diseases.

"We've come beyond the era of just doing GWAS. The last 10 years have provided us with great examples and a framework for doing those studies. Now the challenge is, we've gotten all this information, but how do we really learn biology from it?" said Vijay Sankaran, principal investigator on one of the studies, who is an assistant professor of pediatrics at Harvard Medical School and an associate member at the Broad Institute.

The biggest hurdle has been finding which changes are relevant in non-coding regions of the genome, because the vast majority of GWAS findings lie outside of protein coding regions.

"Being able to interrogate the non-coding genome has been extremely difficult to date. There aren't great tools, particularly if one wants to do this in a way that looks at allelic variation," said Sankaran. "This provides one of the first tools to start to, in a really systematic way, go through and tease apart variants that actually matter from those that are just going along for the ride."

The studies, published in *Cell* this month, show a massively parallel reporter assay (MPRA) can flag variants — SNPs, small insertions or small deletions — that are likely to affect gene expression, from the large number of non-coding hits obtained from genetic association studies such as GWAS or expression quantitative trait loci (eQTL) studies.

MPRA involves testing the effects of individual DNA sequences on gene regulation by inserting each one into a plasmid containing a minimal promoter, a reporter gene and a barcode, then transfecting the plasmids into a cell type of interest to identify which sequences increase reporter gene expression in the context of that cell's regulatory machinery (see "Massive Screen of Small Changes," page 2).

"Before we had this assay, we would have a list of hundreds or thousands of variants that could be the causal variant. What MPRA

MASSIVE SCREEN OF SMALL CHANGES

Two groups from the **Broad Institute of MIT and Harvard** have published a pair of studies in *Cell* showing a massively parallel reporter assay **(MPRA)** can help find human genetic variants that contribute to disease by screening thousands of non-coding sequence variants — SNPs, small insertions or small deletions — that have been associated with specific **disease profiles** in genome-wide association studies **(GWAS)** or with specific **gene expression profiles** in expression quantitative trait loci **(eQTL)** studies. The goal of the assay is to distinguish variants that are likely to cause gene expression changes that contribute to disease from those that are simply co-inherited but not causal.

In the assay, individual non-coding sequences **(red)** containing variants **(colored stripes)** identified in GWAS or eQTL studies are inserted into plasmids containing a minimal promoter **(white)**, a reporter gene **(green)**, and a barcode sequence **(black and white)**. The plasmids are transfected into the cell type of interest, and the amount of reporter gene transcription promoted by each variant is measured by **sequencing** and quantifying the ratio of **RNA** produced to **DNA** plasmids transfected for each barcode. Alleles of a non-coding sequence **(yellow versus blue)** that promotes different levels of transcription — a phenomenon known as allelic skew — are identified as potential causal variants for the disease or trait.

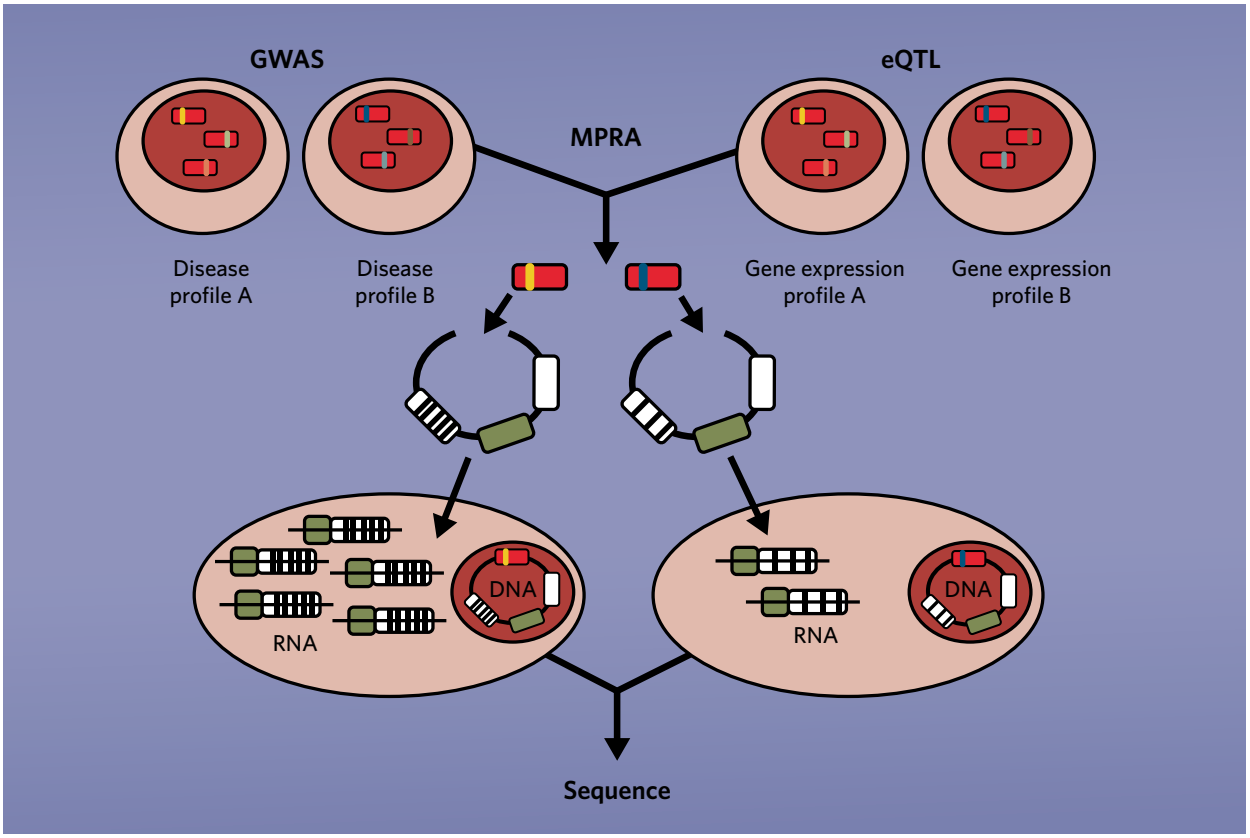

allows us to do is whittle that list down to 10 variants, of which five might have success in the lab as being true causal variants through gene editing experiments," said Ryan Tewhey, the lead author of the second paper.

Tewhey is a postdoctoral fellow at the Broad Institute and the Center for Systems Biology and department of organismic and evolutionary biology at Harvard University.

The MPRA approach was first published by two groups in 2012. "Once upon a time, we would look at reporter assays one by one. What those labs realized is you could simplify this by attaching barcodes into your reporter of interest and turning it into a sequencing problem," said Sankaran.

Now, Sankaran and Tewhey's teams have shown the method can be used to rapidly test how subtle human genetic variations

> "This provides one of the first tools to start to, in a really systematic way, go through and tease apart variants that actually matter from those that are just going along for the ride."
>
> Vijay Sankaran, Broad Institute

in non-coding sequences affect gene expression. "The question was, would the assay's sensitivity tease out the small effect sizes that a variant in the population has. We knew it could find an enhancer, but not necessarily the effects that a single point mutation has in an enhancer," said Tewhey.

SNIPPING THE SNP LIST

Sankaran and Tewhey told BioCentury the two groups began their MPRA projects independently with the goal of benchmarking the approach and ultimately investigating genetic variation in the context of their respective research interests — red blood cell (RBC) traits that impact human health, and the evolution of genetic sequences under selection pressures such as infectious disease. They then collaborated to troubleshoot the method.

The teams each started with a list of variants from GWAS or eQTL studies, which they then screened via MPRA.

GWAS studies find genetic variants that are associated with specific diseases or traits, whereas eQTL studies screen for associations between variants and high or low expression of an array of genes.

Sankaran's team used MPRA in cell lines of human erythroid progenitors — which are RBC precursors — to screen 2,756 genetic variants previously linked to variation in RBC traits. The team identified 32 variants where one allele had a different effect on reporter gene expression than another, a phenomenon called "allelic skew." That suggested inheritance of the different alleles would cause different phenotypes.

For three of those variants, deletion of the corresponding endogenous sequences in the RBC precursors decreased expression of nearby erythropoiesis genes, suggesting the variants had a causal role in gene regulation.

Deletion of one variant, whose minor allele had been previously associated with increased RBC count and decreased RBC volume in GWAS studies, potently inhibited expression of the RNA binding protein RBM38. In cultures of the precursors, knockdown of RBM38 delayed differentiation to RBCs and altered splicing of mRNA transcripts, which could help explain the RBC phenotypes from the GWAS studies.

"Not only did he take these variants and show that they have a regulatory function, but he was able to connect one very strongly to the phenotypic trait from a GWAS," said Tewhey.

In Tewhey's study, the team adapted the MPRA method to screen more variants with greater sensitivity. The idea was to minimize the effect of any "deviant" expression profile of any individual barcode by increasing the total number of barcodes, said Tewhey.

The researchers applied the modified MPRA method to screen genetic variants previously shown to regulate gene expression in eQTL studies of human lymphoblastoid cells — a cell type that can be easily collected to study variation in gene expression across populations.

"You take white blood cells from hundreds of people within a certain population, and you look at the expression levels for all the genes within that cell, and you try to find variants that associate with higher or lower expression of a gene," Tewhey told BioCentury.

The team screened about 30,000 variants linked to gene expression changes in eQTL studies, of which 842 showed allelic skew.

Next the group focused on an allelic skew variant located in an enhancer sequence for the prostaglandin receptor gene PTGER4, which had been previously associated with ankylosing spondylitis in GWAS studies. The more common allele of the variant, which had a cytosine (C) in the SNP position, induced higher reporter gene expression in the MPRA assay than a less common thymine (T) allele. In the eQTL study, the C allele

was also associated with higher PTGER4 expression than the T allele.

Using gene editing, the team showed changing T alleles to C alleles increased PTGER4 expression, while a T to C conversion decreased expression of the gene.

In both studies, the teams looked at whether the alleles also showed functional differences in the genome via DNase hypersensitivity and chromatin immunoprecipitation (ChIP) assays, which measure protein binding at specific loci.

> "Before we had this assay, we would have a list of hundreds or thousands of variants that could be the causal variant. What MPRA allows us to do is whittle that list down to 10 variants, of which five might have success in the lab."
>
> Ryan Tewhey, Broad Institute

"We saw very strong concordance with both the ChIP data and the DNase data. That gave us a lot of confidence that the variants that we were finding were really having some sort of impact endogenously," Tewhey said.

Michael Pazin, program director for functional genomics at the genome sciences division of NIH's National Human Genome Research Institute (NHGRI), told BioCentury the variant's causal effects on PTGER4 expression are convincing, but require follow-up to determine disease relevance. "It shows that those particular variants can actually change the regulation of what they thought was the target gene, but it still doesn't tell you if that particular change causes a change in a trait or disease in people."

Tewhey agreed. "Of course the most difficult step is now turning out to be actually showing that the variants impact phenotype."

Tim Harris, former SVP of precision medicine at Biogen Inc., said this kind of information could help companies prioritize their genetics research around variants that affect pathologies of interest, but noted proving their roles in disease may require long-term experimental models.

"Most of these diseases take some time to develop," Harris said. "The physiological effects of this transcriptional difference are likely going to be evident over time and not immediately."

Based on these and other methods, the Sankaran team estimated between one-third and one-half of variants identified by MPRA have alleles that cause gene expression changes in the cell type of interest. The Tewhey team estimated about two-thirds of MPRA hits were causal in their system.

"For the remaining variants, we don't believe that they're false positives in the sense that MPRA got them wrong. They may have activity when taken out of the genome and tested on this plasmid, but they might be silenced within the genome," Tewhey said.

Both groups estimated the sensitivity of their assay to be less than 25%, meaning there are many false negatives. The authors attribute that in part to the fact that the assay is designed to primarily detect variants that increase rather than decrease gene expression, and to limitations on the length of DNA sequences they can screen in the assay.

"Unfortunately we may miss things because we can't make a long enough construct for technical reasons. As time goes on and synthesis methods improve, we'll be able to do a little better there," said Sankaran.

Next, Tewhey's team plans to pursue larger projects to identify causal variants behind autoimmune disorders and cardiovascular traits.

CASHING IN ON CAUSAL VARIANTS

Tewhey believes MPRAs could reveal the biology underlying otherwise inscrutable GWAS associations.

"I think the biggest value is the ability to lock down the causal variant that gives you the mechanism for that association, and connects you to the gene that's being misregulated," he said.

Pazin said NHGRI's recent call for grant applications to characterize functional elements in the human genome encouraged applicants to pursue MPRAs, among other methods. "I don't think there's any one approach that will solve all of this, but I think that this is a very good approach from the standpoint that it could rapidly test large numbers of elements," he said.

Sankaran thinks understanding the functional effects of subtle genetic variants could inform therapeutic strategies, an idea that has a precedent in his field.

"We know many of these common variants affect outcomes in diseases like sickle cell and the thalassemia syndromes," said Sankaran. "It turns out what we think of as simple Mendelian

blood disorders are a lot more complicated, and some patients are affected more severely than others."

He said his team's previous success in translating GWAS studies into a therapeutic target was part of the impetus for finding a systematic way to identify new leads.

"From GWAS studies, we were able to identify variation in a transcription factor called BCL11A, and later showed that BCL11A is a key regulator of the switch from fetal to adult hemoglobin," Sankaran said. "Most of us express a very low level of fetal hemoglobin, but it turns out if you have diseases like sickle cell disease or thalassemia, continued expression of fetal hemoglobin can be extremely beneficial."

Dana-Farber/Boston Children's Cancer and Blood Disorders Center and Sangamo BioSciences Inc. are developing gene therapy and genome editing approaches targeting BCL11A, respectively. In 2014, Sangamo and Biogen formed a partnership to use Sangamo's zinc finger nuclease (ZFN) technology to develop therapies targeting BCL11A and HBB in β-thalassemia and sickle cell disease.

"That is a discovery we started eight or nine years ago, and it's already leading to a therapy. So our hope is that by better understanding variation in blood traits, there can be other examples that we can go after that are similar to that case," Sankaran said.

The Broad Institute holds a patent on the original MPRA approach, and Tewhey's team has filed a provisional patent on the improved method.

COMPANIES AND INSTITUTIONS MENTIONED

Biogen Inc. (NASDAQ:BIIB), Cambridge, Mass.
Boston Children's Hospital, Boston, Mass.
Broad Institute of MIT and Harvard, Cambridge, Mass.
Harvard Medical School, Boston, Mass.
Harvard University, Cambridge, Mass.
National Human Genome Research Institute (NHGRI), Bethesda, Md.
National Institutes of Health (NIH), Bethesda, Md.
Sangamo BioSciences Inc. (NASDAQ:SGMO), Richmond, Calif.

TARGETS AND COMPOUNDS

BCL11A - B cell CLL lymphoma 11A
HBB - β globin
PTGER4 (Prostanoid EP4 receptor) - Prostaglandin E2 receptor EP4 subtype
RBM38 - RNA binding motif protein 38

REFERENCES

Tewhey, R., et al. "Direct identification of hundreds of expression-modulating variants using a multiplexed reporter assay." *Cell* **(2016)**

Ulirsch, J., et al. "Systematic functional dissection of common genetic variation affecting red blood cell traits." *Cell* **(2016)**

TARGETS & MECHANISMS

HIDE AND SEEK

By Selina Koch, Staff Writer

Duke University researchers and their collaborators have identified the mechanism by which breast cancer cells hide in bone marrow to evade chemotherapy, and developed a two-part strategy for flushing them out. The mechanism falls neatly in the lap of GlycoMimetics Inc., providing a rationale for why the company's next clinical candidate, GMI-1359, might have an advantage in breast cancer.

The compound is a dual inhibitor of the cell adhesion molecule E selectin and CXCR4, the receptor for the chemokine CXCL12. In a paper published last month in *Science Translational Medicine*, the Duke group showed that breast cancer cells gain entry to the bone by binding E selectin in bone blood vessels, and then bind CXCL12 just outside the vessels to take root in the perisinusoidal regions of the bone marrow where they hide out (see "Bad to the Bone," page 7).

Dorothy Sipkins, who led the study and is an associate professor at Duke University Medical Center, told BioCentury that even in the earliest stages of breast cancer, or after treatment when clinical tests show no signs of metastatic disease, bone biopsies have found micrometastases lurking in the marrow. "It's clear that there is something about the bone marrow microenvironment that is very welcoming to certain solid tumors, including breast cancer, but the biology behind that was not well understood," said Sipkins.

Once cancer stem cells are in the bone marrow they are largely sheltered from chemotherapy, and breast cancer cells in particular can lie dormant for long periods of time before reawakening to cause metastatic relapse, she said. "In contrast to most other malignancies where if you haven't relapsed within the first five years you're considered cured, patients with breast cancer can relapse five, 10 or even more years after their initial treatment."

Sipkins' lab is studying the molecular mechanisms by which cancer cells home to the bone and take up residence there, with a goal to "find a way to break the bonds between dormant breast cancer cells and their hideout in the bone."

GlycoMimetics VP and CSO John Magnani told BioCentury the findings support the idea that GMI-1359 — which was designed to prevent metastatic relapse — might be able to drive breast cancer cells out of the bone marrow and keep them out. "This study shows that these two adhesive pathways play distinct roles in the formation of micrometastases in bone, and suggests that blocking them both will be more effective than inhibiting one or the other."

According to Magnani, the company designed the molecule before it knew about the complementary activities of the two targets. But he said evidence had already existed that both E selectin and CXCL12 are expressed in specialized niches in bone and are active in hematologic malignancies, "which is why we made one molecule that can inhibit both."

Magnani, who is a co-author on the study, said the findings both extend the range of possible uses for the compound, and answer the long-standing question in the field about why certain solid tumors metastasize to bone.

BIOCENTURY PRODUCT PROFILE	
INNOVATION STAGE	
Product	GMI-1359, a dual inhibitor of E selectin and CXCR4
Concept	Drive dormant micrometastases out of bone to prevent subsequent disease relapse
Disease	Breast cancer
Competition	1) Chemotherapy 2) E selectin inhibitor 3) CXCR4 or CXCL12 inhibitors
Differentiation	1) Penetrates bone 2) Eliminates existing micrometastases 3) Prevents bone invasion by cancer cells
Administration	Oral
Risks	Dislodged cancer cells may invade other organs
Development status	IND-enabling studies
Patents	Patented
Company; lead investigator	GlycoMimetics Inc.; John Magnani

BAD TO THE BONE

A **Duke University** team has shown how breast cancer cells that have left the primary tumor invade the bone marrow to create dormant micrometastases capable of reawakening years later. The researchers devised a strategy for blocking the mechanism to avoid disease relapse.

The top panel shows the mechanism:

(1) Circulating breast cancer cells (BCCs) bind to **E selectin** expressed on the inner surface of bone blood vessels, which allows transport across the vessel wall into the perisinusoidal region of the marrow.

(2) BCCs bind **CXCL12** on the outer surface of the vessels via the receptor **CXCR4**, forming **dormant** micrometastases.

(3) When the **dormant** cells reactivate, they **proliferate** in distinct zones lateral to the perisinusoidal region.

The bottom panel shows how blocking BCC interactions with bone marrow could prevent the metastatic relapse that commonly occurs in the region:

(1) Inhibiting the binding of BCCs to **E selectin** in blood vessels prevents the cells from invading into the bone marrow tissue.

(2) Inhibiting binding of BCC to **CXCL12** forces **dormant** BCCs already in the marrow back into circulation, which prevents later reactivation of the cells within the bone.

CXCL12 (SDF-1) - Chemokine CXC motif ligand 12; CXCR4 (NPY3R) - CXC chemokine receptor 4; E selectin (SELE; CD62E)

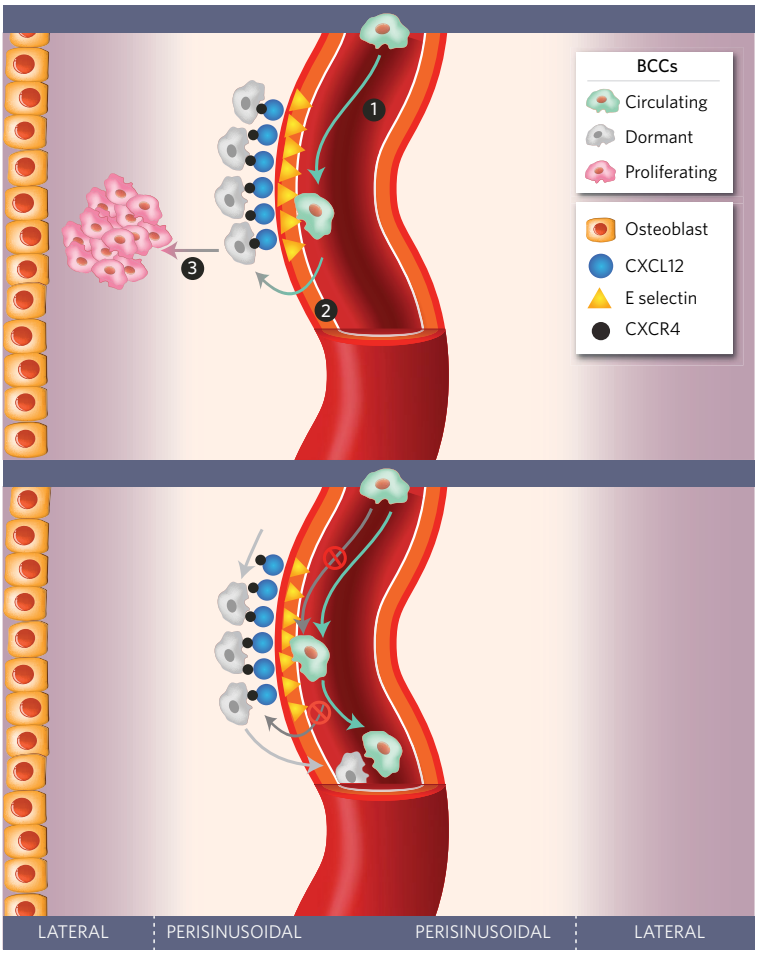

> "It's clear that there is something about the bone marrow microenvironment that is very welcoming to certain solid tumors, including breast cancer, but the biology behind that was not well understood."
>
> Dorothy Sipkins, Duke University

TALE OF TWO TARGETS

According to Sipkins, although the targets had been implicated in the formation of bone micrometastases, it was unclear what roles the two proteins played in the process.

The team's first focus was on the interaction of CXCL12 with its ligand CXCR4, because binding between the two molecules anchor hemopoietic stem cells to bone vasculature, and clinical and preclinical studies have shown that bone micrometastases typically occur in areas with high levels of CXCL12.

"But when we did cell homing studies in our mouse model we saw no effect, zero effect, of inhibiting CXCR4 in just a huge variety of ways," said Sipkins.

Instead, the team turned its attention to E selectin. "We also knew that bone marrow vessels are unique in that they not only express CXCL12 but they also express E selectin in the basal state," whereas most vessels only express E selectin in response to infection, said Sipkins.

Using real-time *in vivo* microscopy in mice injected with fluorescently labeled breast cancer cells, the group showed that the circulating cells adhered to E selectin in bone blood vessels, which suggested E selectin might be involved in allowing entry to the bone marrow.

To determine if binding to E selectin is required for the cells to enter the bone marrow, the group tested GlycoMimetics' E selectin inhibitor GMI-1271 in a patient-derived xenograft mouse model of breast cancer. The compound decreased the number of breast cancer stem cells in the bone marrow threefold compared with vehicle.

GlycoMimetics has GMI-1271 in Phase I/II testing to treat acute myelogenous leukemia (AML).

Sipkins' team then revisited the role of CXCR4-CXCL12 interactions using a tool compound that inhibits CXCR4 and *in vivo* microscopy to test whether the receptor is required for cancer cell retention in bone, despite not acting as a gateway for cancer cell entry. In a xenograft mouse model of breast cancer, a single dose of the CXCR4 inhibitor mobilized 25% of the cancer stem cells present in bone marrow six weeks post engraftment, forcing the cells into circulation, whereas less than 10% of cells in vehicle-treated animals left the bone.

By contrast, although the E selectin inhibitor prevented entry of breast cancer cells into bone marrow through blood vessels, it failed to mobilize breast cancer cells that had already formed micrometastases in the marrow.

"These molecules play different roles in the metastasis of breast cancer cells," said Sipkins. Blockade of CXCR4 alone forces cancer cells into the blood but doesn't stop them from re-entering the bone, whereas blocking E selectin alone prevents additional cancer cells from entering but doesn't influence the cells already present, she said.

The team showed cells associated with CXCL12 that lay close to the site of entry from the blood vessels — in perisinusoidal regions — were dormant, based on expression of specific markers, whereas proliferating cancer cells were present in distinct regions farther away from blood vessels. That supported the idea that CXCR4-CXCL12 interactions maintain the long-lived dormant micrometastases that frequently occur in breast cancer patients.

The Duke team is now determining whether repeat dosing with the combination therapy or with GlycoMimetics' dual inhibitor GMI-1359 can mobilize a greater fraction of the cells, or whether the strategy needs to be combined with inhibition of other types of adhesive interactions to flush out all the cells.

"For hematopoietic stem cells there are certainly other adhesive molecules, and if you inhibit them simultaneously with CXCR4 you get a synergistic effect," said Sipkins.

At least 14 companies have programs targeting CXCR4 in clinical development. Noxxon Pharma AG has the CXCL12 inhibitor olaptesed pegol in Phase II development for chronic lymphocytic leukemia (CLL) and multiple myeloma (MM), and in Phase I for other cancers.

> "This study shows that these two adhesive pathways play distinct roles in the formation of micrometastases in bone, and suggests that blocking them both will be more effective than inhibiting one or the other."
>
> John Magnani, GlycoMimetics

Another priority for Sipkins is to determine the fate of the mobilized cells, including gauging how many of them undergo apoptosis after losing substrate contact, as well as their susceptibility to chemotherapeutic agents.

Once in circulation, Sipkins thinks the mobilized cells are unlikely to form new metastases in different locations. "Patients can have a high tumor burden in the bone and no evidence of disease elsewhere, despite the fact we know that some of the tumor cells are circulating," which suggests the properties that make breast cancer cells particularly suited for entry and adherence within the bone marrow do not support colonization of other potential metastatic sites, she said.

She added that E selectin is normally only expressed in blood vessels of bones and lymph nodes, but that "lymph node metastases are pretty well dealt with with the current therapies. It's really these distant metastases that are the major clinical challenge."

Magnani said E selectin can be up-regulated elsewhere under certain circumstances but that the presence of GMI-1359 should prevent any E selectin-mediated tissue invasion of the cancer cells.

He said the company plans to file an IND for GMI-1359 to treat hematologic malignancies in 3Q16, but has not yet decided whether it will clinically target breast cancer or other solid tumors that "require larger, longer trials."

However, the biotech will continue to collaborate with Sipkins' lab to test GMI-1359 in mouse models of breast cancer. "This paper sets us up perfectly for that," said Magnani.

COMPANIES AND INSTITUTIONS MENTIONED

Duke University, Durham, N.C.
Duke University Medical Center, Durham, N.C.
GlycoMimetics Inc. (NASDAQ:GLYC), Rockville, Md.
Noxxon Pharma AG, Berlin, Germany

TARGETS AND COMPOUNDS

CXCL12 (SDF-1) - Chemokine CXC motif ligand 12
CXCR4 (NPY3R) - CXC chemokine receptor 4
E selectin (SELE; CD62E)
GMI-1271 (E selectin antagonist)
Olaptesed pegol (NOX-A12)

REFERENCES

Price, T., et al. "Dormant breast cancer micrometastases reside in specific bone marrow niches that regulate their transit to and from bone." *Science Translational Medicine* **(2016)**

TOOLS & TECHNIQUES

HOME IS IN THE PLACENTA

By Lauren Martz, Senior Writer

Many drug developers have avoided stepping into what they see as the high risk area of pregnancy-associated complications, leaving diseases such as preeclampsia and fetal growth restriction with little innovation and few treatment options. By taking advantage of biological similarities between solid tumors and the placenta, a group from the University of Manchester has developed a drug delivery technology that could shift the risk-reward balance and spur companies to reopen the book.

In a paper published in *Science Advances* last month, the group, headed by Lynda Harris, a lecturer in pharmaceutics at the university, reported that two peptides known to target solid tumors also home to the surface of the placenta. Drug-loaded liposomes decorated with either peptide accumulated in the outer layers of the placenta without crossing into fetal circulation or accumulating in maternal organs.

The authors wrote the technology can provide "a platform to develop the first generation of placenta-specific therapeutics," and the team has already begun collaborating with Stefan Hansson, a co-founder of A1M Pharma AB and professor and head of the Perinatal Laboratory at Lund University, to deliver recombinant A1M to the placenta. A1M Pharma has the recombinant A1M molecule in preclinical testing for late-onset preeclampsia and acute kidney injury.

"By homing a drug to the placenta, you can use a smaller dose and thereby avoid systemic effects to the mother and baby," said Hansson. "As far as I know, this is the only functional drug delivery that targets the placenta," he added.

In addition to the A1M program, at least two companies have therapeutics in clinical development for preeclampsia, and two others have preclinical candidates for the indication — but none of the clinical or preclinical candidates are targeted to act only in the placenta (see "Preeclampsia Pipeline," page 11).

The landscape for fetal growth restriction is even barer. Several years ago, Ark Therapeutics Group plc was developing a therapeutic for fetal growth restriction, EG103, but the company, which changed its name in 2015 to Premier Veterinary Group plc, is now focusing exclusively on products for veterinary medicine.

> "By homing a drug to the placenta, you can use a smaller dose and thereby avoid systemic effects to the mother and baby."
>
> Stefan Hansson, Lund University

Pregnancy complications such as preeclampsia and fetal growth restriction affect about 10% of pregnancies, and the only effective treatment in either case is early delivery of the baby. Preeclampsia is characterized by a dangerous increase in blood pressure during pregnancy that affects maternal organ function and limits blood and nutrient exchange to the fetus. Fetal growth restriction is a condition that prevents normal growth of the baby.

According to Harris, in most cases, these pregnancy complications are caused by impaired placental growth or function, and studies in animals suggest treating the placenta itself can treat maternal symptoms and help the fetus grow.

The problem is that drugs capable of increasing placental growth or function, such as the growth factor IGF-2, target molecules expressed on other maternal organs, and any crossover from the placenta to fetal circulation can be toxic to the fetus.

COPYING FROM CANCER

To find a system that could target molecules specifically to the outer layers of the placenta, Harris' team reasoned that similarities with some cancers could lead to the discovery of new placenta-specific antigens. The idea was that peptide sequences known to target tumors might also bind the placenta surface.

"The placenta behaves like a well-controlled tumor," wrote the authors, noting it shares the ability to rapidly proliferate, evade immune detection and produce growth factors and cytokines.

The group selected two peptides, CGKRK and cyclic iRGD, that deliver drugs to tumor vessels in different mouse models of cancer.

PREECLAMPSIA PIPELINE

Select products in clinical and preclinical development to treat preeclampsia. At least five companies are developing therapeutics for preeclampsia, but none of the therapeutics in development are specifically targeted to the placenta — the source of the disease. In a new study in Science Advances, a U.K. group suggests targeting therapeutics, including some of those in development, to the placenta using placenta-homing peptide sequences could decrease fetal and maternal toxicity. *Source: BCIQ: BioCentury Online Intelligence*

COMPANY	PRODUCT	DESCRIPTION	PHASE OF DEVELOPMENT
LFB S.A.; **rEVO Biologics Inc.**	ATryn	Recombinant human antithrombin (rhAT) to treat inflammation and cardiovascular damage in preeclampsia	Phase III
Glenveigh Medical LLC	Digibind digoxin immune fab	Polyclonal antibody fragment that neutralizes digoxin to decrease the effects, including vasoconstriction and hypertension, of elevated endogenous digitalis-like factor (EDLF) in preeclampsia	Phase II
A1M Pharma AB (AktieTorget:A1M)	A1M	Recombinant α-1 microglobulin (A1M) to block oxidative stress involved in preeclampsia	Preclinical
Alnylam Pharmaceuticals Inc. (NASDAQ:ALNY)	ALN-AGT	An RNAi therapeutic against angiotensinogen (AGT) that knocks down the target in the maternal liver to decrease blood pressure	Preclinical
Pluristem Therapeutics Inc. (NASDAQ:PSTI; Tel Aviv:PSTI)	PLX-PAD cells	Allogeneic, placenta-derived, expanded (PLX) mesenchymal cell therapy to decrease symptoms of preeclampsia and damage to the placenta	Preclinical

While the iRGD peptide was already known to bind the integrin CD51, the group identified the calcium-binding protein CALR as the molecular target of CGKRK in the placenta (see "No Entry," page 12).

In pregnant mice, fluorescently labeled versions of the peptides accumulated in the placenta, but were not found in other major organs, and didn't affect the size of the fetus or placenta. That suggested the sequences might allow compounds to be safely targeted during pregnancy.

The team conjugated the peptides to liposomes carrying a fluorescent drug analog and showed the particles were specifically delivered to the placenta, where they were detectable for at least 72 hours.

Next the researchers tested the system using IGF-2 as the payload. Targeted liposomes carrying the growth factor increased placental weights compared with IGF-2 alone, empty liposomes or drug-containing liposomes coated with a control peptide. In a mouse model of fetal growth restriction, the IGF-loaded liposomes increased the weight of the smallest pups but caused no significant weight gain in the larger ones, suggesting the treatment could specifically increase weight of growth-restricted babies without causing excessive weight gain above normal levels.

Harris said the researchers are still trying to determine the mechanism that allows the peptides to target the placenta while preventing the drug cargo from crossing over into fetal circulation. "There is presumably some generalized endocytosis pathway that takes up liposomes lacking peptides on the surface, which freely cross into fetal blood, but because our liposomes bind to receptors, they are probably channeled to another pathway," said Harris.

However, while the mouse data were promising Harris noted that mouse models only give a preliminary indication of how the agents might work in disease, and don't include the various co-morbidities present in human disease, citing obesity and high blood pressure as contributing factors that are not modeled in the mice.

To get a better indication of whether the peptides might target efficiently in humans, the group tested the molecules in human placenta explants from different pregnancy stages and showed the free peptides or peptide-coated liposomes bound the syncytiotrophoblast layer of the placenta, which faces the maternal circulation.

WORTH THE RISK

Next, Harris wants to test the targeted liposomes with other drug cargoes in models of placenta-related diseases.

In addition, her group is running a parallel project to screen for new peptides that bind the placenta but not tumors to avoid

NO ENTRY

In a recent paper in *Science Advances*, a University of Manchester group found that a pair of tumor-targeting peptides can home to the placenta, without reaching the fetal circulation. The team proposed that these peptides, or others that target only the placenta and not tumors, could help deliver drugs to the placenta for pregnancy complications including fetal growth restriction and preeclampsia, with low risk for the fetus.

In mouse and *ex vivo* human placenta studies, two peptides, CGKRK and cyclic iRGD, or liposomes decorated with either peptide, accumulated on the surface of the placenta without crossing into fetal circulation and without accumulating in other maternal organs. The iRGD peptide bound the integrin CD51 **(yellow)**, whereas CGKRK bound the calcium-binding protein CALR **(purple)**, both of which are located on the **syncytiotrophoblast** layer — the surface of the placenta that faces the maternal circulation.

While non-targeted liposomes can cross into the fetal circulation **(orange circles)**, liposomes coated with iRGD **(green circles)** or CGKRK **(blue circles)** were found in maternal blood in the placenta and the syncytiotrophoblast layer, but did not pass through to the **cytotrophoblast** cell layer adjacent to the fetal vasculature.

CD51 - Integrin α_v; CALR - Calreticulin

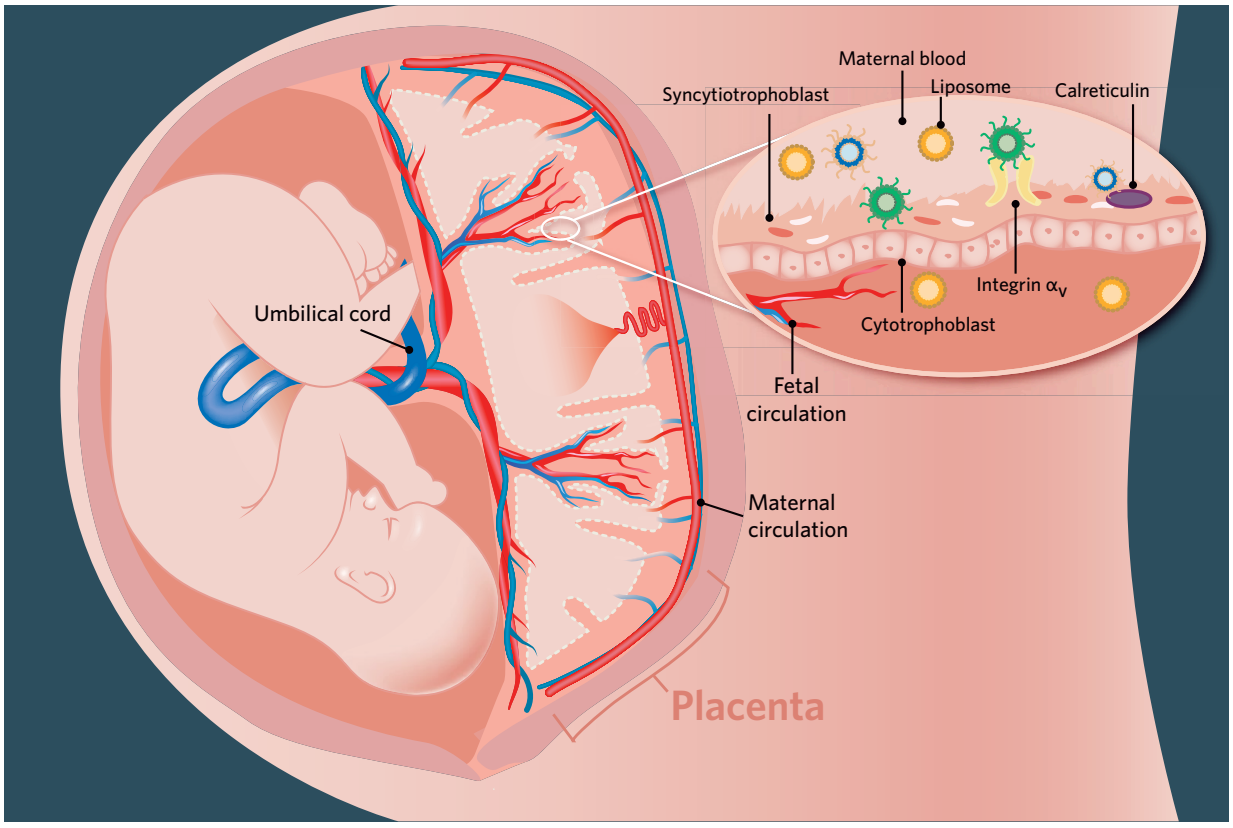

problems caused by targeting both, in the event that a patient carries an unknown tumor.

According to Natalie Hannan, research fellow in the department of obstetrics and gynecology at the University of Melbourne, although screening patients for potential tumors could reduce the risk, accumulation of targeted liposomes in an undetected tumor would be a significant problem because of the types of therapeutics being delivered. For example, directing growth factors to a tumor could accelerate tumor growth.

Harris thinks the targeted liposome approach could lead to uptake of the technology in a variety of pregnancy treatments beyond preeclampsia and fetal growth restriction. For example,

it could be used to prevent surgery to remove the placenta in ectopic pregnancy cases.

She believes that although pregnancy is traditionally a difficult area for drug development, regulators are softening on pregnancy indications.

"I don't think our targeting peptides will make the regulatory pathway easier at first, but more and more, people are trying to find ways to treat pregnant women, and the treatments in the clinic aren't targeted," said Harris.

She noted that clinical trials are already underway in multiple countries examining steroids and Viagra sildenafil for their abilities to increase blood flow to the placenta in pregnant women. Separately, a group from University College London is seeking approval to test a gene therapy targeted at uterine arteries in pregnant women.

"If regulators are open to a gene therapy, I do hope we can get a small trial of our liposomes underway," said Harris.

The peptides have not been patented for placenta-targeted drug delivery because they are already covered under other IP for their tumor-targeting applications. Harris and colleagues are hoping their screens for placenta-specific peptides will identify some that could provide new IP.

COMPANIES AND INSTITUTIONS MENTIONED

A1M Pharma AB (AktieTorget:A1M), Lund, Sweden
Lund University, Lund, Sweden
Premier Veterinary Group plc (LSE:PVG), London, U.K.
University College London, London, U.K.
University of Manchester, Manchester, U.K.
University of Melbourne, Melbourne, Australia

TARGETS AND COMPOUNDS

A1M - α-1 microglobulin
CALR - Calreticulin
CD51 - Integrin α_v
IGF-2 - Insulin-like growth factor-2

REFERENCES

Martz, L. "A1M for preeclampsia." *BioCentury Innovations* **(2016)**

EMERGING COMPANY PROFILE

BOOSTING TRANSMISSION

By Selina Koch, Staff Writer

Muscle weakness associated with myasthenia gravis (MG) is commonly treated with AChE inhibitors that prevent the breakdown of acetylcholine, but the drugs have diverse side effects because the neurotransmitter's receptors are found across the whole nervous system, not just in muscle. Instead, NMD Pharma ApS is developing compounds to maximize the residual muscle activity by targeting an ion channel specific to skeletal muscle fibers.

The autoantibodies generated in MG diminish postsynaptic currents in neuromuscular synapses, preventing muscles from responding properly to nerve discharges. But rather than addressing the underlying cause of the poor synaptic transmission, NMD's goal is to magnify the remaining signal, using small molecule inhibitors that work by amplifying incoming nerve signals to enable muscle contraction.

While CEO Thomas Pedersen said the company is not disclosing the channel's identity, he believes its restriction to the muscle will avoid many of the competitor compounds' side effects. In addition, the strategy could replace or reduce the need for immunosuppressive therapy used widely to counter the generation of the autoantibodies.

"We envision that this could be used quite early on in the disease to improve muscle function, and that some patients may suffice with our compound alone," or require lower doses of AChE inhibitors or immunosuppressants, Pedersen told BioCentury.

In a mouse model of MG, the company's lead compound increased running times in a rotarod test fivefold compared with vehicle.

Pedersen also thinks the compounds will have broad uses across neuromuscular diseases because they provide symptomatic relief "irrespective of whether the underlying cause of neuromuscular junction failure is presynaptic or postsynaptic."

He said NMD chose MG as its lead indication because the endpoints for measuring functional gain in patients are "well described," but the company is also developing the compounds for amyotrophic lateral sclerosis (ALS) and spinal muscular atrophy (SMA).

Although NMD has yet to disclose results in preclinical models of ALS or SMA, COO Paul Little thinks the rotarod results from the MG model can be extrapolated in part because the exercise involves increased breathing, which indicates improved diaphragm function. "The ability to improve breathing would be a huge benefit to patients with ALS," many of whom die of respiratory failure, said Little.

"What ties this together is that these diseases are all associated with reduced neuromuscular transmission," Pedersen added.

NMD PHARMA APS, Aarhus, Denmark
Technology: Small molecules targeting an undisclosed ion channel in skeletal muscle
Disease focus: Neurology
Clinical status: Preclinical
Founded: 2015 by Thomas Pedersen, Ole Nielsen and Claus Olesen
University collaborators: Aarhus University
Corporate partners: None
Number of employees: 10
Funds raised: $3 million
Investors: Lundbeckfond Emerge, Novo Seeds, Capnova
CEO: Thomas Pedersen
Patents: None issued

Pedersen thinks the compounds might also restore more muscle activity than Cytokinetics Inc.'s fast skeletal muscle troponin activators, which act only within fast-twitch muscle fibers, whereas NMD's compounds target both fast- and slow-twitch fibers.

Cytokinetics has the troponin activator tirasemtiv in Phase III for ALS and Phase II for MG. Cytokinetics and Astellas Pharma Inc. have the troponin activator CK-2127107 in Phase II for SMA.

Last week, NMD filed a patent covering use of the approach in a variety of neuromuscular diseases and raised $3 million in seed funding. Pedersen said the round will fund the company for one year, during which it will optimize its lead molecules and explore additional indications. It will then seek a fourth investor to help take the program into the clinic. NMD expects to start its first human trial in 30-36 months and will partner the compound after Phase II trials in MG.

COMPANIES AND INSTITUTIONS MENTIONED

Aarhus University, Aarhus, Denmark
Astellas Pharma Inc. (Tokyo:4503), Tokyo, Japan
Cytokinetics Inc. (NASDAQ:CYTK), South San Francisco, Calif.
NMD Pharma ApS, Aarhus, Denmark

TARGETS AND COMPOUNDS

AChE - Acetylcholinesterase

TRANSLATION IN BRIEF

MUSASHI'S DUAL DUEL

The Musashi genes were originally named for the samurai who fought with two swords because, when discovered in flies, their mutation created double-shafted bristles. Now, a pair of studies double down on the name, showing the genes play a key role in two aggressive cancers and could be exploited therapeutically or diagnostically.

In papers published in *Nature* and the *Proceedings of the National Academy of Sciences*, researchers from the University of California San Diego and the Fox Chase Cancer Center, respectively, showed the genes are major drivers in pancreatic ductal adenocarcinoma (PDAC) and non-small cell lung cancer (NSCLC).

Since the first Musashi gene, Musashi RNA-binding protein 1 (MSI1), was discovered in 1994, followed by the second one, Musashi homolog 2 (MSI2), eight years later, the RNA regulators have been associated primarily with stem cell function, in particular in the nervous system.

Until now, most of the focus has been on MSI1, which has been tied to several cancers, including glioblastoma, breast and colon cancer. But using unbiased approaches, the teams found MSI2 to have a dominant role regulating metastasis and therapy resistance in PDAC and NSCLC.

Tannishtha Reya, principal investigator of the *Nature* study, told BioCentury that her team, which focuses on mechanisms that drive benign pancreatic lesions to become malignant, investigated the genes because their expression is "normally high in stem cells and progenitor cells, and becomes extinguished as cells differentiate." In addition, she said, "it is actually very low in benign lesions and it becomes up-regulated as cancers progress." Reya is a professor of pharmacology at UCSD.

> "It is actually very low in benign lesions and it becomes up-regulated as cancers progress."
>
> Tannishtha Reya, UCSD

The UCSD group tested levels of MSI1 and MSI2 in patient pancreatic tumor samples and showed levels of the proteins increased from well-differentiated, grade 1 disease to poorly differentiated, grade 3 disease.

Using "reporter mice" that enabled MSI-expressing cells to be tracked and isolated, the group found that pancreatic cancer cells expressing MSI2 were highly lethal when transplanted into healthy mice, but cells lacking MSI2 did not cause disease. In addition, MSI2-positive cells were enriched in the circulating tumor cell population and were more tumorigenic than circulating MSI2-negative cells. Moreover, the MSI2-positive cells were the predominant population surviving chemotherapy in mice.

"I think the novel element was our ability to build this preclinical model and visualize the cells within the cancer that are actively expressing this gene," said Reya. Importantly, she added, "the cells that do express it are much more aggressive drivers of oncogenic progression."

Finally, the researchers showed that genetic and pharmacologic depletion of both MSI genes decreased tumor growth, prevented pancreatic neoplasias from advancing to adenocarcinomas, and increased survival time roughly twofold.


THINKSTOCK

Reya said she is interested in developing a therapeutic inhibitor of MSI1 and MSI2 and has worked with Ionis Pharmaceuticals Inc. (NASDAQ:IONS) on antisense oligos.

In the *PNAS* study, a team led by Yanis Boumber discovered the biomarker potential of MSI2 by looking for drivers of metastasis in lung cancer. Boumber was formerly an assistant professor at the Fox Chase Cancer Center, and is now an assistant professor in the department of internal medicine at the University of New Mexico.

By screening tissue microarrays, the team showed that MSI2 protein levels were higher in primary lung tumor samples from 123 NSCLC patients than in normal lung tissue. Independent analysis of 59 patient samples from the Cancer Genome Atlas Research Network showed that RNA levels of MSI2 were elevated in primary lung tumors and correlated with poor patient survival. In contrast, MSI1 levels were normal in all samples examined.

MSI2 RNA and protein levels were also elevated in lymph node metastases in a 14-patient cohort. In addition, shRNA depletion of MSI2 decreased cell invasiveness in human and mouse NSCLC lines *in vitro* compared with a control shRNA.

Boumber noted that while MSI1 might also be involved, "MSI2 is the main driver based on our work of the metastatic invasion in lung cancer."

The team believes that MSI2 could be a predictive biomarker for aggressiveness in NSCLC, and Boumber plans to investigate its activity in other cancers as well.

Reya has filed patents on diagnostic and therapeutic MSI functions, which are available for licensing. She has not patented the MSI reporter mice but is interested in collaborations to use the mice for drug testing. Boumber's work is unpatented. *Fox, R., et al. "Image-based detection and targeting of therapy resistance in pancreatic adenocarcinoma." Nature (2016); Kudinov, A., et al. "Musashi-2 (MSI2) supports TGF-β signaling and inhibits claudins to promote non-small cell lung cancer (NSCLC) metastasis." Proceedings of the National Academy of Sciences USA (2016)*

— Michael Leviten

PREFERRING THE FETAL BRAIN

A team at Ohio State University has shown that an opioid antagonist readily enters a fetus' brain but has limited entry into an adult brain, raising the prospect that a peripherally selective compound could be used to prevent or reduce neonatal opioid dependence without compromising the mother.

The idea is to avoid interfering with treatment for pregnant women with opioid dependence, which usually involves managed maintenance with methadone or buprenorphine. Although effective in the mother, the managed maintenance strategy doesn't prevent opioid dependence in the infant upon birth, which results in neonatal abstinence syndrome, often leads to premature birth, and causes a range of other symptoms that require extended stays in ICUs.

The only therapy for neonatal opioid dependence is oral methadone at birth and treatment to alleviate withdrawal symptoms during opioid weaning.

Now, Wolfgang Sadee, professor of medicine and pharmacology, and John Oberdick, associate professor of neuroscience at the Ohio State University College of Medicine, believe they have uncovered a way to prevent neonatal abstinence syndrome by

> "Our main goal is to reduce the length of stay in the ICU, reduce severity of withdrawal, and even prevent premature birth."
>
> John Oberdick, Ohio State

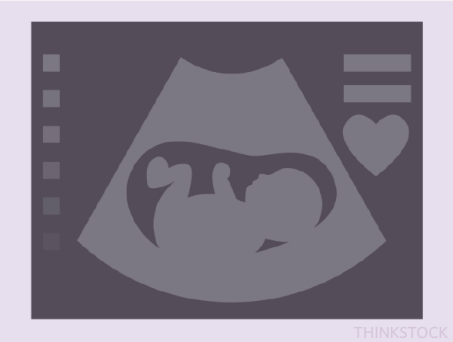
THINKSTOCK

intervening prior to birth. "Our main goal is to reduce the length of stay in the ICU, reduce severity of withdrawal, and even prevent premature birth," Oberdick told BioCentury.

In earlier studies, Sadee's group had found the naltrexone metabolite 6β-naltrexol acted as a potent opioid antagonist, but was peripherally selective and did not readily enter the adult brain. The researchers hypothesized that because the compound does not cross the adult blood-brain barrier (BBB), but does cross other membranes, it might cross the placenta. Because the fetal BBB is undeveloped until shortly after birth, they also guessed the compound would enter the fetal brain.

In a paper published last month in the *Journal of Pharmacology and Experimental Therapeutics*, the researchers showed the compound had unimpeded entry into the fetal brain in mice, but was relatively excluded from the adult brain. "We saw no difference in liver concentrations between the mother and fetus, but brain concentrations had at least a tenfold difference" said Sadee.

Because the BBB takes about three weeks to fully develop in mice after birth, the team used the early postnatal mouse as a behavioral model for testing 6β-naltrexol in opioid dependence, establishing first that the compound readily entered the brain of early postnatal pups.

The researchers administered 6β-naltrexol along with morphine from postnatal days 12 to 17, then induced withdrawal using naloxone. 6β-naltrexol decreased characteristic withdrawal behaviors including jumping, paw wringing and teeth chattering compared with vehicle.

However, while Oberdick said the postnatal mouse model is roughly equivalent to a third trimester or newborn human, he acknowledged a key difference from neonatal abstinence syndrome in human newborns. In humans, withdrawal occurs immediately upon birth.

"We would like to do proof-of-concept studies in rhesus monkeys — a non-human primate model — to see when the BBB develops, see if 6β-naltrexol enters the fetus and if it has the same pharmacokinetic behavior and distribution in non-human primates as in mice, and then show if there are the same behavioral effects in a dependence model," said Oberdick.

Sadee added that the next step is to show the efficacy of combination therapy with opioid maintenance compounds, "eventually testing the efficacy of naltrexol *in utero* with methadone or opioid therapy."

The authors believe another strength of the study is that it shows the feasibility of selectively targeting the fetal brain. "There may be similar applications where it may be possible to take advantage of compounds that don't make it through the BBB but can cross into the fetus, thereby treating problems that affect the fetus," said Sadee.

The university has filed a provisional patent application on this work, and it is available for licensing. *Oberdick, J., et al. "Preferential delivery of an opioid antagonist to the fetal brain in pregnant mice." Journal of Pharmacology and Experimental Therapeutics (2016)*

— Mary Romeo

DISTILLERY

THE DISTILLERY brings you this week's most essential scientific findings in therapeutics, distilled by *BioCentury Innovations* editors from a weekly review of more than 400 papers in 41 of the highest-impact journals in the fields of biotechnology, the life sciences and chemistry. The Distillery goes beyond the abstracts to explain the commercial relevance of featured research, including licensing status and companies working in the field, where applicable. This week in therapeutics includes important research findings on targets and compounds, grouped first by disease class and then alphabetically by indication.

THERAPEUTICS

AUTOIMMUNE DISEASE; HEPATIC

INDICATION: Scleroderma; liver fibrosis

Mouse studies suggest agonizing thyroid hormone receptor could help treat liver fibrosis and scleroderma-associated fibrosis. In a mouse model of liver fibrosis, the endogenous thyroid hormone receptor agonist triiodothyronine (T3) decreased levels of liver fibrosis markers compared with no treatment. In a mouse model of scleroderma, T3 decreased collagen deposition and dermal thickening. Next steps could include testing other thyroid hormone receptor agonists in the models.

Ligand Pharmaceuticals Inc. and Viking Therapeutics Inc. have MB07811 (VK2809), a thyroid hormone receptor β agonist, in Phase I testing to treat hypercholesterolemia and preclinical testing to treat fatty liver disease and non-alcoholic steatohepatitis (NASH).

QuatRx Pharmaceuticals Co. has sobetirome, a thyroid hormone receptor β agonist, in Phase I testing to treat dyslipidemia.

Roche and Madrigal Pharmaceuticals Inc. have 3196 (MGL-3196; VIA-3196), a selective thyroid hormone receptor β agonist, in Phase I testing to treat dyslipidemia.

TARGET/MARKER/PATHWAY: Thyroid hormone receptor
LICENSING STATUS: Patent and licensing status unavailable
PUBLICATION DETAILS: Alonso-Merino, E. et al. *Proc. Natl. Acad. Sci. USA*; published online May 31, 2016
doi:10.1073/pnas.1506113113
CONTACT: Ana Aranda, Autonomous University of Madrid, Madrid, Spain
e-mail: aaranda@iib.uam.es

CANCER

INDICATION: Acute myelogenous leukemia (AML)

In vitro and mouse studies suggest inhibiting RPS6KB1 could help treat AML and other hematologic malignancies. In a human AML cell line, an RPS6KB1 inhibitor tool compound decreased cell growth compared with vehicle. In a xenograft mouse model of AML, the inhibitor increased survival. Next steps could include testing RPS6KB1 inhibitors in additional models of AML and other hematologic malignancies.

Merck KGaA has M2698, a dual inhibitor of RPS6KB1 and protein kinase B (AKT; AKT1; PKB; PKBA), in Phase I testing to treat solid tumors.

TARGET/MARKER/PATHWAY: Ribosomal protein S6 kinase 70kDa polypeptide 1 (RPS6KB1; S6K1)
LICENSING STATUS: Patent and licensing status unavailable
PUBLICATION DETAILS: Ghosh, J. et al. *J. Clin. Invest.*; published online June 13, 2016
doi:10.1172/JCI84565
CONTACT: Rebecca J. Chan, Indiana University School of Medicine, Indianapolis, Ind.
e-mail: rchan@iupui.edu
CONTACT: Reuben Kapur, same affiliation as above
e-mail: rkapur@iupui.edu

THERAPEUTICS

CANCER

INDICATION: Breast cancer

Cell culture and mouse studies suggest inhibiting PTK6 could help treat triple-negative breast cancer (TNBC). In breast tumor samples from 60 TNBC patients, PTK6 was expressed in 44 (74%) and highly expressed in seven (12%). In human TNBC cell lines, PTK6 knockdown increased anoikis and decreased proliferation, migration and levels of epithelial-mesenchymal transition (EMT) markers compared with normal PTK6 expression. In a xenograft mouse model of TNBC, PTK6 knockdown or pretreatment of the mice with a PTK6 inhibitor tool compound decreased the number of lung metastases compared with normal PTK6 expression or vehicle pretreatment. Next steps could include testing the inhibitor in patient-derived xenograft models of TNBC.

TARGET/MARKER/PATHWAY: Protein tyrosine kinase 6 (PTK6)
LICENSING STATUS: Patent and licensing status unavailable
PUBLICATION DETAILS: Ito, K. et al. *Cancer Res.*; published online June 14, 2016
doi:10.1158/0008-5472.CAN-15-3445
CONTACT: Hanna Y. Irie, Icahn School of Medicine at Mount Sinai, New York, N.Y.
e-mail: hanna.irie@mssm.edu

INDICATION: Cancer

In vitro and mouse studies suggest inhibiting SLC7A5 could help treat various cancers. In human colon, lung and kidney cancer cell lines, gene knockout or pharmacological inhibition of SLC7A5 decreased proliferation compared with normal SLC7A5 expression or vehicle. In a xenograft mouse model of colon cancer, SLC7A5 knockout decreased tumor growth compared with normal SLC7A5 expression. Next steps could include testing SLC7A5 inhibition in additional models of cancer.

TARGET/MARKER/PATHWAY: Solute carrier family 7 member 5 (SLC7A5; LAT1)
LICENSING STATUS: Patent and licensing status unavailable
PUBLICATION DETAILS: Cormerais, Y. et al. *Cancer Res.*; published online June 14, 2016
doi:10.1158/0008-5472.CAN-15-3376
CONTACT: Jacques Pouyssegur, University of Nice-Sophia Antipolis, Nice, France
e-mail: jacques.pouyssegur@unice.fr

INDICATION: Cancer; breast cancer; pancreatic cancer

Cell culture and mouse studies suggest inhibiting ALDOA could help treat breast, pancreatic and other cancers. In a human pancreatic cancer cell line, siRNA targeting ALDOA decreased proliferation compared with scrambled siRNA. In a human breast cancer cell line, an ALDOA inhibitor tool compound decreased proliferation compared with vehicle. In an orthotopic xenograft mouse model of metastatic breast cancer, shRNA targeting ALDOA decreased the number of lung and liver metastases and increased survival compared with scrambled shRNA. Also in the model, the tool compound decreased tumor growth compared with vehicle. Next steps could include testing the ALDOA inhibitor in other solid tumor models.

TARGET/MARKER/PATHWAY: Aldolase A (ALDOA)
LICENSING STATUS: Patent and licensing status unavailable
PUBLICATION DETAILS: Grandjean, G. et al. *Cancer Res.*; published online June 3, 2016
doi:10.1158/0008-5472.CAN-16-0401
CONTACT: Garth Powis, Sanford Burnham Prebys Medical Discovery Institute, La Jolla, Calif.
e-mail: gpowis@sbpdiscovery.org

THERAPEUTICS

CANCER

INDICATION: Cancer

In vitro and mouse studies identified a protein inhibitor of the integrin CD51/CD61 that could help treat cancer. *In silico* analysis of the binding interaction of CD2 analogs with CD51/CD61 and *in vitro* binding assays of the analogs identified a protein that bound CD51/CD61 outside the known CD2 binding site with a K_d of 4.3 nM. In a xenograft mouse model of CD51/CD61-driven prostate cancer and an orthotopic xenograft mouse model of breast cancer, the compound decreased tumor growth and tumor angiogenesis compared with vehicle, without overt toxicity in the liver, heart, lung, spleen or kidney. Next steps could include testing and improving safety and efficacy of the compound in animal models of other CD51/CD61-driven cancers.

Allegro Ophthalmics LLC, Hanmi Pharmaceutical Co. Ltd and Senju Pharmaceutical Co. Ltd. have Luminate (ALG-1001), an oligopeptide against CD51/CD61 and integrin $\alpha_v\beta_5$, in Phase II testing to treat vitreomacular traction (VMT), diabetic macular edema (DME) and diabetic retinopathy.

Merck KGaA has Impetreve cilengitide, an integrin inhibitor targeting CD51/CD61 and integrin $\alpha_v\beta_5$, in Phase II testing to treat head and neck cancer and lung cancer and preclinical testing to treat melanoma.

Tactic Pharma LLC has ATN-161, an integrin inhibitor targeting CD51/CD61 and integrin $\alpha_v\beta_1$, in Phase II testing to treat brain cancer and Phase I to treat head and neck cancer.

TARGET/MARKER/PATHWAY: Integrin $\alpha_v\beta_3$ (CD51/CD61)

LICENSING STATUS: Patent and licensing status unavailable

PUBLICATION DETAILS: Turaga, R. et al. *Nat. Commun.*; published online May 31, 2016

doi:10.1038/ncomms11675

CONTACT: Zhi-Ren Liu, Georgia State University, Atlanta, Ga.

e-mail: zliu8@gsu.edu

INDICATION: Lung cancer

Cell culture and mouse studies identified an inhibitor of mutant EGFR that could help treat lung cancer. Chemical screening of a compound library in a protein expression assay and optimization of hits identified an allosteric EGFR inhibitor that bound the L858R and T790M EGFR mutants with IC_{50} values of 9 and 600 nM, respectively, and bound EGFR harboring both mutations with an IC_{50} of 3 nM. In a mouse model of EGFR-mutant lung cancer, the allosteric inhibitor plus cetuximab decreased tumor growth compared with either agent alone. In mice, the allosteric inhibitor had a half-life of two hours and an oral bioavailability of 26%. Next steps could include optimizing and testing the inhibitor in other models of lung cancer.

Eli Lilly and Co. and Merck KGaA market Erbitux cetuximab to treat colorectal and head and neck cancers and have the compound in Phase III testing for gastric cancer and Phase II testing for biliary and breast cancers.

TARGET/MARKER/PATHWAY: Epidermal growth factor receptor (EGFR)

LICENSING STATUS: Patent and licensing status unavailable

PUBLICATION DETAILS: Jia, Y. et al. *Nature*; published online May 25, 2016

doi:10.1038/nature17960

CONTACT: Michael Eck, Dana-Farber Cancer Institute, Boston, Mass.

e-mail: eck@crystal.harvard.edu

THERAPEUTICS

CANCER

INDICATION: Pancreatic cancer

Patient sample, cell culture and mouse studies suggest inhibiting DNMT1 could help treat pancreatic ductal adenocarcinoma (PDAC). In patient tumor samples, levels of DNMT1 mRNA were higher in cancer stem cells (CSCs) than in non-CSCs. In a human PDAC cell line, DNMT1 knockout decreased expression of cancer stem cell markers and sphere formation compared with normal DNMT1 expression. In patient-derived PDAC cells, a DNMT1 inhibitor tool compound or Dacogen decitabine decreased proliferation and levels of stem cell markers and proliferation markers compared with vehicle. In a patient-derived xenograft mouse model of PDAC, pretreatment of tumor cells with the tool compound decreased tumor number compared with vehicle pretreatment. Next steps could include testing DNMT1 inhibitors to treat existing PDAC tumors.

Otsuka Pharmaceutical Co. Ltd., Eisai Co. Ltd. and Johnson & Johnson market Dacogen, a hypomethylating agent that inhibits DNA methyltransferase, to treat myelodysplastic syndrome (MDS), and have the compound approved to treat acute myelogenous leukemia (AML) and in Phase I testing to treat ovarian cancer.

Otsuka has guadecitabine (SGI-110), a small molecule DNA methyltransferase inhibitor, in Phase II testing to treat AML, MDS, liver and ovarian cancers and Phase I testing to treat solid tumors.

TARGET/MARKER/PATHWAY: DNA (cytosine-5-)-methyltransferase 1 (DNMT1)

LICENSING STATUS: Patent and licensing status unavailable

PUBLICATION DETAILS: Zagorac, S. et al. *Cancer Res.*; published online June 3, 2016

doi:10.1158/0008-5472.CAN-15-3268

CONTACT: Christopher Heeschen, Barts Cancer Institute, Pacific Palisades, Calif.

e-mail: christopher.heeschen@gmail.com

INDICATION: Prostate cancer

Cell culture and mouse studies identified a BET bromodomain protein degrader that could help treat castration-resistant prostate cancer (CRPC). Chemical synthesis and testing in three human CRPC cell lines of small molecules linking BRD4- and vHL-binding scaffolds identified a compound, ARV-771, that degraded BRD2, BRD3 and BRD4 with IC_{50} values less than 5 nM and decreased proliferation compared with a BET inhibitor tool compound and the BET inhibitor OTX015. In two xenograft mouse models of CRPC, ARV-771 decreased tumor growth compared with OTX015. Next steps by Arvinas LLC include testing the safety of ARV-771 in mice.

Arvinas has ARV-771 in preclinical development for CRPC.

Mitsubishi Tanabe Pharma Corp. and Merck & Co. Inc. have OTX015, a synthetic small molecule inhibitor of BRD2, BRD3 and BRD4, in Phase II testing to treat recurrent glioblastoma multiforme (GBM) and Phase I testing to treat hematologic malignancies and solid tumors.

TARGET/MARKER/PATHWAY: BET bromodomain proteins; bromodomain containing 2 (BRD2); BRD3; BRD4; von Hippel-Lindau tumor suppressor (vHL)

LICENSING STATUS: Patent status unavailable; available for licensing

PUBLICATION DETAILS: Raina, K. et al. *Proc. Natl. Acad. Sci. USA*; published online June 6, 2016

doi:10.1073/pnas.1521738113

CONTACT: Kevin G. Coleman, Arvinas LLC, New Haven, Conn.

e-mail: kevin.coleman@arvinas.com

THERAPEUTICS

DERMATOLOGY

INDICATION: Dermatology

Patient sample and mouse studies suggest the NFE2L2 activator sulforaphane could help treat pachyonychia congenita, which is caused by mutations in keratin-encoding genes. In patient skin samples, levels of phosphorylated NFE2L2 were lower than in skin samples from healthy volunteers. In a mouse model of pachyonychia congenita, topical application of sulforaphane decreased skin lesions and epidermal thickening compared with topical vehicle. Next steps could include testing sulforaphane in other models of pachyonychia congenita.

Evgen Pharma plc has sulforaphane (SFX-01) in Phase II testing to treat stroke, Phase I testing to treat prostate cancer and preclinical development to treat breast cancer and multiple sclerosis (MS).

TARGET/MARKER/PATHWAY: Nuclear factor (erythroid-derived 2)-like 2 (NFE2L2; NRF2)

LICENSING STATUS: Patent and licensing status unavailable

PUBLICATION DETAILS: Kerns, M. et al. *J. Clin. Invest.*; published online May 16, 2016

doi:10.1172/JCI84870

CONTACT: Pierre A. Coulombe, The Johns Hopkins University, Baltimore, Md.

e-mail: coulombe@jhu.edu

ENDOCRINE / METABOLIC

INDICATION: Menopause

Cell culture and mouse studies identified inducers of ESR1 activity that could help treat menopause without uterine side effects. Chemical modification and screening of estradiol and bisphenol A analogs identified four compounds with lower binding affinity for ESR1 than estradiol, including one whose complex with ESR1 had a half-life that was more than 1,900 times lower than the half-life of estradiol-ESR1 complex. In a mouse model of menopause-associated endothelial injury, that compound increased endothelial repair with comparable potency to estradiol. In a mouse model of menopause, all four compounds decreased weight gain with potency comparable to estradiol, without inducing the uterine growth associated with estradiol. Next steps could include testing the compounds in larger animal models of menopause.

TARGET/MARKER/PATHWAY: Estrogen receptor (ESR1)

LICENSING STATUS: Patent and licensing status unavailable

PUBLICATION DETAILS: Madak-Erdogan, Z. et al. *Sci. Signal.*; published online May 24, 2016

doi:10.1126/scisignal.aad8170

CONTACT: Benita Katzenellenbogen, University of Illinois, Champaign, Ill.

e-mail: katzenel@illinois.edu

GENITOURINARY

INDICATION: Genitourinary

Patient sample and mouse studies suggest promoting NOS3 activity with Viagra sildenafil could help prevent preeclampsia. In patient placental tissue samples or vascular endothelium from a mouse model of preeclampsia, markers of NOS3 activity were lower than in samples from healthy volunteers or mice with normal pregnancies. Also in the mouse model, Viagra decreased uterine vascular resistance, hypertension and angiotensin II sensitivity — a marker of preeclampsia — in the dam and increased birth weight in the offspring compared with vehicle. Next steps could include testing further safety and efficacy of Viagra in pregnant mice.

Pfizer Inc. markets Viagra, a phosphodiesterase-5 (PDE-5) inhibitor, to treat erectile dysfunction (ED) and hypertension and has the compound in Phase II testing to treat single-ventricle heart disease.

TARGET/MARKER/PATHWAY: Endothelial cell nitric oxide synthase 3 (NOS3; eNOS)

LICENSING STATUS: Patent and licensing status unavailable

PUBLICATION DETAILS: Burke, S. et al. *J. Clin. Invest.*; published online June 6, 2016

doi:10.1172/JCI83918

CONTACT: Suzanne D. Burke, Beth Israel Deaconess Medical Center, Boston, Mass.

e-mail: sdburke@bidmc.harvard.edu

CONTACT: S. Ananth Karumanchi, same affiliation as above

e-mail: sananth@bidmc.harvard.edu

THERAPEUTICS

INFECTIOUS DISEASE

INDICATION: HIV/AIDS

In vitro studies suggest the DDX58 agonist Soriatane acitretin could help treat HIV. In T cells from healthy volunteers infected *ex vivo* with HIV, Soriatane decreased levels of viral DNA 72 hours after infection compared with vehicle, and Soriatane plus the HDAC inhibitor Zolinza vorinostat, a reactivator of latently infected cells, reduced viral DNA to undetectable levels, whereas neither agent alone did so. In $CD4^+$ T cells from HIV patients on antiretroviral therapy, Soriatane alone or with Zolinza decreased viral DNA levels compared with vehicle or a combination of mAbs against CD3 and CD28. Also in the patient-derived cells, Soriatane increased apoptosis of infected cells but not uninfected cells, whereas the anti-CD3 and anti-CD28 mAbs increased apoptosis of both cell types. Next steps include investigating the mechanisms downstream of DDX58 activation.

GlaxoSmithKline plc markets the oral retinoid Soriatane to treat psoriasis.

Merck & Co. Inc. markets Zolinza for cutaneous T cell lymphoma (CTCL) and has the compound in Phase III testing for mesothelioma, Phase I/II testing for graft-versus-host disease (GvHD) and Phase I testing for brain cancer.

TARGET/MARKER/PATHWAY: DEAD box polypeptide 58 (DDX58; RIG-I); histone deacetylase (HDAC)

LICENSING STATUS: Unpatented; unavailable for licensing

PUBLICATION DETAILS: Li, P. et al. *Nat. Med.*; published online June 13, 2016

doi:10.1038/nm.4124

CONTACT: Peilin Li, San Francisco Veterans Affairs Medical Center, San Francisco, Calif.

e-mail: Peilin.li@ucsf.edu

INDICATION: Viral infection

Patient sample studies suggest inhibiting ISG15 could help treat viral infections. *In vitro*, stimulation with interferon α (IFNα) and IFNβ of fibroblasts from ISG15-deficient volunteers induced more persistent expression of the antiviral RNA-binding protein IFIT1 than stimulation of fibroblasts from healthy volunteers. In fibroblast-based viral infectivity assays, the IFN-stimulated, ISG15-deficient fibroblasts enabled less replication of herpes simplex virus 1 (HSV-1), human cytomegalovirus (HCMV), vesicular stomatitis virus (VSV), influenza virus A, Sendai virus, Rift Valley fever virus and Nipah virus than IFN-stimulated fibroblasts with normal ISG15 expression. Next steps include screening a compound library for ISG15 inhibitors.

TARGET/MARKER/PATHWAY: Interferon-stimulated gene 15 (ISG15); interferon induced protein with tetratricopeptide repeats 1 (IFIT1)

LICENSING STATUS: Unpatented; licensing status unapplicable

PUBLICATION DETAILS: Speer, S. et al. *Nat Commun.*; published online May 19, 2016

doi:10.1038/ncomms11496

CONTACT: Sandra Pellegrini, Institut Pasteur, Paris, France

e-mail: Sandra.Pellegrini@pasteur.fr

CONTACT: Dusan Bogunovic, Icahn School of Medicine at Mount Sinai, New York, N.Y.

e-mail: Dusan.Bogunovic@mssm.edu

THERAPEUTICS

INFECTIOUS DISEASE; CANCER

INDICATION: Viral infection; melanoma

Mouse studies suggest PSGL-1 inhibitors could help treat chronic viral infections or melanoma. In a mouse model of chronic lymphocytic choriomeningitis virus (LCMV) infection, knockout of PSGL-1 decreased viral loads in serum, liver and kidney; decreased T cell expression of PD-1 and other inhibitory receptors in the spleen, kidney and liver; increased the accumulation of virus-specific T cells in spleen, lung, liver and kidney; and increased serum levels of interferon γ (IFNγ), tumor necrosis factor α (TNFα) and other inflammatory cytokines compared with normal PSGL-1 expression. In a mouse model of melanoma, knockout of PSGL-1 increased the number of tumor-infiltrating T cells and the fraction of T cells that expressed interleukin-2 (IL-2), IFNγ and TNFα and decreased tumor growth and levels of PD-1 in tumor-infiltrating T cells. Next steps could include identifying small molecule inhibitors of PSGL-1.

TARGET/MARKER/PATHWAY: P selectin glycoprotein ligand-1 (PSGL-1; CD162; SELPLG)

LICENSING STATUS: Patent and licensing status unavailable

PUBLICATION DETAILS: Tinoco, R. et al. *Immunity*; published online May 17, 2016

doi:10.1016/j.immuni.2016.04.015

CONTACT: Linda M. Bradley, Sanford Burnham Prebys Medical Discovery Institute, La Jolla, Calif.

e-mail: lbradley@sbpdiscovery.org

NEUROLOGY

INDICATION: Pain

Rat studies suggest inhibiting MIR500A could help treat neuropathic pain. In rat models of chemotherapy-induced and surgery-induced neuropathic pain, spinal dorsal horn levels of MIR500A were higher than in spinal dorsal horns of normal rats. Also in the models, MIR500A knockout decreased thermal and mechanical allodynia compared with normal MIR500A expression. Next steps could include identifying and testing MIR500A inhibitors in animal models.

TARGET/MARKER/PATHWAY: MicroRNA-500a (MIR500A)

LICENSING STATUS: Patent and licensing status unavailable

PUBLICATION DETAILS: Huang, Z.-Z. et al. *J. Neurosci.*; published online June 8, 2016

doi:10.1523/JNEUROSCI.0646-16.2016

CONTACT: Wen-Jun Xin, Sun Yat-Sen University, Guangzhou, China

e-mail: xinwj@mail.sysu.edu.cn

TECHNIQUES

BIOMARKERS

TECHNOLOGY: Gene profiling

Liver levels of SQSTM1 could help diagnose liver cancer. In 121 patients with early stage disease, levels of SQSTM1 in liver tissue correlated with cancer recurrence and poor survival. Liver levels of SQSTM1 were also higher in two patients with chronic liver diseases associated with the risk of liver cancer and one patient who had both liver cirrhosis and early stage liver cancer. Next steps could include validating SQSTM1 levels in the liver as a diagnostic marker in larger cohorts of liver cancer patients.

DESCRIPTION: Liver levels of sequestosome 1 (SQSTM1; p62) to diagnose liver cancer

LICENSING STATUS: Patent and licensing status unavailable

PUBLICATION DETAILS: Umemura, A. et al. *Cancer Cell*; published online May 19, 2016

doi:10.1016/j.ccell.2016.04.006

CONTACT: Jorge Moscat, Sanford Burnham Prebys Medical Discovery Institute, La Jolla, Calif.

e-mail: jmoscat@sbpdiscovery.org

CONTACT: Michael Karin, University of California San Diego, La Jolla, Calif.

e-mail: karinoffice@ucsd.edu

TECHNOLOGY: Gene profiling

Genetic profiling of circulating tumor cells could be used to predict prostate cancer prognosis and stratify patients for treatment. RNA transcripts from 1,321 human prostate tumors were used to create a prostate cancer classification system that stratifies patients into three disease subgroups based on expression levels of genes involved in various molecular pathways. In a proof-of-concept study, patients stratified into one subgroup using a 37-gene panel on circulating tumor cells or prostate tissue samples had increased rates of Xtandi enzalutamide resistance and metastatic progression and decreased overall survival compared with other subgroups. Next steps could include optimizing the assay to improve accuracy.

Medivation Inc. and Astellas Pharma Inc. market Xtandi, an oral androgen receptor antagonist, to treat prostate cancer, and have the compound in Phase III to treat breast cancer and Phase II to treat liver cancer.

DESCRIPTION: Genetic profiling of circulating tumor cells to stratify prostate cancer patients

LICENSING STATUS: Patent and licensing status unavailable

PUBLICATION DETAILS: You, S. et al. *Cancer Res.*; published online June 14, 2016

doi:10.1158/0008-5472.CAN-16-0902

CONTACT: Michael Freeman, Cedars-Sinai Medical Center, Los Angeles, Calif.

e-mail: michael.freeman@cshs.org

TECHNIQUES

DRUG PLATFORMS

TECHNOLOGY: Cell therapy

An artificial *in vitro* niche could help preserve muscle stem cell quiescence before transplant to enhance regenerative potency after transplant. The niche consisted of engineered artificial muscle fibers composed of collagen type I (COL1), integrin $\alpha_4\beta_1$ (CD49D/CD29) and laminin plus a quiescence-promoting culture media containing the hormones somatostatin and transforming growth factor β (TGF-β), the clinical compounds Elcitonin elcatonin and glesatinib, and four tool compounds: a pan-cyclin dependent kinase (CDK) inhibitor; an activator of adenylyl cyclases; a p38 mitogen-activated protein kinase (p38 MAPK; MAPK14) inhibitor; and an inhibitor of vascular endothelial growth factor receptor 2 (VEGFR-2; KDR/Flk-1), fibroblast growth factor receptor (FGFR) and epidermal growth factor receptor (EGFR). In a mouse model of muscle injury, transplant of muscle stem cells cultured in the artificial niche engrafted and expanded more extensively than transplants of stem cells cultured in standard growth media without muscle fibers. In mice receiving transplants and subjected to a second injury, transplants of cells cultured in the artificial niche also expanded more extensively. Next steps include scaling up the artificial niche culture system.

Asahi Kasei Pharma Corp. markets Elcitonin, an eel calcitonin derivative, for pain associated with osteoporosis.

Mirati Therapeutics Inc. has glesatinib (MGCD265), a dual inhibitor of c-Met receptor tyrosine kinase (c-MET; MET; HGFR; c-Met proto-oncogene) and AXL receptor tyrosine kinase (AXL; UFO), in Phase II testing for solid tumors and Phase I/II testing for head and neck cancer and non-small cell lung cancer (NSCLC).

DESCRIPTION: In vitro system to preserve muscle stem cell quiescence pre-transplant and regenerative potency post-transplant

LICENSING STATUS: Unpatented; licensing status not applicable

PUBLICATION DETAILS: Quarta, M. et al. *Nat. Biotechnol.*; published online May 30, 2016

doi:10.1038/nbt.3576

CONTACT: Thomas Rando, Stanford University, Stanford, Calif.

e-mail: rando@stanford.edu

TECHNOLOGY: Structural analyses

Structural analyses of PRC2 bound to an inhibitor or histone H3 substrate could help guide the development of PRC2 inhibitors for cancer that bypass known mechanisms of resistance. Analysis of co-crystals of a pyridone-based PRC2 inhibitor and a complex of three PRC2 subunits — embryonic ectoderm development (EED), suppressor of zeste 12 homolog (SUZ12) and a modified version of enhancer of zeste homolog 2 (EZH2) — showed the inhibitor bound a pocket formed by an activation loop and the I-SET domain of EZH2, and mutations associated with resistance to pyridone-based PRC2 inhibitors were predicted to disrupt this interaction. Analysis of co-crystals of the three PRC2 subunits, two PRC2 cofactors — jumonji and AT-Rich interaction domain containing 2 (JARID2) and acyl-CoA synthetase medium-chain family member 3 (ACSM3) — and an oncogenic histone H3 substrate containing a K27M mutation that prevented PRC2 methylation showed the mutant substrate bound a channel within EZH2's SET domain that interacts with the lysine residue of the wild-type histone. *In vitro*, mutant and wild-type histone H3 bound PRC2 with K_d values of 3.3 μM and 52 μM, respectively. Next steps could include structure-based design of PRC2 inhibitors that can inhibit the mutant enzyme or its interaction with the mutant histone H3.

DESCRIPTION: Structural analyses of polycomb repressive complex 2 (PRC2) bound to an inhibitor and a mutant histone H3 substrate

LICENSING STATUS: Patent and licensing status unavailable

PUBLICATION DETAILS: Brooun, A. et al. *Nat. Commun.*; published online Apr. 28, 2016

doi:10.1038/ncomms11384

CONTACT: Alexei Brooun, Pfizer Inc., San Diego, Calif.

e-mail: alexei.brooun@pfizer.com

CONTACT: Ketan Gajiwala, same affiliation as above

e-mail: ketan.gajiwala@pfizer.com

LICENSING STATUS: Patent and licensing status unavailable

PUBLICATION DETAILS: Justin, N. et al. *Nat. Commun.*; published online Apr. 28, 2016

doi:10.1038/ncomms11316

CONTACT: Steven Gamblin, Francis Crick Institute, London, U.K.

e-mail: steve.gamblin@crick.ac.uk

SCIENTIFIC ADVISORY BOARD

EDITORIAL & RESEARCH

NEWSROOM:
pressreleases@biocentury.com

SAN CARLOS, CA:
+1 650-595-5333; Fax: +1 650-595-5589

CHICAGO:
+1 312-755-0798; Fax: +1 650-595-5589

WASHINGTON, DC:
+1 202-462-9582; Fax: +1 202-667-2922

UNITED KINGDOM:
+44 (0)1865-512184; Fax: +1 650-595-5589

Editor: C. Simone Fishburn, Ph.D.

Associate Editor: Michael J. Haas

Senior Writers: Michael Leviten, Ph.D.; Lauren Martz

Staff Writers: Selina Koch, Ph.D.; Mary Romeo; Karen Tkach, Ph.D.; Mark Zipkin

Director of Research: Walter Yang

Copy Editor: Claire Quang

CORPORATE, SUBSCRIPTIONS & PRIVACY

BioCentury's mission is to provide value-added business information & analysis for life science companies, investors, academia and government on the strategic issues essential to the formation, development and sustainability of life science ventures.

BioCentury Inc.
BioCentury International Inc.

MAIN OFFICES
PO Box 1246
San Carlos CA 94070-1246
+1 650-595-5333; Fax: +1 650-595-5589

CORPORATE
Chairman: Karen Bernstein, Ph.D.

President & CEO: David Flores

Vice President/Commercial Operations: Thomas Carey

Vice President/Administration & CFO: Bennet Weintraub

Publisher: Eric Pierce

Executive Editor and Director, New Ventures: Joshua L. Berlin

Senior Director/Commercial Operations: Tim Tulloch

Director/Business Intelligence: Chris Dokomajilar

Director/Multimedia Business Development: Jamie Gould

Director/Digital Product Manager: Ravid Lazinsky,

Director/Marketing & Promotional Services: Greg Monteforte

Director/Administration & Human Resources: Susan Morgan

Director/Publishing: Jenny Nichols

SUBSCRIBER SERVICES

Subscriber Services: subscribe@biocentury.com

Account Managers: Orlando Abello; Matt Krebs; Michelle Ortega; Ron Rabinowitz

BUSINESS SERVICES
Accounting & Billing: finance@biocentury.com

Conferences: conferences@biocentury.com

Data Solutions Support: support@biocentury.com

Privacy Policy: privacy@biocentury.com

Reprints/Permissions:

businessservices@biocentury.com

PRIVACY & ADVERTISING
In accordance with its Privacy Policy, BioCentury does NOT sell its customer information or usage data to third parties.
BioCentury does NOT sell advertising in the BioCentury, BioCentury Innovations or BioCentury Week in Review. BioCentury is pleased to acknowledge its conference partners and sponsors through unpaid promotional announcements in its publications. BioCentury MAY accept paid promotional messages from sponsors, which are displayed only on BioCentury's websites.